ALMA MATER STUDIORUM · UNIVERSITÀ DI BOLOGNA

DOTTORATO DI RICERCA IN MATEMATICA

Cicolo XXXVI

Settore Concorsuale di afferenza: 01/A4
Settore Scientifico disciplinare: MAT/07

BEYOND PAIRWISE INTERACTION: THE CUBIC MEAN-FIELD ISING MODEL

Presentata da: GODWIN OSABUTEY

Coordinatore Dottorato:
Prof. GIOVANNI MONGARDI

Supervisore:
Prof. PIERLUIGI CONTUCCI

Co-supervisori:
Prof.ssa CECILIA VERNIA
Prof. EMANUELE MINGIONE

Esame finale anno 2024

Contents

Acknowledgement

To my beloved father, Emil Osabutey,
whose unwavering support and love continue to inspire me.
Though you are no longer with us, your guidance lives on
in every achievement.

Introduction

In this thesis, the Ising model, initially formulated with two-spin interactions, is extended to include three-spin interactions. The extended version incorporates the necessary mathematical rigor to investigate the effect of three-spin interactions on the formation of phase separations. This section of the thesis provides an introduction to the Ising model, offering a historical background on its development. It includes an overview of the thesis, introduces the extension of the Ising model to a three-spin model, and outlines the structure of the thesis.

The Ising model was originally proposed by the German physicist Wilhelm Lenz and his graduate student, Ernst Ising, during the early 1920s as a model for ferromagnetism. It is notable that Ising, received the credit for the model rather than his advisor, which is uncommon in scientific nomenclature. Lenz's interest in Curie's law, proposed by Pierre Curie in 1895 [1], which describes the properties of magnetic susceptibility of a material in relation to temperature and an applied external magnetic field, motivated his study. In his work [2], Lenz made the assumption that elementary magnets have only two possible opposite directions; that laid the groundwork for Ising's subsequent investigations on ferromagnetism under his guidance [3].

Pierre Curie's observation in 1895 [1] noted that magnets lose their magnetic properties when heated beyond a certain critical temperature known as the Curie temperature. Regardless of the specific temperature, the underlying phenomenon remains the same: a magnet can only exhibit magnetisation in the presence of an external magnetic field below the Curie temperature, while above it, the magnet behaves as a paramagnetic material. This phenomenon is called phase transition between a paramagnetic and a ferromagnetic phase. Curie drew parallels between the behaviour of ferromagnetic and paramagnetic phases in magnets and the liquid and gas phases in fluids concerning temperature and external fields.

In [4], Pierre Weiss in 1907 proposed an explanation for Curie's observations [1]

based on the interactions between atoms within a magnetic material. He introduced the mean-field approximation theory, suggesting that each atom experiences the combined effect of all other atoms within the material. Weiss's theoretical predictions using this model aligned remarkably well with experimental measurements. Together with Curie's observation this assumption gave rise to a mean-field model, now called the Curie-Weiss model. While this model offered valuable insights, it did not fully capture the complexities of phase transitions.

The work of Pierre Curie [1] forms the basis of the work carried out by Lenz and latter generalised or modified by Ising. Lenz in his work [2], failed to propose an explicit form for the interaction between elementary magnets or magnetic particles. He explained the typical behaviour of a paramagnet, which has zero magnetisation when no magnetic field is applied, and a magnetisation when such a magnetic field is applied, but Lenz made no mention of what will later be referred to as the ferromagnetic behaviour [5]. Although Lenz did not say much about the ferromagnetic behaviours, he made an important contribution: according to [3], Lenz noted that "For ferromagnetic bodies, in addition to the temperature dependence of the susceptibility, one has to explain first of all the fact of spontaneous magnetisation, as is observed in magnetite and pyrites..."

Lenz's work [2] laid the foundation for Ising's contributions, specifically in describing the interactions between elementary magnets or magnetic particles. Ising assumed that interactions between magnets decay rapidly with distance, primarily considering the influence of neighbouring magnets. Additionally, he postulated that the configuration requiring the minimum energy occurs when neighbouring atoms act in the same direction. These assumptions led to the formulation of the mathematical model discussed in the subsequent chapters of this thesis. Ising further assumed that the elementary magnets are arranged in a linear chain to facilitate analysis.

Ising's analysis of the one-dimensional variant of his model resulted in the correct conclusion that a linear chain of two-state spins cannot undergo a phase transition at finite temperature. However, when extending his conclusions to two and three dimensions, Ising's predictions were proven to be incorrect. Despite some attempts to generalise the model, including non-nearest neighbour interactions and variations in spin directions, an explanation for ferromagnetism remained elusive [5]. Ising conjectured that the model was insufficient for describing ferromagnetism, even when considering higher-dimensional spin arrangements.

Ising's work, published in 1925 [6], has gained attention for its unexpected impact, as it revealed a superficial understanding of the profound problems addressed in twentieth-century physics. Although Ising's conclusions were incorrect, the model he proposed encapsulated essential aspects of phase transitions, critical phenomena, and many-body problems. The two-dimensional version of the Ising model was later successfully solved by Lars Onsager [7], while on the three-dimensional lattice remains unsolved. However, continued progress and numerical techniques have shed further light on the problem's structure. Despite its analytical challenges, the Ising model and its variants have found applications in diverse fields such as condensed matter physics, physical chemistry, neuroscience, and the study of complex systems.

Heisenberg provided another model of ferromagnetism based on quantum mechanics a few years following Ising's work, in which the "classical" spins of the Ising model are substituted with electron quantum spins [8]. The Heisenberg model aims to explain ferromagnetism through the interplay of electron spin angular momentum in atoms, whereas the Ising model relied on their magnetic moments. In certain ways, the Ising model is indeed a semi-classical variant of the Heisenberg model, and as such it contradicted recent advances in quantum mechanics. The disparity between the Heisenberg model's tremendous prediction success and the challenge of aligning the Ising model with recent advancements in contemporary physics nearly discredited the model as a good explanation of ferromagnetic materials.

The Ising model [6] is a valuable source of ideas and methods for studying statistical dependences in networks. By definition the Ising model naturally fits the problem of describing pairwise interactions among dichotomic variables. The model is represented on a lattice, with a molecule or atom having a discretised magnetic moment that assumes only two directions with values $+1$ for an upward and -1 for a downward direction at each lattice site i. The spin of a magnetic moment at site i is represented as $\sigma_i = \pm 1$. These spins interact with their neighbours via an interaction potential which may induce alignments of the neighbours. The interaction between neighbouring spins is favourable if the neighbours have the same spin alignment (i.e., both are $+1$ or both are -1), and unfavourable otherwise. The two possible states indicate whether two spins i and j are aligned and thus parallel $(\sigma_i \cdot \sigma_j = +1)$ or antiparallel $(\sigma_i \cdot \sigma_j = -1)$. If the two magnetic moments are aligned, the system is in a state with lower energy otherwise in a state with higher energy. To minimise the energy, the system therefore tends to align all magnetic moments in one direction.

Overview

In the early 1970s, a rigorous analysis of the nature of phase transitions in multi-spin systems lacking the usual spin-reversal symmetry drew a lot of attention because it was discovered that their critical behaviours differed from that of the nearest-neighbour two-spin interacting model [9–11]. The Ising model with three-spin interactions is one of such multi-spin systems that have been considered [11].

In this thesis, the mean-field Ising spin model with three-spin interactions is investigated both for the forward and the inverse problem. Note that lower energy state for the system with three-spin interaction is not an indication of spin alignments, since different spin orientations can lead to the same energy levels. The aim of this thesis is not to argue on the importance of three-spin interactions, but to gain a theoretical understanding of their role in the occurrence of phase separation.

The interest in such a model comes from two large fields of research. The first is condensed matter physics, where the three-spin interaction plays a role in the description of the phase separation phenomena of some magnetic alloys [12] lacking spin-flip symmetry. Those physical systems cannot be described by the sole use of a two-spin interaction, while a three-spin term captures some features of their behaviour [9]. This fact is well paralleled by the Ginibre theorem about functions of spin configurations that are fully classified by an orthonormal base of k-body interactions [13]. Those physical phenomena are well described by statistical mechanics models on regular lattices in finite (d=2,3) dimensions. While some of those models have an exact solution in very special cases [10, 11], it is well known that the mean-field approximation provides an analytically viable setting and a fair description of the phase separation. In those cases, the term mean-field approximation is understood in the sense of a special class of probability measure where the Boltzmann-Gibbs variational principle is optimised: instead of minimising the free energy over all probability measures, one restricts it to product measures on single spins [14, 15].

The other field in which the three-spin (i.e., three-body) interactions came to play a role is that of the applications to complex systems, in particular those of a socio-technical nature where the social network structure with long-range interaction represents a realistic description of the phenomenon and not an approximation of its finite-dimensional version [16–19]. In this case, from a mathematical perspective, the introduction of the three-body interaction entails moving from a graph-theoretical environment of vertices and edges to a richer hypergraph setting where

the three-body terms, representing the faces of the hypergraph, are also taken into account.

The presence of the three-spin interactions brings technical difficulties in the analysis of the model. In particular, the non-convex energy contribution due to the cubic power prevents the use of the Hubbard-Stratonovich transform, which instead is very efficient in the case of quadratic interactions. More precisely, even if the thermodynamic limit of the free energy can be easily computed by large deviation arguments, the fluctuations of the order parameter cannot be analysed with the classical rigorous methods for a mean-field system with pairwise interaction [20–22]. In order to overcome this obstacle we need a fine control on the N-asymptotic behaviour of the partition function that is obtained by a method similar to that recently introduced in [23].

Layout of thesis

The first chapter of the thesis provides some mathematical background to the Ising model with two-spin interaction and an external magnetic field.

The Ising model with three-spin interaction is formally introduced in chapter two. In chapter two, the considered model has three- and two-spin interactions and an external magnetic field. The large N behaviour governing the system, thermodynamic limit of the pressure density, is shown to exist using methods based on large deviations machinery. The equilibrium properties of the system are then investigated by generating phase plots for the order parameter. The phase properties of the model is thoroughly studied using the mean-field approximation theory. Some basic concepts and properties of the model, such as the existence and uniqueness of phase transitions, the properties of the magnetic order parameter and an order parameter with a critical point characterised by critical exponents are analysed in the subsequent chapters 3 and 4.

In chapter three, the equilibrium measure for large volumes is shown to have three pure states in the phases of the model in the absence of an external field. These phases include the two with opposite magnetisation and an unpolarised one with zero magnetisation, merging at the critical point. The Central Limit Theorem is shown to hold for a suitably rescaled magnetisation, while its violation with the typical quartic behaviour appears at the critical point.

In the fourth chapter, the equilibrium and phase properties of the Ising model

with three-spin interaction and an external field are studied. The thermodynamic properties of the model reveals two coexistence curves, signifying two distinct second-order phase transitions, dependent on the domain of the interaction parameter. The critical exponents of the magnetic order parameter are calculated in all directions of the phase space and show their agreement with the mean-field universality class.

Chapter five of this thesis deals with the inverse problem for the Ising model with three-spin interaction where the couplings and bias between particles describing the microscopic interactions are computed from its statistical properties. In this chapter the inverse problem is solved following an analytical approach, i.e., naive mean-field method or method of moments. To compute the couplings and bias, we first obtain analytical formulas for the system's macroscopic variables in the thermodynamic limit where they provide explicit expressions of the parameters. Starting from configuration data generated according to the distribution of the model we reconstruct the free parameters of the system and test the robustness of the inversion procedure both in the region of uniqueness of the solutions and in the region where multiple thermodynamic phases are present.

In chapter six, a multipopulated version of the model introduced in chapter two is studied. Here, the spin particles are partitioned into $r-$blocks and the thermodynamic limit of the pressure density is shown to exist using methods from large deviations. It is shown that the Central Limit Theorem holds for a vector of rescaled block magnetisation when the limiting pressure per particle has unique global maximiser and local multivariate Gaussian fluctuations for the vector of block magnetisation around multiple global maximisers. A bipopulated version of the model is then used as a paradigm to model a complex system made of Human (H) and AI agents. The system is studied analytically using a simple model where two-body and three-body interactions among units are present. The interactions and the relative size α ($0 \leq \alpha \leq 1$) of the two populations are the control parameters that can be changed to drive the system through different phases with transitions of different orders between them. It is shown that for suitable values of the interaction parameters, arbitrarily small values of α may trigger dramatic changes for the system, and the results are interpreted in terms of the Human-AI ecosystem.

Chapter 1

The Ising model

The Ising model was introduced to explain the ferromagnetic behaviour of some types of metals or alloys. These materials, after being exposed to an external magnetic field, develop magnetisation with the same sign as the field. When the field is switched off, the materials show two different behaviours that depend on the temperature at which the magnetisation is induced. If the temperature (T) is below a certain critical value, T_c, the materials retain a certain degree of magnetisation, called spontaneous magnetisation, while at a temperature greater than or equal to the critical value they do not exhibit such property. As the temperature approaches its critical value from below, the spontaneous magnetisation disappears.

Let us consider the finite $d-$dimensional integer lattice $\{d = 2, 3, ...\}$, $\mathbb{Z}^d$, and a finite subset $\Lambda \subset \mathbb{Z}^d$. Let $G = (\Lambda, E)$ be a finite graph such that the spins are located in the vertex-set Λ and the edge-set E represents the set of the links between neighbouring spins which describe their interactions. For each vertex $i \in \Lambda$, a collection of the microstates of the spins is given as $(\sigma_i : i \in \Lambda) = \sigma \in \{-1, 1\}^{|\Lambda|} = \Omega_\Lambda$, where σ is the spin configuration representing the state of the magnetic material.

1.1 The model

The energy of a spin configuration σ on G is defined as the sum of the interactions over all pairs of spins and addition of the interaction of each spin with an external magnetic field:

$$H_G(\sigma) = -\sum_{i,j \in E} J_{i,j}\sigma_i\sigma_j - \sum_{i \in \Lambda} h_i\sigma_i. \tag{1.1}$$

Equation (1.1) is the Hamiltonian of the system for a given spin configuration σ; it is called the nearest neighbour ferromagnetic Ising model if the following choices are made: $J_{i,j} = J > 0$ when $|i - j| = 1$, $J_{i,j} = 0$ if $|i - j| \neq 1$, and $h_i = h \in \mathbb{R}$. In this case, the first sum is over all nearest neighbour pair of spins in Λ which reflects the fact that the interactions vanish at long distances, J measures the interaction strength between neighbouring pair of spins and h is the strength of an applied external magnetic field. The ferromagnetic property of the model is implied by the sign of the interaction strength J such that, minimisation of the Hamiltonian (1.1) in the whole configuration space Λ requires neighbouring spins to align. Note that, by definition of equation (1.1), one can extend the Ising model to incorporate non-nearest neighbour interactions when the constraint on $|i - j| = 1$ is relaxed and anti-ferromagnetic interactions when $J_{i,j} = J$ can be negative.

It is important to note that the Hamiltonian (1.1) can give rise to a rich diversity of behaviours depending on the choice of $J_{i,j}$: ferromagnetism, frustration, glassy systems, etc, of which only the first will be discussed while the others are beyond the scope of this thesis.

A key focus in statistical mechanics is the computation of the probability of a system being in a particular state, given the definition of the Hamiltonian for a specific configuration. The probability measure for each configuration $\sigma \in \Omega_\Lambda$, associated with the Hamiltonian (1.1) in a finite-volume system, is expressed by the Gibbs measure:

$$\mu_G(\sigma) = \frac{\exp(-\beta H_G(\sigma))}{Z_G}, \tag{1.2}$$

where $Z_G = \sum_{\sigma \in \Omega_\Lambda} \exp(-\beta H_G(\sigma))$ is the *normalising constant* on G, also called the *partition function*, $\beta = 1/T > 0$ is the inverse of the temperature. Note that the likelihood of observing a certain configuration depends largely on the external field and the spin orientations. If the strength of an applied external field h is nonzero for a given spin configuration $\tilde{\sigma}$, whose spin orientations are all aligned in the direction of h, then $\tilde{\sigma}$ has the least energy, since $J > 0$. Hence, the probability $\mu_G(\tilde{\sigma})$ is the largest one when compared to those for all other configurations $\sigma \neq \tilde{\sigma} \in \Omega_\Lambda$.

An important observation is that, in the absence of a magnetic field (that is, when $h = 0$), even though local spin alignment is favoured by the Hamiltonian (1.1), neither of the $+1$ or -1 orientations is favoured globally. Namely, if $-\sigma$ denotes the spin-flipped configuration in which $(-\sigma)_i = -\sigma_i$, then $H_G(-\sigma) = H_G(\sigma)$; this implies that $\mu_G(-\sigma) = \mu_G(\sigma)$. The model is then said to be invariant under global spin flip. Whereas, when $h \neq 0$, this symmetry no longer holds.

For any given observable g on Ω_Λ, i.e., $g(\sigma) : \Omega_\Lambda \to \mathbb{R}$, we denote by $\langle g(\sigma) \rangle$ its average value with respect to the measure (1.2) as:

$$\langle g(\sigma) \rangle_G = \frac{\sum_{\sigma \in \Omega_\Lambda} g(\sigma) e^{-\beta H_G(\sigma)}}{Z_G}. \tag{1.3}$$

The normalising factor Z_G plays a crucial role in computing the *Gibbs free energy*, which is the *generating functional* of the moments of (1.2) via suitable derivatives of:

$$F_G = -\frac{1}{\beta} \log Z_G \tag{1.4}$$

and its thermodynamic limit defined as,

$$f_G = -\frac{1}{\beta} \lim_{\Lambda \uparrow \mathbb{Z}^d} \frac{1}{|\Lambda|} \log Z_G, \tag{1.5}$$

provided it exists. A quantity of central importance is the *magnetisation density* or *magnetic order parameter* for a given configuration $\sigma \in \Omega_\Lambda$, which provides information about the balance between the two spin values of the system. The magnetic order parameter is defined as:

$$m_\Lambda(\sigma) = \frac{1}{|\Lambda|} M_\Lambda \tag{1.6}$$

where $M_\Lambda = \sum_{i \in \Lambda} \sigma_i$ is the *total magnetisation*. Notice that, once equation (1.4) is computed, the Gibbs state of m_Λ can be obtained as

$$\langle m_\Lambda \rangle_G = \frac{\partial F_G}{\partial h} \tag{1.7}$$

and in the thermodynamic limit, the average magnetisation density (1.7), is given by

$$m(\beta J, \beta h) = \lim_{\Lambda \uparrow \mathbb{Z}^d} \langle m_\Lambda \rangle_G = \frac{\partial f_G}{\partial h}. \tag{1.8}$$

As it has already been pointed out, the Gibbs distribution is invariant under a global spin-flip when $h = 0$. Hence, as a consequence and by symmetry, $\langle m_\Lambda \rangle = 0$, and $m(\beta J, 0) = \lim_{\Lambda \uparrow \mathbb{Z}^d} \langle m_\Lambda \rangle = 0$ for all temperatures.

Let's consider the behaviour of the system when $\beta \downarrow 0$ (*infinite temperature*) and $\beta \uparrow \infty$ (*zero temperature*). In the limit as $\beta \to 0$, the Gibbs distribution converges to a uniform distribution on Ω_Λ for all spin configurations $\sigma \in \Omega_\Lambda$. In this case, M_Λ becomes the sum of independent and identically distributed random variables. On the other hand, when $\beta \uparrow \infty$, the Gibbs distribution concentrates on those configurations that minimise the Hamiltonian, the so-called *ground states*

and different behaviours appear depending on the value of β. The ground states of the model, can easily be identified as the configuration having all of its spins equal $+1$ or -1. This gives exactly two ground states, namely, $\sigma^+ \in \Omega_\Lambda$ and $\sigma^- \in \Omega_\Lambda$, where σ^+ represents a configuration with all of its spins pointing up (i.e., $\sigma_i = +1$ for all i) and σ^- represents a configuration with all the spins pointing down (i.e., $\sigma_i = -1$ for all i). Therefore, due to the invariant property of the Gibbs measure, it's easy to verify that:

$$\lim_{\beta \uparrow \infty} \mu_G(\sigma; h = 0) = \begin{cases} \frac{1}{2}, & \text{if} \quad \sigma \in \{\sigma^+, \sigma^-\} \\ 0, & \text{otherwise} \end{cases} . \tag{1.9}$$

This implies that, with equal probability the system has higher chance of getting *frozen* in one of the two ground states in the limit of very low temperatures (T). In this case, there exists a global order in the system called *spontaneous magnetisation*, given that the majority of the spins have the same sign. Hence, we say that the symmetry under a global spin flip is *spontaneously broken*, since configurations belonging to one of the two is favoured.

Now, let's discuss the behaviour of the system when $0 < \beta < \infty$. If $\beta > 0$ and finite, there exists a critical value β_c such that for all $\beta < \beta_c$, $m(\beta J, \beta h) \to 0$ as $h \to 0^+$. On the other hand, if $\beta > \beta_c$ and $h \to 0^+$, then $m(\beta J, \beta h)$ converges to a positive number, while when $h \to 0^-$ it converges to a negative number [20].

If β is sufficiently small (i.e., in the high temperature regime), the interaction is not strong enough to produce any order, and the limiting Gibbs measure is uniquely determined. In contrast, when β is sufficiently large (in the low-temperature regime), the interaction becomes so strong that a long-range order appears: the bias towards neighbour pairs of aligned spins then implies that the Gibbs measure prefers configurations with either a vast majority of plus spins or a vast majority of minus spins, and this preference even survives in the infinite volume limit. We say that the system thus undergoes a phase transition and a spontaneous magnetisation has occur.

1.2 The mean-field Ising model

This section explores a simplified version of the Ising model discussed earlier using mean-field theory. By imposing this mean-field assumption, we can derive a simplified version of the Ising model known as the Curie-Weiss model. In this

approximation, the interactions between spins are no longer explicitly dependent on their neighbours but are instead replaced by an effective mean interaction parameter. While this simplification may not capture all the intricacies of the original Ising model, it still provides valuable insights into the system's behaviour observed at high and low temperatures, especially in relation to phase transitions. At high temperatures, the spins tend to be more disordered, resulting in a paramagnetic phase. On the other hand, at low temperatures, the spins tend to align, leading to a ferromagnetic phase. These different phases are characterised by distinct thermodynamic properties, which can be analysed using the concepts of free energy or pressure density.

Let us now explore an intuitive rationale of the mean-field approximation. Consider an Ising spin system with $\sigma_i = \pm 1$ as described by (1.1) on $\mathbb{Z}^d$. The first term in (1.1) represents the energy contribution arising from the interaction between the spin σ_i (where $i \in \Lambda$) and its neighbouring spins on the lattice. Now, the contribution of a single spin σ_i can be expressed as follows [24]:

$$-J \sum_{j:j\sim i} \sigma_i \sigma_j = -2dJ\sigma_i \left(\frac{1}{2d} \sum_{j:|i-j|=1} \sigma_j \right) \qquad (1.10)$$

where $j \sim i$ denotes the sum over all nearest neighbour spins and the $2d$ is the number of nearest neighbour spins of spin σ_i. It is evident that the contribution of a given spin to the total energy of the system relies on the interaction of σ_i, $i \in \Lambda$, and the local magnetisation density, represented by the average of its $2d$ nearest neighbours: $\frac{1}{2d} \sum_{j:j\sim i} \sigma_j$. Notably, the nearest neighbour interaction is replaced by a local magnetisation density, which varies from one point to another within the lattice. The mean-field approximation involves making an extreme assumption about the nature of interactions in the following manner: each spin variable interacts with every other spin at any site of the lattice, regardless of their distance, and each local magnetisation can be approximated by a global one. Consequently, the specific structure of the lattice becomes irrelevant, and the sole crucial factor is the number of spins, represented by a positive integer N. Thus, we may simplify our notation by taking $\Lambda \equiv \{1, \ldots, N\}$, and the configuration space becomes $\Omega_N = \{-1, +1\}^N$. Therefore, the mean-field Ising model, also known as the Curie-Weiss model, is defined as:

Definition 1.2.1. *The Hamiltonian of the Curie–Weiss model for any configuration*

of spins $\sigma = (\sigma_i)_{i \leq N} \in \{-1, +1\}^N = \Omega_N$, can be defined as:

$$H_N(\sigma) = -\frac{J}{2N} \sum_{i,j=1}^{N} \sigma_i \sigma_j - h \sum_{i=1}^{N} \sigma_i. \tag{1.11}$$

The resulting system can be characterised as a spin model residing on a complete graph comprising N vertices, where every pair of distinct vertices is interconnected by an edge. The model is defined by a constant coupling parameter $J > 0$ and an external magnetic field parameter $h \in \mathbb{R}$. It is noteworthy that the Hamiltonian (1.11) exhibits invariance under spin flip $(\sigma \to -\sigma)$ for transformation of $h \to -h$.

The primary observable of this system, known as the magnetisation density, is expressed as:

$$m_N(\sigma) = \frac{1}{N} \sum_{i=1}^{N} \sigma_i \tag{1.12}$$

and as a consequence, (1.11) becomes

$$H_N(\sigma) = -N \left(\frac{J}{2} m_N^2(\sigma) + h m_N(\sigma) \right). \tag{1.13}$$

Here, the mean-field model is expressed in terms of the magnetisation density, and it involves a quadratic term and a linear term that depends on the values of J, h, and $m_N(\sigma)$. For any configuration $\sigma \in \Omega_N$, the Gibbs distribution associated to it can be written as:

$$\mu_N(\sigma) = \frac{\exp(-\beta H_N(\sigma))}{Z_N} \tag{1.14}$$

and

$$Z_N = \sum_{\sigma \in \Omega_N} e^{-\beta H_N(\sigma)} \tag{1.15}$$

is the normalisation factor also called the *partition function* and β is the usual inverse temperature. Let us now examine the Hamiltonain (1.13) in the absence of the external field $h = 0$. Notably, due to the invariance property of the Hamiltonian (1.11) under global spin flip for $h = 0$, the magnetisation density exhibits a symmetric distribution, specifically, $\mu_N(m_N(-\sigma) = -m) = \mu_N(m_N(\sigma) = m)$, leading to the particular case of $\langle m_N \rangle = 0$. As previously discussed for the Ising model on G, when βJ is small, it is expected that the spins would be essentially independent. However, when βJ is large, the most probable configurations would involve most spins having the same orientation, effectively approaching one of the two ground states where all spins are equal. To be more precise, there exists a critical point J_c

of βJ such that, when $\beta J < J_c$, the magnetisation density $m_N(\sigma)$ is approximately 0 (zero) with high probability, whereas if $\beta J > J_c$, the following condition holds:

$$m_N(\sigma) \simeq \begin{cases} +m & \text{with probability close to } 1/2, \\ -m & \text{with probability close to } 1/2 \end{cases}.$$

It is important to observe that as N tends to infinity, the limiting distribution of the magnetisation is as follows:

$$\lim_{N \to \infty} \mu_N(m_N(\sigma)) \begin{cases} \delta_0 & \text{if } \beta J < J_c, \\ \frac{1}{2}(\delta_{+m} + \delta_{-m}) & \text{if } \beta J > J_c \end{cases}. \qquad (1.16)$$

Here, δ_m represents a Dirac probability measure on the interval $[-1, 1]$. Notably, for large N and $\beta J > J_c$, this implies that the typical magnetisation values observed during configuration sampling are close to either $+m$ or $-m$. However, it is crucial to reiterate that this fact does not contradict the overall average magnetisation being zero when $h = 0$, i.e., $\langle m_N \rangle = 0$.

Moving forward, we consider β to be absorbed by the parameters J and h, and we simply write $\beta J = J$ and $\beta h = h$. The focus now shifts to the thermodynamic properties of the model, which are dictated by the large N behaviour of the pressure per particle. The pressure per particle, denoted as p_N, represents, up to a negative multiplicative factor, the specific Gibbs free energy per site of the system when $\beta = 1$ and is defined as:

$$p_N = \frac{1}{N} \log Z_N. \qquad (1.17)$$

Notice that, by the use of mean-field approximation, we can characterise the macroscopic behaviour of the physical system through the magnetisation density $m_N(\sigma)$. The goal is to find an explicit expression of (1.17) in terms of the order parameter, the magnetisation density, and then we impose at the same time a minimisation of the energy and a maximisation of the entropy. This endeavor typically leads to a self-consistency equation, also known as the mean-field equation, which allows us to study the phase properties the system. In this context, the self-consistency equation serves to determine the equilibrium magnetisation.

Note that the exisitence of thermodynamic limit for (1.17):

$$p := \lim_{N \to \infty} p_N \qquad (1.18)$$

can be shown by a straightforward application of Varadhan's integral lemma [20, 25, 26] which we will not illustrate here. The limiting pressure per particle (1.18) satisfies a one dimensional variational problem:

Definition 1.2.2. *For any $m \in [-1, 1]$, let $\phi(m) = U(m) - I(m)$ such that,*

$$U(m) = \frac{J}{2}m^2 + hm$$

is the energy contribution coming from (1.11) and

$$I(m) = \frac{1-m}{2} \log\left(\frac{1-m}{2}\right) + \frac{1+m}{2} \log\left(\frac{1+m}{2}\right)$$

is the binary entropy, expressing the logarithmic number of ways m can be obtained from $\sigma \in \Omega_N$. Then the limiting pressure per particle has the following variational representation:

$$p = \sup_m \phi(m). \tag{1.19}$$

Proofs of the preceding results can be achieved using various methods (see [20, 25, 26], wherein the results are derived through the machinery of large deviations). Interested readers can find a comprehensive analysis of the thermodynamic limit of the Gibbs measure in them.

Another approach, known as Guerra's interpolation method, can be utilised to demonstrate the existence of thermodynamic limit of the pressure per particle [27, 28]. The fundamental concept is to compare the pressure per particle of a large system comprising N spin sites with two independent subsystems, each composed of N_1 and N_2 sites, respectively, where $N_1 + N_2 = N$. It has been demonstrated by Ruelle [29], that if one can establish that the pressure function is sub-extensive, or possibly super-extensive, with an essential condition that it remains stable and does not oscillate, and that it is bounded, then, by Fekete Lemma, the sequence $F_N, F_{N+1}, ..., F_\infty$ must converge.

Now, from Definition 1.2.2 notice that $U(m)$ and $I(m)$ are both convex, but $\phi(m)$ is not always convex for some fixed values of J and h and its supremum can be obtained following the stationarity condition:

$$\frac{\partial}{\partial m}\phi(m)|_{\overline{m}} = J\overline{m} + h - \left[\frac{1}{2} \log\left(\frac{1+\overline{m}}{1-\overline{m}}\right)\right] = 0. \tag{1.20}$$

From the above equation, we have that

$$\overline{m} = \tanh(J\overline{m} + h). \tag{1.21}$$

Here, $\overline{m}$, is called the magnetic order parameter, and (1.21) is the self-consistency equation also known as the mean-field equation. Therefore, for fixed J and h,

$$p(\overline{m}; J, h) = \frac{J}{2}\overline{m}^2 + h\overline{m} - \left[\frac{1-\overline{m}}{2} \log\left(\frac{1-\overline{m}}{2}\right) + \frac{1+\overline{m}}{2} \log\left(\frac{1+\overline{m}}{2}\right)\right]. \tag{1.22}$$

The investigation of the limiting pressure per particle commences with an examination of its behaviour with respect to the coupling strength (J) and subsequently applies it to analyse the magnetic order parameter's typical behaviour. Figure 1.1
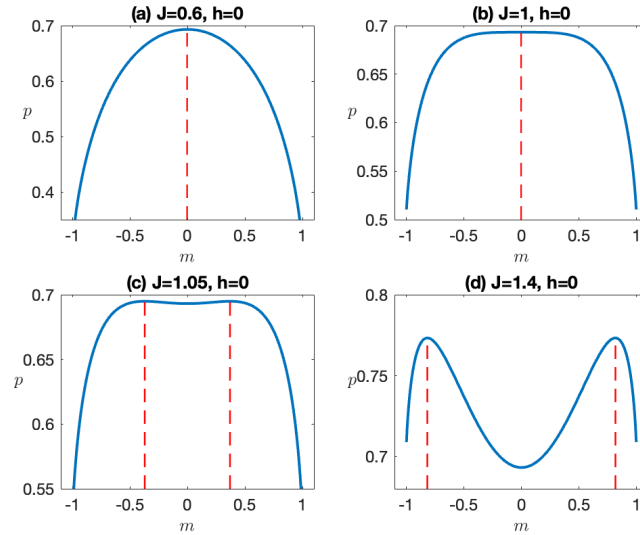
Figure 1.1: Pressure per particle p, of the system as a function of the magnetic order parameter $\overline{m}$, with $h = 0$ and varrying J.

illustrates the case of no applied magnetic field, $h = 0$, starting at high temperature, i.e., J is small. The pressure per particle as a function of m resembles a downward-pointing parabola with its maximum at $m = 0$, as depicted in Figure 1.1 (a). As temperature decreases, i.e., by increasing the value of J, the curve around $m = 0$ becomes flatter. At a critical value of $J = J_c = 1$, as shown in Figure 1.1 (b), the maximum becomes so flat that the second derivative approaches zero. Consequently, the curve transforms from a parabolic shape to that of a fourth-order function. Further decreasing the temperature leads to the splitting of the single maximum at $m = 0$ into two maxima at small positive and negative values of m, as depicted in Figure 1.1 (c). As the temperature continues to decrease, the maxima move outward and eventually approach ± 1, as shown in Figure 1.1 (d).

An important observation here is that at high temperature, the system tends to adopt a state with no magnetic order, i.e., $m = 0$, due to the favouring effect of entropy. Conversely, at low temperature, the system tends to take on a state with some magnetic order (m). In the absence of an external magnetic field, the system has no preference for the direction of the magnetic order (up or down),

and thus randomly selects one of the maxima with either positive or negative m. This low-temperature state with spontaneous magnetic order, not induced by an external field, is referred to as the ferromagnetic phase. On the other hand, the high-temperature state without spontaneous magnetic order is called the paramagnetic phase. The transition from the paramagnetic to the ferromagnetic phase at a specific temperature signifies a phase transition.

Another significant observation is the point of symmetry: the high-temperature paramagnetic phase exhibits symmetry between up and down directions, with no preference for either. However, in the low-temperature ferromagnetic phase, this symmetry is broken, and the system randomly selects one direction or the other. This spontaneous random selection is termed *spontaneous symmetry breaking*. Importantly, the high-temperature state possesses more symmetry and is disordered, while the low-temperature state has less symmetry and is more ordered. In this context, order denotes the absence of symmetry; it signifies broken symmetry.

The behaviour of the magnetic order parameter (1.21) for $h = 0$ can be described by Figure 1.2 below.
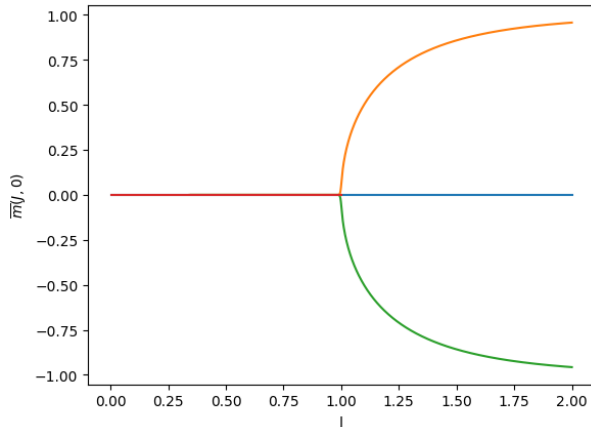
Figure 1.2: Magnetic order parameter, $\overline{m}$, as a function of J at $h = 0$.

The curves in Figure 1.2 represent all the solutions of (1.21). The orange curve corresponds to the positively polarised stable phase, the green curve is the negatively polarised stable phase, the red curve denotes the paramagnetic phase above which the symmetry is broken and the blue curve is an unstable phase of the system (see Figure 1.1 for comparison). The red, orange and green curves are the ones that realise the supremum of the variational principle (1.19). The magnetic order parameter exhibits continuity with respect to J, leading to the classification of

the critical phenomenon as a continuous phase transition or a second-order phase transition. The term "second-order phase transition" arises from the discontinuity's impact on the fluctuations of the magnetisation, which diverge at J_c.

Now, let's examine the behaviour of the pressure per particle and its maximiser(s) in the presence of a very small applied magnetic field (h) as depicted in Figure 1.3 and Figure 1.4. It becomes evident that with the magnetic field h present,
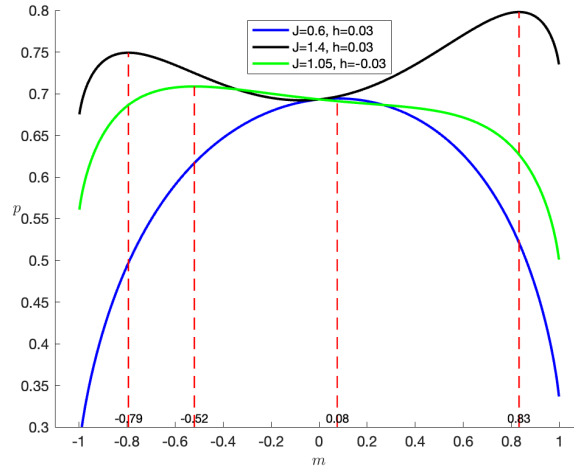
Figure 1.3: Pressure per particle p as a function of the magnetic order parameter $\overline{m}$, for fixed h and J.

the free energy has its global maximum with the same sign as h. This behaviour is also evident in Figure 1.4 where the magnetic order exhibits the same sign as h, while varying J.

The occurrence of a phase transition is a result of two competing effects. The first one tends to minimise the energy contribution and to introduce order in the system by aligning the spins, i.e., $m \to \pm 1$. On the other hand, the second effect aims to maximise entropy, driving the system towards a configuration with random spins and zero magnetic order. The balance between these opposing requirements leads the system to undergo a critical behaviour as $J \to 1$, which we will describe in terms of the critical exponent of $\overline{m}$.

Notice that, when $J \leq 1$ and $h = 0$, the only solution for $\overline{m}$ in (1.21) is $\overline{m} = 0$. However, when $J > 1$, $\overline{m}$ has a unique solution $m^* > 0$. Our interest now lies in understanding the critical behaviour of (1.21) in the absence of a magnetic field as $J \to 1$. Notice that the value of m^* approaches 0 as $J \to 1$ from the left. As a result, the hyperbolic tangent term in equation (1.21) with $h = 0$ can be approximated
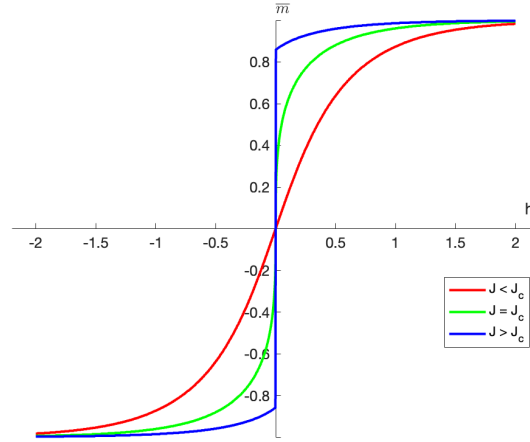
Figure 1.4: Magnetic order parameter $\overline{m}$ of the system as a function of h for fixed J. For the red curve (i.e., $J < J_c$), the magnetic order parameter is a continuous function of the external field h, while in the blue curve (i.e., $J > J_c$) it is discontinuous and has a jump.

using Taylor's expansion as follows:

$$m^* = Jm^* - \frac{J^3 m^{*3}}{3} + J^3 m^{*3} o(Jm^*) \tag{1.23}$$

where $o(Jm^*) \to 0$ and $m^* \to 0$. A direct computation shows that

$$m^*(J) \sim \sqrt{\frac{3(J-1)}{J^3}} \quad \text{as} \quad J \to 1^+. \tag{1.24}$$

Chapter 2

The three-spin Ising model

This chapter introduces the Ising model with three-spin interactions and explores some of its equilibrium properties. Unlike the two-spin model, lower energy states in the three-spin model do not necessarily indicate spin alignments, as different spin orientations can give the same energy levels due to the presence of the three. Applying large deviations techniques, we obtain the limiting pressure associated with the system, revealing the presence of phase transitions in a system that lacks the conventional spin-reversal symmetry. Notably, the infinite-volume properties of the three-spin model exhibit novel phenomena that are absent in the two-spin mean-field case. Additionally, we consider the three-spin model as a lattice gas model and compute its equilibrium state.

2.1 The cubic mean-field Ising model

Consider a system of N interacting spins with an internal degree of freedom $\sigma_i = \{-1, +1\}$ which represents the possible state of a spin. Define the Hamiltonian of the system by,

$$H_N(\sigma) = -\sum_{\langle i,j,k \rangle} K_{i,j,k} \sigma_i \sigma_j \sigma_k - \sum_{\langle i,j \rangle} J_{i,j} \sigma_i \sigma_j - \sum_i h_i \sigma_i, \qquad (2.1)$$

where $\sigma \in \{-1, +1\}^N = \Omega_N$ is a configuration of the system. The first term in the Hamiltonian captures the modulation of interactions between triplets of spins, while the second term the modulation of interaction between pairs of spins and the third term represents the effect of an applied magnetic field on each spin. The parameters $K_{i,j,k}, J_{i,j}$ are families of real parameters that tune the interactions among triples and pair of spins respectively while h_i is also a real parameter representing an

external field acting on each spin. To simplify the model, we assume isotropic interactions and fields and apply the mean-field approximation. This allows us to set $K_{ijk} = K/3N^2$, $J_{i,j} = J/2N$ and $h_i = h$ in the Hamiltonian, where K, J and h are real numbers representing the strength of interaction between spins and the external magnetic field, respectively. The factors $1/3N^2$ and $1/2N$ of the interaction strength accounts for the triple and double counting of interactions between spins over the sum in (2.1) respectively, and ensure that the Hamiltonian is linear in N.

Observe that the Hamiltonian (2.1) is particularly interesting as an example of a spin system lacking the usual spin-up and spin-down reversal symmetry. For a given spin configuration $\sigma \in \Omega_N$, the observable of interest, namely the magnetisation per particle, is defined as:

$$m_N(\sigma) = \frac{1}{N}\sum_{i=1}^{N}\sigma_i, \qquad m_N \in [-1,1]. \tag{2.2}$$

Now, substituting the expression for magnetisation into (2.1), we obtain:

$$\begin{aligned}
H_N(\sigma) &= -\frac{K}{3N^2}\sum_{i,j,k=1}^{N}\sigma_i\sigma_j\sigma_k - \frac{J}{2N}\sum_{i,j=1}^{N}\sigma_i\sigma_j - h\sum_{i=1}^{N}\sigma_i \\
&= -N\bigg(\underbrace{\frac{K}{3}m_N^3(\sigma) + \frac{J}{2}m_N^2(\sigma) + hm_N(\sigma)}_{=U_N}\bigg).
\end{aligned} \tag{2.3}$$

Here, the mean-field model is expressed in terms of the magnetisation per particle, and it involves cubic and quadratic terms and a linear term that depend on the values of K, J, h, and $m_N(\sigma)$.

The Boltzmann-Gibbs state on a configuration σ is given by

$$\mu_N^{KJh}(\sigma) = \frac{e^{-H_N(\sigma)}}{Z_N}\prod_{i=1}^{N}d\rho(\sigma_i), \tag{2.4}$$

where $Z_N = \sum_{\tilde{\sigma}\in\Omega_N}e^{-H_N(\tilde{\sigma})}\prod_{i=1}^{N}d\rho(\tilde{\sigma}_i) = \int_{\mathbb{R}}e^{-NU_N(m_N)}Q_N(m)$ is the partition function of the system, ρ is the distribution of a single spin such that: $\rho(a) = 1/2(\delta_{a-1} + \delta_{a+1})$ and $a \in \{-1, +1\}$ and the measure Q_N is the law of the empirical mean m_N under the Gibbs measure (2.4) denoting the product probability measure of single spins. For a given observable $g(\sigma)$ the Boltzmann-Gibbs expectation $\omega_N(g(\sigma))$ is defined as follows:

$$\omega_N(g(\sigma)) = \frac{\sum_{\sigma\in\Omega_N}g(\sigma)e^{-H_N(\sigma)}}{Z_N} \tag{2.5}$$

and the moment generational function, i.e., pressure per particle, associated with the system is defined as:

$$p_N = \frac{1}{N} \log Z_N \ . \tag{2.6}$$

The pressure per particle p_N defined here, coincide up to a multiplicative factor with the free energy and its thermodynamic limit $p = \lim_{N \to \infty} p_N$ exists.

2.2 Existence of thermodynamic limit

To prove the existence of thermodynamic limit of p_N and study its properties, the standard Gaussian transformation, i.e., the Hubbard-Stratonovich transform, fails due to the non-convex nature of (2.3). Notwithstanding, methods from large deviation theory using extreme value distributions (i.e., tail estimation) and combinatorial methods which relies on Stirling's approximation to compute a bound on the pressure per particle. The Varadhan's integral lemma [20, 25, 26] also as a large deviation machinery can be used to verify the existence of thermodynamic limit of (2.6).

2.2.1 Large deviations techniques

Large deviation theory explains how, on an exponential scale, the likelihood of a very rare event decaying to zero is characterized. To be more precise, large deviations are formally defined as follows [25, 26]:

Definition 2.2.1. *Let $\{\mu_\epsilon\}$ be a family of probability measures defined on $(\chi, \mathcal{B})$ for a sequence of positive numbers $\{\epsilon \to 0\}$, where χ is a topological space and $\mathcal{B}(\chi)$ a Borel σ-field of χ. $\{\mu_\epsilon\}$ satisfy a large deviation principle (LDP) with a rate function I that is lower semicontinuous, $I : \mathcal{X} \to [0, \infty]$, and has compact level sets such that the following holds:*

$$- \inf_{x \in T} I(x) \leq \liminf_{\epsilon \to 0} \epsilon \log \mu_\epsilon(T) \leq \limsup_{\epsilon \to 0} \epsilon \log \mu_\epsilon(R) \leq - \inf_{x \in R} I(x)$$

for each open set T and closed set R in χ.

Observe that (2.3) is a representation of (2.1) in its macroscopic state due to the introduction of the magnetisation density $m_N(\sigma)$ for a given configuration σ. In this case, computing μ_N^{KJh} for a given configuration with $m_N(\sigma) = m \in [-1, 1]$ involves finding the number of such configurations that share the same value of

m. This is a consequence of the fact that different microstates (i.e., orientations of the spins) can produce the same macroscopic behaviour (i.e., $m_N(\sigma)$) and that μ_N^{KJh} assigns equal probability to configurations that have the same magnetisation density.

Remark 2.2.2. *The normalising constant, Z_N, in (2.4) can be written as:*

$$Z_N = \sum_{m \in S_m} A_N(m)e^{-H_N(\sigma)} \tag{2.7}$$

where $S_m = \{-1 + \frac{2k}{N}, k = 0, \ldots, N\}$ is the spectrum of the magnetisation and $A_N(m) = \text{card}\{\sigma \in \{-1, 1\}^N : m_N(\sigma) = m\}$ is a count of all microscopic configuration of the spins sharing the same magentisation.

From the definition of $A_N(m)$ one can compute a bound on it to obtain a closed form of the normalising constant and use it to prove the existence of thermodynamic limit of the pressure density describing the asymptotic properties of the system. To achieve this we employ the same argument of Talagrand [30]:

Lemma 2.2.1. *Let $\Omega_N = \{+1, -1\}^N$ denote the set of all possible configurations of σ. Then for $A_N(m) \in \mathbb{N}$ the following inequalities hold:*

$$\frac{1}{L\sqrt{N}}e^{-NI(m)} \leq A_N(m) \leq e^{-NI(m)}$$

where L is a universal constant and,

$$I(m) = \frac{1-m}{2}\log\left(\frac{1-m}{2}\right) + \frac{1+m}{2}\log\left(\frac{1+m}{2}\right).$$

Proof. Using that $\mu_N^{KJh}(\sigma)$ assigns equal probability to configurations having the same $m_N(\sigma)$, to obtain the number of such configurations becomes a combinatorial problem such that:

$$A_N = \binom{N}{\frac{N(1+m)}{2}} = \frac{N!}{\left(\frac{N(1+m)}{2}\right)!\left(\frac{N(1-m)}{2}\right)!} \tag{2.8}$$

where $\frac{N(1+m)}{2}$ corresponds to the number of spins with $+1$ orientation and $\frac{N(1-m)}{2}$ the number of spins with -1 orientation.

To obtain the lower bound of A_N, we consider the case when $N(1 + m)$ is even and apply Stirling's formula. Using Stirling's approximation of a factorial,

$N! = N^N e^{-N} \sqrt{2\pi N}(1 + \mathcal{O}(1/N))$, we have that:

$$\binom{N}{\frac{N(1+m)}{2}} = \frac{N!}{\left(\frac{N(1+m)}{2}\right)! \left(\frac{N(1-m)}{2}\right)!}$$

$$= \frac{N^N \sqrt{2}}{\left[\left(\frac{N(1+m)}{2}\right)^{\left(\frac{N(1+m)}{2}\right)} \left(\frac{N(1-m)}{2}\right)^{\left(\frac{N(1-m)}{2}\right)} \sqrt{\pi N(1-m^2)}\right]} \cdot (1 + \mathcal{O}(N^{-1}))$$

$$= \sqrt{\frac{2}{\pi N(1-m^2)}} \cdot$$

$$\cdot \frac{1}{\exp \ln \left[\left(\frac{(1+m)}{2}\right)^{\left(\frac{N(1+m)}{2}\right)} \left(\frac{(1-m)}{2}\right)^{\left(\frac{N(1-m)}{2}\right)}\right]} \cdot (1 + \mathcal{O}(N^{-1}))$$

$$= \sqrt{\frac{2}{\pi N(1-m^2)}} \cdot$$

$$\cdot \exp\left(-N \underbrace{\left(\frac{1-m}{2} \ln\left(\frac{1-m}{2}\right) + \frac{1+m}{2} \ln\left(\frac{1+m}{2}\right)\right)}_{=I(m)}\right) \cdot (1 + \mathcal{O}(N^{-1})).$$

The lower bound follows from the last equality.

Let's suppose that the spins σ_i are independent such that $\mu_N^{KJh}(\sigma_i = +1) = \mu_N^{KJh}(\sigma_i = -1) = 1/2$. Then the upper bound of A_N can be obtained using tail estimation. Observe that, if σ_i are independent for all $i = 1, ..., N$, then all configurations of Ω_N, have equal probability of having a magnetisation m and thus,

$$A_N = 2^N \mu_N^{KJh}(m_N(\sigma) = m) \leq 2^N \mu_N^{KJh}\left(\sum_{i=1}^N \sigma_i \geq Nm\right).$$

The last inequality above follows from the definition of $m_N(\sigma)$ and leads to a tail estimation, since σ_i is a random variable assumed to be independent and distributed with equal probability for both -1 and $+1$ spins (i.e., $\rho = 1/2(\delta_{x-1} + \delta_{x+1})$). Therefore, for any $\lambda > 0$,

$$\mu_N^{KJh}\left(\sum_{i=1}^N \sigma_i \geq Nm\right) \leq \exp\left(-\lambda mN\right) \prod_{i=1}^N \mathbb{E}_\rho \exp\left(\lambda \sigma_i\right) \qquad (2.9)$$

$$= \exp\left(N(-\lambda m + \ln \cosh\left(\lambda\right))\right).$$

Optimising over all λ, we obtain that

$$\lambda = \operatorname{arctanh}(m) = \frac{1}{2} \ln\left(\frac{1+m}{1-m}\right)$$

and it follows that since $1/\cosh^2(y) = 1 - \tanh^2(y)$, then $\ln\cosh(\lambda) = -1/2\ln(1 - m^2)$. Substituting this observation into (2.9), we have that

$$A_N \leq \exp(-NI(m)).$$

$I(m)$ is the entropy associated to m. It quantifies the disorder in the system for a given configuration σ. Notice that the results obtained here gives a large deviations approximation of the Gibbs measure for the event $m_N(\sigma) = m$. $\qquad \square$

Using the result of Lemma 2.2.1, we can obtain a bound on the normalising constant. Notice that the sum over the spectrum S_m of the partition function has $N + 1$ terms. Since we are interested in behaviour of the system in the exponential scale, we keep only the dominating terms [24, 30];

$$\frac{1}{L}\frac{1}{\sqrt{N}}\exp\left(N\left(\max_{m\in[-1,1]}f(m)\right)\right) \leq Z_N \leq (N+1)\exp\left(N\left(\max_{m\in[-1,1]}f(m)\right)\right) \tag{2.10}$$

where,

$$f(m) = \frac{K}{3}m^3 + \frac{J}{2}m^2 + hm - I(m)$$

and $I(m)$ is the entropy associated to m.

Now with the expanded form of the normalising constant, the existence of thermodynamic limit of the pressure per particle governing the asymptotic behaviour of the system follows:

$$-\frac{1}{N}\left(\ln L + \frac{1}{2}\ln N\right) + \max_{m\in[-1,1]}f(m) \leq p_N \leq \frac{1}{N}\ln(N+1) + \max_{m\in[-1,1]}f(m)$$

and

$$p = \lim_{N\to\infty}p_N = \max_{m\in[-1,1]}f(m).$$

Hence

$$p = \max_{m\in[-1,1]}\left\{\frac{K}{3}m^3 + \frac{J}{2}m^2 + hm - I(m)\right\}. \tag{2.11}$$

Notice from (2.11) that, p simply describes the asymptotic behaviour of the partition function Z_N, which indicates its growth or decay depending on the sign of the maximiser.

Varadhan's integral lemma

The Varadhan's integral lemma studied in Theorem II.7.1 of [20], Theorem 4.3.1 of [25] and Theorem 5 of [26] will be used to assess the variational formula for the

pressure per particle obtained in (2.11). In the sequel we will use the following notation: let $\mathcal{X} = [-1, 1] \subset \mathbb{R}$ be a compact space such that $m_N(\sigma) \in \mathcal{X}$. Further, for every positive integer N, we define the map $U_N : \mathcal{X} \to \mathbb{R}$ as:

$$U_N(m_N) = \frac{K}{3} m_N^3(\sigma) + \frac{J}{2} m_N^2(\sigma) + h m_N(\sigma). \qquad (2.12)$$

Notice that U_N for all N is uniformly bounded by the sum of the absolute values of $|\frac{K}{3} + \frac{J}{2} + h|$. Now, observe that since $\mathcal{X}$ is a closed and bounded, i.e., compact, subset of $\mathbb{R}$ and $m_N \mapsto U_N(m_N)$ is continuous for every N, it follows that the function U_N is equicontinuous. This is because U_N is defined for all values of N on the map $m_N \mapsto U_N(m_N)$ (see Theorems 7.13 and 7.24 of [31]). Again, suppose that m_N converge to $m \in [-1, 1]$, as $N \to \infty$, then it follows from Theorem 7.25 of [31], that $U_N \to U$ uniformly:

$$
\begin{aligned}
U(m) &= \frac{K}{3} m^3 + \frac{J}{2} m^2 + hm \\
&= \lim_{N \to \infty} U_N(m_N).
\end{aligned}
\qquad (2.13)
$$

Recall from (2.4) that

$$Z_N = \int_{\mathcal{X}} e^{-N U_N(m_N)} Q_N(m)$$

is the partition function of the system and the measure Q_N is the law of the empirical mean m_N under the Gibbs measure (2.4). Here, Q_N represents the product probability measure of the spins and has a large deviation property with a sequence of positive numbers $\{a_N : N = 1, 2, ...\}$ which tends to ∞ and a good rate function $I : \mathcal{X} \to [0, \infty]$ [26] following the results obtained from Lemma 2.2.1.

The interest is to show that the pressure per particle associated to Hamiltonian (2.3) admits a thermodynamic limit. This limiting behaviour is given by the following proposition:

Proposition 2.2.1. *For choices of the parameters K, J and h the limiting pressure admits the following variational representation:*

$$p(K, J, h) := \lim_{N \to \infty} p_N = \sup_{m \in [-1, 1]} \Phi(m), \qquad (2.14)$$

where $\Phi(m) = U(m) - I(m)$ with

$$U(m) = \frac{K}{3} m^3 + \frac{J}{2} m^2 + hm \qquad (2.15)$$

is the energy contribution and

$$I(m) = \frac{1-m}{2} \log\left(\frac{1-m}{2}\right) + \frac{1+m}{2} \log\left(\frac{1+m}{2}\right) \qquad (2.16)$$

is the binary entropy contribution.

The following theorem leads to the results of Proposition 2.2.1 which is taken from Theorem II.7.1 of [20], signifying the leading order asymptotic behaviour of the partition function (2.6):

Theorem 2.2.3. *Let $\mathcal{X}$ be a complete separable metric space, $\mathcal{B}(\mathcal{X})$ the Borel σ-field of $\mathcal{X}$, and $\{Q_N; N = 1, 2, ...\}$ a sequence of probability measures on $\mathcal{B}(\mathcal{X})$. Assume that Q_N has a large deviation property with rate N and rate function I, $I : \mathcal{X} \to \mathbb{R}$. Further, let the sequence of functions $U_N : \mathcal{X} \to \mathbb{R}$ be equicontinuous converging point-wise to a function $U : \mathcal{X} \to \mathbb{R}$.*
(a) Suppose that $\sup_{m \in \mathcal{X}} U(m) < \infty$, then $\sup_{m \in \mathcal{X}}\{U(m) - I(m)\} < \infty$ and

$$\lim_{N \to \infty} \frac{1}{N} \log \int_{\mathcal{X}} \exp[NU_N(m_N)] Q_N(m) = \sup_{m \in \mathcal{X}} [U(m) - I(m)]. \qquad (2.17)$$

(b) More generally, for some constant B, if U satisfies

$$\lim_{B \to \infty} \limsup_{N \to \infty} \frac{1}{N} \log \int_{\{U \geq B\}} \exp[NU_N(m_N)] Q_N(m) = -\infty, \qquad (2.18)$$

then the limit (2.17) holds and is finite. In particular, if U_N is bounded above on the union of the supports of Q_N, then (2.18) is satisfied and thus the limit (2.17) holds and is finite.

Proof. The lower bound for (2.17) is derived first then following condition (2.18), we proof an upper bound for (2.17). Lastly, we show that when (2.17) is finite then condition (2.18) holds and that completes the proof. Recall that $U_N(m_N)$ is equicontinuous and uniformly bounded. The interest here is to prove that the limiting pressure per particle has the following variational form:

$$\lim_{N \to \infty} \frac{1}{N} \log \int_{\mathcal{X}} \exp[NU_N(m_N)] Q_N(m) = \sup_{m \in \mathcal{X}} [U(m) - I(m)].$$

Now, note that, since Q_N has large deviation property with good rate function I, it may be written heuristically as: $dQ_N/dx \approx e^{-NI(x)}$. Then for any $x \in \mathcal{X}$,

$$Z_N = \int_{\mathcal{X}} e^{NU(x)} Q_N(x) \approx \int_{\mathcal{X}} e^{N(U(x) - I(x))} dx. \qquad (2.19)$$

This integral above has the form of a so called *Laplace integral*, which is known to be dominated for large N by its largest integrand when it is unique. Employing Laplace approximation or a saddle-point approximation of the integral, is justified in the context of large deviation theory since the corrections to this approximation are sub-exponential in N, as are those of large deviations principles. This verifies (2.17) without the need of further clarification but for completeness a detailed step-by-step approach is included. The Laplace integral of the partition function uses heuristic approximations, which lead to results popularly referred to as the Varadhan Theorem [32,33], which rigorously handles all the heuristic approximations. As such, Varadhan's Theorem can be considered a rigorous and general expression of the Laplace principle.

Step 1

Let m be an arbitrary point in $\mathcal{X}$ and $\delta > 0$. Since the sequence U_N is equicontinuous, it is the case that the functions U_N are lower semicontinuous. Hence, there exists a neighbourhood G of m such that $\inf_{y \in G} U_N(y) \geq U_N(m) - \delta$ for $N = 1, 2, 3, ...$. Since G is an open set, the lower large deviation bound can be defined as

$$\liminf_{N \to \infty} \frac{1}{N} \log Q_N(G) \geq -I(G). \tag{2.20}$$

Hence,

$$\begin{aligned}
\liminf_{N \to \infty} \frac{1}{N} \log Z_N &\geq \liminf_{N \to \infty} \frac{1}{N} \log Z_N(G) \\
&\geq \liminf_{N \to \infty} \frac{1}{N} \log \left[\int_G \exp[NU_N(m_N)] Q_N(m) \right] \\
&\geq \liminf_{N \to \infty} U_N(x) + \liminf_{N \to \infty} \frac{1}{N} \log Q_N(G) \\
&\geq U(m) - \delta - I(m) \\
&= U(m) - I(m) - \delta.
\end{aligned}$$

In the second and third inequality of the equation above, it has been used that Q_N has a large deviation property and U_N is lower semicontinuous on a complete separable metric space $\mathcal{X}$ with a compact level set [25,26]. Now, since $m \in \mathcal{X}$ and $\delta > 0$ are arbitrary chosen,

$$\liminf_{N \to \infty} \frac{1}{N} \log Z_N \geq \sup_{m \in \mathcal{X}} \{U(m) - I(m)\}. \tag{2.21}$$

Step 2

For the upper bound, let assume that the function U_N is continuous and uniformly bounded on $\mathcal{X}$ such that $\sup_{m\in\mathcal{X}} U(m)$ is finite, i.e., there exists a constant M such that $\sup_{m\in\mathcal{X}} U(m) \leq M$. Then for a non-negative rate function I, $\sup_{m\in\mathcal{X}}\{U(m) - I(m)\} < \infty$ and $\sup_{m\in\mathcal{X}}\{U(m) - I(m)\} > -\infty$. Hence, (2.18) holds trivially.

Let A be a Borel subet of $\mathcal{X}$ and define for $m \in A$,

$$I(A) = \inf_{m\in A} I(m) \qquad \text{and} \qquad Z_N(A) = \int_A e^{NU_N(m)} Q_N(m).$$

Suppose again that there exists $B < \infty$ such that for every $m \in \mathcal{X}$, $U(m) \leq B$ and $C < \min(B, sup_{m\in\mathcal{X}}\{U(m) - I(m)\})$. Now, let define the closed set $W_{n,q}$ for $q = 1, ..., n$ as

$$W_{n,q} = \left\{ m \in \mathcal{X} : C + \frac{q-1}{n}(B-C) \leq U(m) \leq C + \frac{q}{n}(B-C) \right\}.$$

From the above we have that $\bigcup_{q=1}^{n} W_{n,q} = \{m \in \mathcal{X} : U(m) \geq C\}$ and then the upper large deviation bound becomes

$$\limsup_{N\to\infty} \frac{1}{N} \log Q_N(W_{n,q}) \leq -I(W_{n,q}).$$

Therefore,

$$\begin{aligned}
\limsup_{N\to\infty} \frac{1}{N} \log Z_N(\{m \in \mathcal{X} : U(m) \geq C\}) &\leq \max_{q=1,...,n}\left\{C + \frac{q}{n}(B-C) - I(W_{n,q})\right\} \\
&\leq \max_{q=1,...,n} \sup_{m\in W_{n,q}}\{U(m) - I(m)\} + \frac{B-C}{n} \\
&\leq \sup_{m\in\mathcal{X}}\{U(m) - I(m)\} + \frac{B-C}{n}.
\end{aligned}$$

Taking limit as $n \to \infty$

$$\limsup_{N\to\infty} \frac{1}{N} \log Z_N(\{m \in \mathcal{X} : U(m) \geq C\}) \leq \sup_{m\in\mathcal{X}}\{U(m) - I(m)\}.$$

Note that $Z_N(\{m \in \mathcal{X} : U(m) \leq C\}) \leq e^{NC}$, hence

$$\begin{aligned}
\limsup_{N\to\infty} \frac{1}{N} \log Z_N &\leq \max\left\{C, \sup_{m\in\mathcal{X}}\{U(m) - I(m)\}\right\} \\
&= \sup_{m\in\mathcal{X}}\{U(m) - I(m)\}.
\end{aligned} \tag{2.22}$$

Now, since $Z_N(\{m \in \mathcal{X} : U(m) \leq C\}) \leq e^{NC}$, it follows that

$$\limsup_{N \to \infty} \frac{1}{N} \log Z_N \leq \max \left\{ C, \sup_{m \in \mathcal{X}} \{U(m) - I(m)\} \right\} = \sup_{m \in \mathcal{X}} \{U(m) - I(m)\}. \quad (2.23)$$

Step 3

Here, for a continuous real valued function U_N, we prove that the limit (2.17) satisfies (2.18). Recall from (2.21), that

$$\liminf_{N \to \infty} \frac{1}{N} \log Z_N \geq \sup_{m \in \mathcal{X}} \{U(m) - I(m)\}.$$

Equation (2.18) implies that,

$$\limsup_{N \to \infty} \frac{1}{N} \log Z_N < \infty \quad \text{and} \quad \sup_{m \in \mathcal{X}} \{U(m) - I(m)\} < \infty$$

follows from (2.21). According to (2.18), there exists a constant $B > 0$ such that

$$\limsup_{N \to \infty} \frac{1}{N} \log Z_N(\{m \in \mathcal{X} : U(m) > B\}) \leq \sup_{m \in \mathcal{X}} \{U(m) - I(m)\}.$$

Now, let's define $\overline{U}(m) = \min[U(m), B]$ and $\overline{Z}_N = \int_{\mathcal{X}} e^{N\overline{U}_N(m)} Q_N(m)$. $\overline{U}$ satisfy the hypothesis in (a) of Theorem 2.2.3. Hence, we have that

$$Z_N = Z_N(\{m \in \mathcal{X} : U(m) \leq B\}) + Z_N(\{m \in \mathcal{X} : U(m) > B\})$$
$$= \overline{Z}_N + Z_N(\{m \in \mathcal{X} : U(m) > B\}).$$

Therefore,

$$\limsup_{N \to \infty} \frac{1}{N} \log Z_N \leq \max \left[\sup_{m \in \mathcal{X}} \{\overline{U}(m) - I(m)\}, \sup_{m \in \mathcal{X}} \{U(m) - I(m)\} \right]$$
$$= \sup_{m \in \mathcal{X}} \{U(m) - I(m)\}.$$

This completes the proof of part (b) of Theorem 2.2.3. □

Observe that to obtain the supremum over $m \in [-1, 1]$ of Φ as described by the variational principle (2.14) we have to find the stationary conditions of Φ which can be obtained by taking suitable derivatives. The derivative of Φ w.r.t m:

$$\frac{d}{dm} \Phi(m)\big|_{\overline{m}} = K\overline{m}^2 + J\overline{m} + h - \left[\frac{1}{2} \log \left(\frac{1 + \overline{m}}{1 - \overline{m}} \right) \right] = 0. \quad (2.24)$$

From the above equation, we have that

$$\overline{m}(K, J, h) = \tanh(K\overline{m}^2 + J\overline{m} + h). \tag{2.25}$$

The structure of the probability measure identified by the variational principle (2.14) select stable solutions, i.e., a small stochastic disturbance of the system will produce small changes on the average behaviour of the system unless it is close to a second order phase transition. Equation (2.25) is the stationarity condition, which acts as a self-consistency equation, and must be satisfied by the solutions of the variational principle (2.14). The mean-field equation (2.25) can be solved by suitable numerical methods, of which the interest is to select those solutions that realise the supremum of Φ in (2.14). Hence, among those solutions, we identify for which values of $\overline{m}$, Φ is maximised. The quantity $\overline{m}$ is called the order parameter of the model. On the other hand, one can obtain the solutions of (2.25) by maximising Φ over all $m \in \mathcal{X}$ and selecting those that achieve the maximum.

The variational principle (2.14) depends on three parameters, K, J and h. To better understand its behaviour, we begin the analyses by studying: first, its behaviour as a function of the cubic parameter K, by setting $J = h = 0$ and secondly, generate phase diagrams of the order parameter (2.25). The overall phase diagram that emerges presents novel features. When $J = h = 0$, (2.14) becomes:

$$p(\overline{m}; K, 0, 0) = \frac{K}{3}\overline{m}^3 - \left[\frac{1 - \overline{m}}{2} \log\left(\frac{1 - \overline{m}}{2}\right) + \frac{1 + \overline{m}}{2} \log\left(\frac{1 + \overline{m}}{2}\right)\right]. \tag{2.26}$$

A numerical investigation of (2.26) for fixed values of the interaction parameter is shown in Figure 2.1 and reveals a critical point of K above which the system transition from one state to another. In **(a)** it can be observed that when K is small, i.e., 0.7, there is only one maximum which is at zero. When K is increased to 1.3, in **(b)**, the maximum still remains at zero and there begins to be a rise of another maximum point towards $+1$. From **(c)** and **(d)** two global maximum points are observed resulting in the same value of the variational principle. Hence there are two values of $\overline{m}$ and a unique K at which the derivative of equation (2.26) is zero for the result in **(c)** and **(d)**. This unique K-value for which the system has two global maximisers can be approximated using an appropriate iterative numerical optimisation technique, such as the Levenberg–Marquardt algorithm. As can be seen in the Figure 2.1, the critical value of K, is approximated to be ± 2.0162. It's worth mentioning that the values 1.3 and 0.7 for K in Figures 2.1(a) and 2.1(b) respectively have no particular meaning, but they are chosen as two examples of
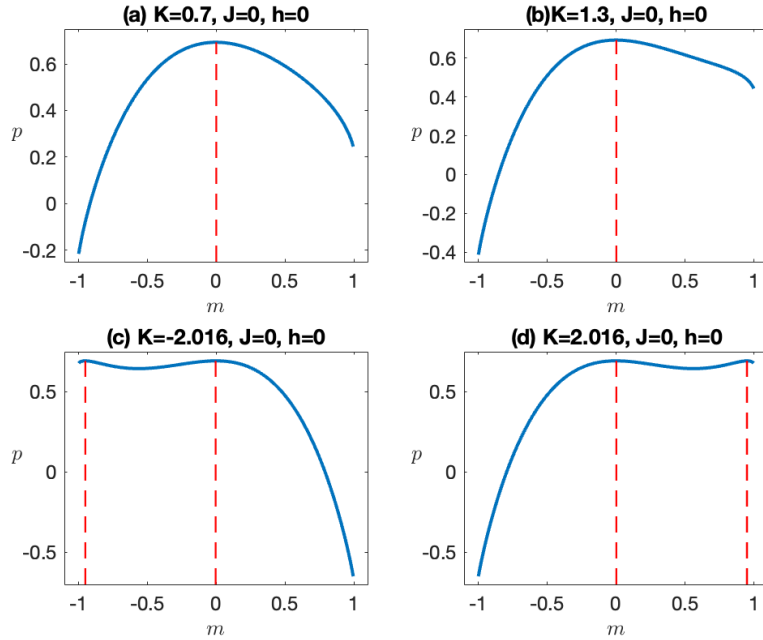
Figure 2.1: Variational free energy of the cubic mean-field model for $J = h = 0$ as a function of m in blue curves and the red dashed lines denote the point at which it gets maximised.

relatively low values, while ± 2.0162 is chosen because they turn out to be critical points from the numerical solution of self-consistency equation (2.25).

Now, for any $K > 2.0162$, p has a unique global maximum point, likewise when $K < -2.0162$. Hence, $K \approx \pm 2.0162$ is the critical value of K. From this observation, it is clear that the magnetic order parameter (m) that realises the supremum of the variational principle for $J = h = 0$ remains at zero until $K \approx \pm 2.0162$, where there will be a jump. Let call $K_c = \pm 2.0163$ as the critical value.

Unlike the quadratic mean field model that, for $h = 0$, has a second order continuous phase transition in J, the cubic case analysed here displays a remarkable *discontinuous first order phase transition* in K when $J = h = 0$ shown in Figure 2.2. Starting from small absolute valued K-s and increasing or decreasing it, the value $\overline{m}$ characterising the stable stationary solutions (see Figure 2.2 in blue) remains at zero until $K = K_c \approx \pm 2.016295$ where suddenly we observe a jump in the order parameter. The phase diagram of the order parameter (2.25) for $J = 1$ and $h = 0$ is shown in Figure 2.3 and it can be observed to be continuous.

The behaviour of the order parameter in the planes $(K, J, 0)$ and $(K, 0, h)$ is
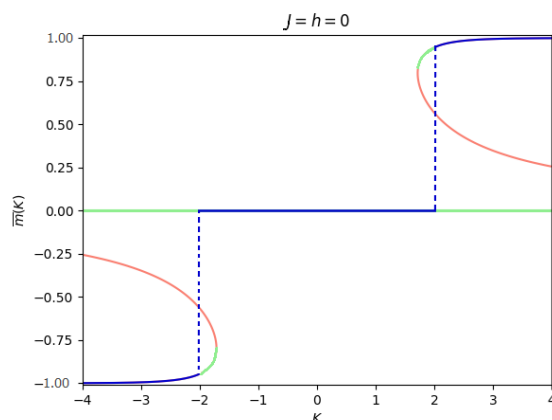
Figure 2.2: Magnetic order parameter, $\overline{m}$, of the system for $J = h = 0$ as a function of K. There is a transition in $\overline{m}$ from zero to positively polarised magnetisation when crossing $K \approx 2.0162$ from below and a transition from zero to negative average opinion when crossing $K \approx -2.0162$ from above. The curves represent all the solutions of the stationary condition (2.25), the blue ones corresponds to the global stable ones, i.e., the solution that realise the supremum of Φ for $J = h = 0$, the green ones are locally stable solutions and the red ones are the unstable solutions.
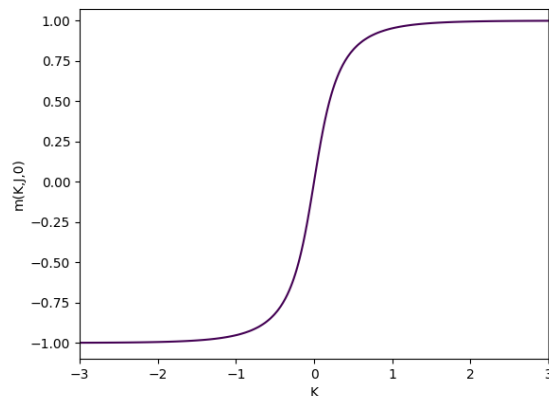
Figure 2.3: Magnetic order parameter $\overline{m}$ as a function of K at $J = 1$ and $h = 0$.

shown in Figure 2.4, while the case $(0, J, h)$ correspond to the classical two-body mean-field model. The behaviour of the order parameter in the planes $(K, J, 0)$ and $(K, 0, h)$ will further be investigated in chapters 3 and 4 but we only give an overview in this section. The asymptotic properties of the limiting free energy in those cases, i.e., in the plane $(K, J, 0)$ and $(K, 0, h)$, will be studied in details in subsequent

Chapters 3 and 4. In panel **(a)** of Figure 2.4, when $J = 0$, we can observe the behaviour found in Figure 2.2 which indicates jumps at $K \approx \pm 2.0162$ and when $K = 0$, we obtain the solution of the model with only two-spin interaction (i.e., classical two-spin mean-field model). For $J < 1$, one can observe the presence of three distinct phases: the one with negative magnetic order (in blue), the one with zero magnetic order, i.e., no order, (in gray) and the one with positive magnetic order (in red). The zero magnetic order, which is a stable paramagnetic state, corresponds a state with no spontaneous magnetic order. It is an indication of symmetry in the spin orientation (i.e., +1 and -1) with no preference for one over the other. As K increases or decreases, the symmetry is broken, and the system shifts to either a positive or negative state. In that region therefore a progressive increase in K from negative to positive values encounter two consecutive jumps. In panel **(b)** of Figure 2.4 the system observes two distinct *second order phase transitions* in the magnetic order parameter h and K falls within certain thresholds.
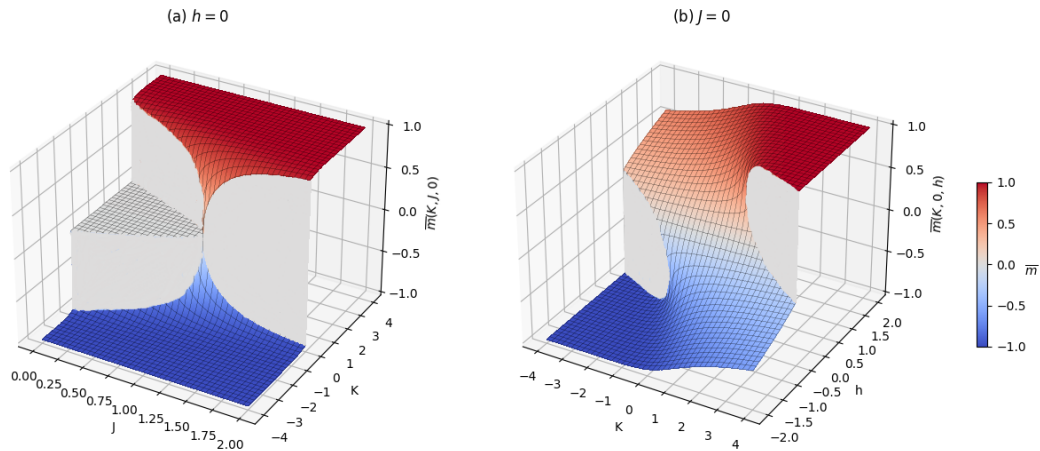
Figure 2.4: Magnetic order parameter of the cubic mean-field model. In panel **(a)**, $h = 0$ while in **(b)** $J = 0$. When $J = 0$ in **(a)**, we observe the global stable solution found in Fig 2.2 which indicates jumps at K_c and when $K = 0$, we obtain the solution of the simple Ising model without cubic interaction. For fixed $J < 1$ and moving along K the system presents two jumps separated by a plateau at zero. Those two jumps coalesce into a single one when J cross the unit value. In **(b)** we observe a discontinuity in the magnetic order parameter for two separated jumps when h and K falls within certain thresholds.

2.3   Three-spin interacting lattice gas model

Let us consider the Hamiltonian of a system defined on a lattice with N sites. Here, each site on the lattice is either occupied by a gas particle or it's vacant. We define the occupancy of site i as $\eta_i = 1$ when i is occupied and $\eta_i = 0$ when site i is vacant. The model describing the system is given as follows:

$$\tilde{H}_N(\eta) = -\frac{\tilde{K}}{3N^2} \sum_{i,j,k=1}^{N} \eta_i \eta_j \eta_k - \frac{\tilde{J}}{2N} \sum_{i,j=1}^{N} \eta_i \eta_j - \tilde{h} \sum_{i=1}^{N} \eta_i, \qquad (2.27)$$

where $\eta \in \{0,1\}^N$. Let's define the average density of the particles for a given configuration η of the lattice as:

$$\upsilon_N(\eta) = \frac{1}{N} \sum_{i=1}^{N} \eta_i, \qquad (2.28)$$

hence,

$$\tilde{H}_N(\eta) = -N \left(\underbrace{\frac{\tilde{K}}{3} \upsilon_N^3(\eta) + \frac{\tilde{J}}{2} \upsilon_N^2(\eta) + \tilde{h} \upsilon_N(\eta)}_{=\tilde{U}_N(\upsilon_N(\eta))} \right).$$

Proposition 2.3.1. *Given choices of the parameters $\tilde{K}, \tilde{J}$ and $\tilde{h}$ the large number limit of the negative free energy per site related to the Hamiltonian* (2.27) *has the following variational representation:*

$$\tilde{p}(\tilde{K}, \tilde{J}, \tilde{h}) = \sup_{x \in [0,1]} \zeta(x), \qquad (2.29)$$

where $\zeta(x) = \left[\tilde{U}(x) - \tilde{I}(x) \right]$ with

$$\tilde{U}(x) = \frac{\tilde{K}}{3} x^3 + \frac{\tilde{J}}{2} x^2 + \tilde{h} x \qquad (2.30)$$

is the energy contribution of the Hamiltonian and

$$\tilde{I}(x) = x \log(x) + (1 - x) \log(1 - x) \qquad (2.31)$$

is the entropy contribution, expressing the logarithm of the number of ways the value x can be produced with different η configuration.

The solution of the Hamiltonian is obtained as the stationary condition(s) of the variational pressure defined in (2.29) with interest in the ones that realise the supremum. These stationary points $\overline{x}$ of ζ are derived as:

$$\frac{d}{dx}\zeta(x)|_{\overline{x}} = \tilde{K}\overline{x}^2 + \tilde{J}\overline{x} + \tilde{h} - \left[\log\left(\frac{\overline{x}}{1-\overline{x}}\right)\right] = 0 \tag{2.32}$$

and

$$\overline{x} = \frac{e^{\tilde{K}\overline{x}^2 + \tilde{J}\overline{x} + \tilde{h}}}{1 + e^{\tilde{K}\overline{x}^2 + \tilde{J}\overline{x} + \tilde{h}}} \tag{2.33}$$

Equation (2.33) represents the average density of particles on the lattice and is commonly referred to as the logistic function. Importantly, the statistical mechanical model discussed in this section establishes a connection between the Ising model with three-spin interactions on the lattice and the classical logistic model with interactions.

Remark 2.3.1. *It is noteworthy that the stationary points of the variational principle in (2.29) describe a special case within a class of probabilistic choice models found in socioeconomic literature, known as logit models. Other examples of probabilistic choice models include probit models and generalized extreme-value models. This raises the question: what are the statistical mechanical analogues of these models? Insights gained from these statistical mechanical models will significantly contribute to the understanding of socioeconomic models.*

Chapter 3

Three- and two-spin interactions: the KJ Ising model

In this chapter, we thoroughly investigate the equilibrium properties of the Ising model described by (2.1) under the condition of zero external field (i.e., $h = 0$). Several intriguing characteristics of the model are explored, including the existence and properties of phase transitions that delineate different phases of the system, the limiting behaviour of the magnetisation, the magnetisation's behaviour along phase boundaries, and its behaviour approaching the critical point of the system. In particular, our findings demonstrate that the equilibria of the system encompass not only positively and negatively polarised states but also a stable unpolarised state, which arises due to the presence of a non-zero cubic term that breaks the spin-flip symmetry. Moreover, we conduct a comprehensive analysis of the fluctuations of the magnetisation density across the entire phase space, with particular focus on its behaviour during phase separation and near the critical point.

We establish that the critical exponent for the magnetisation takes on a value of zero in the direction of unpolarised states in the phase space, and further identify the occurrence of phase transitions in the antiferromagnetic region of the model. The study offers valuable insights into the intricate equilibrium properties of the Ising model with three-spin interactions and highlights the significance of the cubic term's influence on the system's behaviour. The results discussed here can be found in the reference list as [34].

3.1   Definitions and main results

It worth noticing that the parameters K and h, appearing in equation (2.1), both act as a symmetry breaking parameter when the other is absent. In order to emphasis their different role we will restrict the attention to the case where $h = 0$. Indeed the model for $K = 0$ is well known as the classical two-spin interacting Curie-Weiss model. Hence, the Hamiltonian to be considered in this chapter is

$$
\begin{aligned}
H_N^{KJ}(\sigma) &= -\frac{K}{3N^2} \sum_{i,j,k=1}^{N} \sigma_i \sigma_j \sigma_k - \frac{J}{2N} \sum_{i,j=1}^{N} \sigma_i \sigma_j \\
&= -N \left(\frac{K}{3} m_N^3(\sigma) + \frac{J}{2} m_N^2(\sigma) \right)
\end{aligned}
\tag{3.1}
$$

on an N interacting Ising spin lattice with $\sigma = (\sigma_i)_{i \leq N} \in \{-1, +1\}^N$, where $(K, J) \in \mathbb{R}^2$ and $m_N(\sigma)$ is defined by (2.2).

The parameters K and J tune the interactions among triples and pair of spins respectively. The Hamiltonian (3.1) is particularly interesting as an example of a spin system lacking the usual spin-up and spin-down reversal symmetry. Let's observe that, the Hamiltonian (3.1) is invariant under the transformation $K \mapsto -K$ and $\sigma_i \mapsto -\sigma_i$, hence, without loss of generality, we can study the model only for $K \geq 0$.

The Hamiltonian (3.1) induces a Boltzmann-Gibbs probability measure on the configuration space given by:

$$
\mu_N^{KJ}(\sigma) = \frac{e^{-H_N^{KJ}(\sigma)}}{Z_N},
\tag{3.2}
$$

where $Z_N = \sum_{\sigma \in \{-1, +1\}^N} \exp\left(-H_N^{KJ}(\sigma) \right)$ is the partition function. In equation (3.2) we set the usual inverse temperature β to 1 since it can be absorbed in the parameters.

Our aim is to obtain a complete characterisation of the model's *phase diagram*, an analysis of the asymptotic distribution of the magnetisation in the presence and absence of phase transitions, the *fluctuations* of the suitably rescaled magnetisation w.r.t. the Boltzmann-Gibbs measure (3.2) at and away from the critical point, and the computation of the *critical exponents*.

All the above properties are strictly related to the analytical properties of the *free energy* of the system, which is the starting point of our analysis. Let us recall that the thermodynamic pressure, i.e., the generating functional, has the same form as (2.6):

$$p_N = \frac{1}{N} \log Z_N \tag{3.3}$$

which equals the free energy up to a minus sign. The thermodynamic limit of (3.3) can be easily computed applying Varadhan's integral lemma [20, 25, 26], obtaining:

Proposition 3.1.1. *Given that $(K, J) \in \mathbb{R}^2$ the limiting pressure (3.3) admits the following variational representation:*

$$p := \lim_{N \to \infty} p_N = \sup_{m \in [-1,1]} \phi(m), \tag{3.4}$$

where $\phi(m) = U(m) - I(m)$ with

$$U(m) = \frac{K}{3} m^3 + \frac{J}{2} m^2 \tag{3.5}$$

is the energy contribution and

$$I(m) = \frac{1-m}{2} \log \left(\frac{1-m}{2} \right) + \frac{1+m}{2} \log \left(\frac{1+m}{2} \right) \tag{3.6}$$

is the binary entropy contribution.

The variational principle (3.4) has solution(s) that satisfy the stationarity condition,

$$m = \tanh(Km^2 + Jm) \tag{3.7}$$

sometimes called the consistency equation. A careful analysis shows that, among the solutions of (3.7), the function $\phi(m)$ in (3.4) can have one or two global maximisers in the interval $(-1, 1)$ for fixed (K, J) (see Figure 3.1).

In particular, we can divide the parameter space $(K, J) \in \mathbb{R}_+ \times \mathbb{R}$ accordingly to the following:

Proposition 3.1.2 (Phase diagram)**.** *For any $K > 0$, there exists $J = \gamma(K)$ such that the function $m \mapsto \phi(m)$ has a unique maximum point m^* for $(K, J) \in (\mathbb{R}_+ \times \mathbb{R}) \backslash \gamma$. Moreover, on the curve γ there are two global maximisers, $0 = m_0 < m_1$ and the limit as $K \to 0$ of $\gamma(K)$ identifies the critical point $(K_c, J_c) = (0, 1)$ where the magnetisation takes the value $m_c = 0$. The explicit definition of $J = \gamma(K)$ will be given in Proposition 3.2.3.*

In physical terms, the presence of two global maximisers corresponds to the existence of two different thermodynamic equilibrium phases, whereas the curve γ represents the coexistence curve. Let's note that m_0 and m_1 represent a stable
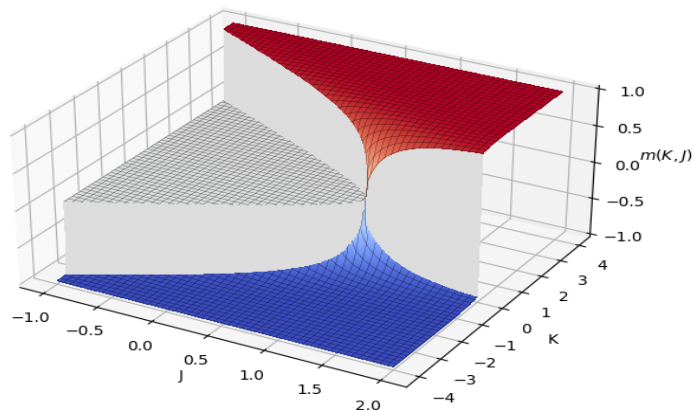
Figure 3.1: Stable solutions of the mean-field equation as a function of K and J. There are three stable phases presented here: the positive polarised phase depicted in red, the unpolarised phase given as the gray plateau, and the negative polarised phase denoted by the blue colour. At the critical point, $(K, J) = (0, 1)$, the three phases of the cubic model as well as the two phases of the Curie-Weiss plane $(K = 0)$ coalesce.

paramagnetic state and a positively polarised state, respectively. The paramagnetic state is characterised by the absence of spontaneous magnetic order and the presence of symmetry between the up and down spin, with no preference for either direction. The jump from the paramagnetic state to the polarised state, namely when the magnetisation jumps from m_0 to m_1, represents a *first-order phase transition* [35], which is markedly different from the quadratic mean-field model $(K = 0)$ having a second-order phase transition in J. More precisely if we denotes by $m^*(K, J)$ the unique maximizer of ϕ, for any $\bar{K} > 0$ there exists $\bar{J} = \gamma(\bar{K}) \in (-\infty, 1)$ such that

$$0 = \lim_{J \to \bar{J}^-} m(J, \bar{K}) \neq \lim_{J \to \bar{J}^+} m(J, \bar{K}) > 0.$$

This behaviour is somehow reminiscent of the Curie-Weiss Potts model analyzed in [36] where for any value of the parameter q a first order phase transition is observed. Numerical simulations of the phase diagram described in Proposition 3.1.2 can be seen in Figure 3.2.

In the standard Curie-Weiss model, when $J > 0$ we know that as soon as $h > 0$ one obtains a positive magnetisation. The reason is that the energy contribution due to h favours only spins aligned with $sign(h)$. On the contrary, in our system, $J, K > 0$, the energy contribution due to K can be minimised by configurations
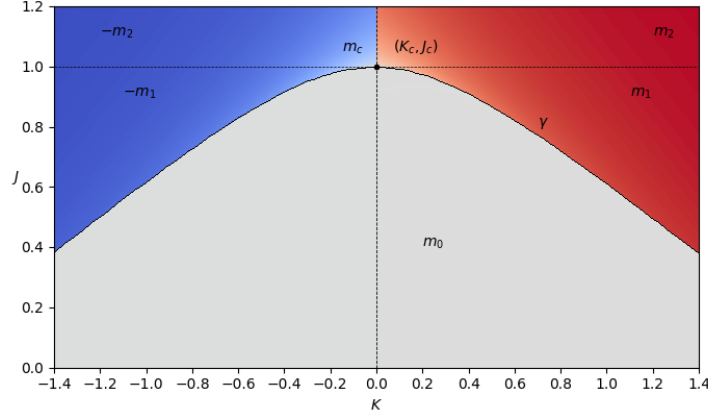
Figure 3.2: Phase diagram of the model with coexistence curve γ and the critical point (K_c, J_c) in the (K, J) plane.

containing both up and down spin signs. This implies that the entropy contribution can dominate also for small but non-zero K, giving a zero magnetisation.

Finally, we study the behaviour of the limiting value of the magnetisation near the critical point $(K_c, J_c) = (0, 1)$ namely the critical exponents of the model. The average value of the magnetisation will be given by the Law of Large Numbers (LLN) in Theorem 3.3.1 and denoted by $m^*(K, J)$. The following proposition describes the critical behaviour of $m^*(K, J)$ when $(K, J) \to (K_c, J_c)$ from various directions.

Proposition 3.1.3. *Let $m^*(K, J)$ be the unique maximiser of $\phi(m)$ defined in Corollary 3.2.1. Given $\alpha \in \mathbb{R}$ consider the lines*

$$J(K) = 1 + \alpha K \ , \ \ K > 0 \tag{3.8}$$

and the function $m^*(K) \equiv m^*(K, J(K))$. Then, for $K \to 0^+$, the following holds

$$m^*(K) \sim \begin{cases} \sqrt{3\alpha}\sqrt{K}, & \text{for} \quad \alpha > 0 \\ 3K, & \text{for} \quad \alpha = 0 \\ 0, & \text{for} \quad \alpha < 0 \end{cases} \tag{3.9}$$

Remark 3.1.1. *Notice that when $\alpha < 0$ the critical exponent is 0. The case $K = 0$ and $J \to 1^+$ corresponds to the classical mean-field Ising model (i.e., Curie-Weiss model) shown in Chapter 1 and is well known that*

$$m^*(0, J) \sim \sqrt{\frac{3(J-1)}{J^3}}. \tag{3.10}$$

3.2   Properties of the Solution

This section contains the proofs of the above results by studying the properties of the stationary points of the variational principle, $\phi(m, K, J)$, in equation (3.4) and is organised as follows:

In Sections 3.2.1 and 3.2.2, we prove Proposition 3.1.2 by studying the properties of the function $\phi(m)$ appearing in the variational problem (3.4). Finally, in Section 3.2.3, we compute the critical exponents of the model described by Proposition 3.1.3.

3.2.1   Phase diagram

Proof of Proposition

The complete proof of Proposition 3.1.2 follows from Propositions 3.2.1, 3.2.2, 3.2.3 and 3.2.4 below. Let us start studying in detail the variational principle (3.4) and observe that the function $\phi(m)$ satisfies

$$
\begin{aligned}
\frac{\partial}{\partial m}\phi(m) &= Km^2 + Jm - \frac{1}{2}\log\left(\frac{1+m}{1-m}\right), \\
\frac{\partial^2}{\partial m^2}\phi(m) &= 2Km + J - \frac{1}{1-m^2}.
\end{aligned}
\tag{3.11}
$$

Therefore the variational pressure $\phi(m)$ attains it maximum in at least one point $m = m(K, J) \in (-1, 1)$, which satisfy

$$
\frac{\partial}{\partial m}\phi(m) = 0, \qquad \text{i.e.,} \quad m = \tanh\left(Km^2 + Jm\right). \tag{3.12}
$$

Indeed, from (3.11) $\lim_{m\to -1+}\phi'(m) = +\infty$ and $\lim_{m\to 1-}\phi'(m) = -\infty$. Therefore, there exists $\epsilon > 0$ such that $\phi(m)$ is strictly increasing on $[-1, -1+\epsilon]$ and strictly decreasing on $[1-\epsilon, 1]$. This implies that, the local maximisers of $\phi(m)$ does not include -1 and $+1$. Notice also that, since $K > 0$, if $\bar{m} > 0$ then $\phi(\bar{m}) > \phi(-\bar{m})$; therefore the supremum of $\phi(m)$ cannot be reached at negative values.

A complete classification of the critical points of $\phi(m)$ is contained in the following proposition:

Proposition 3.2.1. *(Classification of critical points) For all $K > 0$ and $J \in \mathbb{R}$, the solutions to equation (3.12) can be described as follow:*

Define the function

$$\Psi(K) := \min_{m \in [0,1]} \frac{g(m,K)}{m} < 1 \tag{3.13}$$

where $g(m,K) := \operatorname{arctanh}(m) - Km^2$ and set $J_c = 1$. Then:

a. *for $J < \Psi(K)$, there exists a unique solution, $m_0 = 0$, and it is the maximum point of $\phi(m)$,*

b. *for $\Psi(K) < J < J_c$, equation (3.12) has three solutions i.e., $m_0, m_1 > m_3 > 0$. Furthermore, m_0, m_1 are local maximum points while m_3 is a local minimum point of $\phi(m)$,*

c. *for $J = \Psi(K)$, there exist two solutions, m_0 and $m_1 > 0$, where m_0 is the maximum point of $\phi(m)$ and m_1 is an inflection point.*

d. *If $J \geq J_c$, there exists a unique positive solution m_2 which is the only maximum point of $\phi(m)$ in equation (3.4).*

Proof. Let us start by noticing that $m = 0$ is always a solution of (3.12). Moreover,

$$\phi''(0) \begin{cases} < 0, & \text{if } J < 1 \\ > 0, & \text{if } J > 1 \end{cases}.$$

Now, let's rewrite (3.12) as

$$mJ = \underbrace{\left[\operatorname{arctanh}(m) - Km^2 \right]}_{= g(m,K)}. \tag{3.14}$$

The solutions of (3.12) are the intersections between the line mJ and the function $g(m,K)$. Therefore the function $\Psi(K)$ in (3.13) is a benchmark to study the number of solutions of $\phi'(m) = 0$ when J varies. Indeed by definition, $\Psi(K)$ represents the smallest value of J in order to have a positive solution for (3.14). Let us start collecting some properties of the function $g(m,K)$. By definition we have that

$$g'(m,K) = \left[\frac{1}{1-m^2} - 2Km \right]$$

$$g''(m,K) = \left[\frac{2m}{(1-m^2)^2} - 2K \right]. \tag{3.15}$$

This implies that,

$$\begin{cases} g'(0, K) = 1, \\ g''(0, K) = -2K < 0 \quad \text{for all } K > 0. \end{cases}$$

Since the function $m \mapsto \dfrac{2m}{(1 - m^2)^2}$ is strictly increasing on $[0, 1)$, then $g''(m, K) = 0$ has only one solution, namely $g(m, K)$ has only one inflection point. Moreover, observe that, as $m \to 1^-$, $g(m, K) \to +\infty$.

a. If $J < \Psi(K)$ then it's clear that (3.12) has a unique solution $m_0 = 0$ which is a maximum point since in this case $\phi''(0) < 0$.

b. If $\Psi(K) < J < J_c$, continuity of g and the fact that for $m \to 1^-$, $g(m, K) \to +\infty$, imply that (3.12) has three solutions, m_0, m_1 and m_3, where m_1 and m_3 are positive. It's also easy to check using the properties of the function $g(m, K)$ that m_0 and m_1 are local maxima while m_3 is a local minima.

c. If $J = \Psi(K)$, then there is only one intersection point m_4 between the line mJ and the function $g(m, K)$. Standard reasoning allows to conclude that m_4 is an inflection point for ϕ.

d. Finally suppose that $J \geq J_c$. The fact that $g'(0, K) = 1$ and $g''(0, K) = -2K < 0$ for $K > 0$, means that the line mJ starts above the function g. Now, since g has at most one inflection point and $g(m, K) \to +\infty$ as $m \to 1^-$, one can conclude that there exist a unique positive solution $m_2 \in (0, 1)$ of $\phi'(m) = 0$.

$\square$

The solutions made mention in Proposition 3.2.1 are displayed in Figure 3.3. In the next proposition we obtain the differentiability of the solution(s) of the consistency equation (3.12) with respect to the parameters J and K.

Proposition 3.2.2. *(Regularity properties). Let m_0, m_1 and m_2 be the (local) maxima of ϕ described in Proposition 3.2.1. Then for $K > 0$, the following properties hold:*

(a) m_1 is continuous in its domain namely $\Psi(K) \leq J < J_c$ and C^∞ in its interior, while m_2 is C^∞ in its domain, namely $J \geq J_c$.
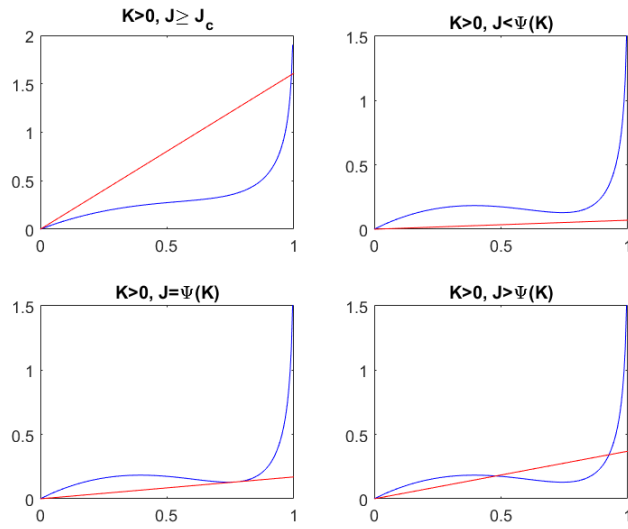
Figure 3.3: The points of intersection between the blue curve $g(m, K)$ as defined in (3.14) and red curve $f(m) = Jm$. The solution of the equation (3.12) are the points of intersection between $g(m, K)$ and $f(m)$.
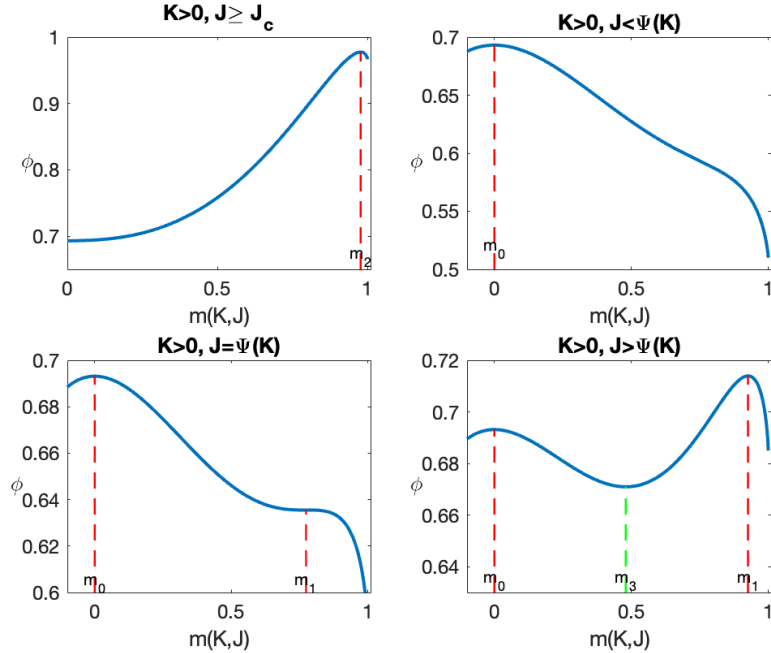
Figure 3.4: The variational free energy, ϕ as a function of $m(K, J)$ for fixed K and J.

(b) $\phi''(m_0) = \phi''(0) < 0$, $\phi''(m_1) < 0$ for $\Psi(K) < J < J_c$, and $\phi''(m_2) < 0$ for $J \geq J_c$.

Moreover, for any $i \in \{0, 1, 2\}$ it holds that

$$\frac{\partial}{\partial J}\phi(m_i) = \frac{1}{2}m_i^2, \qquad \frac{\partial}{\partial K}\phi(m_i) = \frac{1}{3}m_i^3 \tag{3.16}$$

$$\frac{\partial m_i}{\partial J} = -\frac{m_i}{\phi''(m_i)}, \qquad \frac{\partial m_i}{\partial K} = -\frac{m_i^2}{\phi''(m_i)}. \tag{3.17}$$

Proof. Since $m_0 = 0$ there is nothing to prove for it. We focus on the properties of m_1 and m_2.

(a) Let's start with m_1 and take (K, J) in its domain, namely $D := \{(K, J) | K > 0, \Psi(K) \leq J < J_c\}$. We define $\tau(K, J) = \left(\frac{1}{J} - 1\right)\frac{J}{K} > 0$ and $\tilde{\phi}(m) := \phi(m)|_{[\tau(K,J),1]}$. Observe from (3.12) that,

$$m_1 = \frac{1}{J}\left[\underbrace{\operatorname{arctanh}(m_1)}_{\geq m_1} - Km_1^2\right]$$

$$\implies m_1 \geq \left(\frac{1}{J} - 1\right)\frac{J}{K} = \tau(K, J).$$

Hence, m_1 is the unique maximum point of $\tilde{\phi}(m)$, then by the Berge's maximum theorem A.2.1 (see [37,38]), m_1 is continuous for $(K, J) \in D$. To prove the smoothness of m_1 on the interior of its domain it's enough to show that $\phi''(m_1) < 0$ and then apply the implicit function theorem A.2.2 (see [31, 38]). Let $G(m) := \phi''(m)$ then,

$$\frac{\partial G}{\partial m}(m) = 2K - \frac{2m}{(1 - m^2)^2}$$

$$\frac{\partial^2 G}{\partial m^2}(m) = -\frac{2(3m^2 + 1)}{(1 - m^2)^3} < 0 \quad \forall\, m \in [0, 1)$$

and hence,

$$\begin{cases} G(0) = J - 1 < 0, \quad \forall\, J < J_c \\ G'(0) = 2K > 0, \quad \forall\, K > 0 \\ G''(0) = -2 \\ \lim_{m \to 1^-} G(m) = -\infty \quad \forall\, K > 0 \text{ and } J < J_c. \end{cases} \tag{3.18}$$

We want to prove that $G(m_1) < 0$ if $\Psi(K) < J < J_c$. Clearly since m_1 is a local maximiser it's enough to show that $G(m_1) \neq 0$. Recall that m_1 is the biggest positive solution of $\phi'(m) = 0$. It's easy to check that $G(m) = 0$ has at most two solutions. Assume by contradiction that $G(m_1) = 0$ if $\Psi(K) < J < J_c$, then $G(m) < 0$ or $G(m) > 0$ in a left neighbourhood of m_1.

- Suppose that $G(m) < 0$ in a left neighbourhood of m_1 then $G(m)$ cannot be always negative, otherwise $\phi'(m)$ is decreasing and, since $\phi'(0) = 0$ then $\phi'(m) = 0$ can not have more than one solution. This contradicts point $b)$ of Proposition 3.2.1. Therefore there exists an interval where $G(m) > 0$ but keeping in mind the properties of G in (3.18) and the fact that G is continuous, this implies that there are at least three solutions for $G(m) = 0$, but this is impossible because we already observed that $G(m) = 0$ has at most two solutions.

- Suppose that $G(m) > 0$ in a left neighbourhood of m_1, then $G(m) = 0$ has in addition to m_1 another solution that we denote by $\bar{m}$. Clearly $\bar{m} < m_3$ otherwise m_3 cannot satisfies $\phi'(m_3) = 0$. Therefore $G(m) \equiv \phi''(m) > 0$ if $m_3 < m < m_1$ and this contradicts the fact that $\phi'(m_3) = \phi'(m_1) = 0$.

Let's focus on m_2. Since for $K > 0$ and $J \geq J_c$, m_2 is the only maximiser of $\phi(m)$ it's enough to show that $\phi''(m_2) < 0$ to get smoothness of m_2 by using the implicit function theorem. Let's note that if $J \geq J_c$ then $\phi''(0) \geq 0$ and $\phi''(m) = 0$ has a unique positive solution. Furthermore, $\phi(m)$ has a unique maximum point, $m_2 \in (0, 1)$ and $\phi'(m_2) = 0$. It is easy to show that $\phi''(m_2) \neq 0$ by contradiction. Let's assume that $\phi''(m_2) = 0$ then $\phi''(m) > 0$ for $m < m_2$, therefore, using the Taylor's series expansion of $\phi(m)$ around m_2 one gets $\phi(m) > \phi(m_2)$ which contradicts the fact that m_2 is the global maximum.

Therefore by the implicit function theorem A.2.2, since $\phi''(m) \neq 0$ on the interior of the domains of m_1 and m_2, we can conclude that m_1 and m_2 are C^∞.

(b) We already proved that for any $i \in \{0, 1, 2\}$, $\phi''(m_i) < 0$ for suitable K, J. For the second part a direct computation shows that:

$$
\begin{aligned}
\frac{\partial}{\partial J}\phi(m_i) &= \left.\frac{\partial}{\partial m}\phi(m)\right|_{m=m_i}\frac{\partial m_i}{\partial J} + \frac{m_i^2}{2} \\
&= \frac{m_i^2}{2}
\end{aligned}
\tag{3.19}
$$

and similarly,

$$
\begin{aligned}
\frac{\partial}{\partial K}\phi(m_i) &= \left.\frac{\partial}{\partial m}\phi(m)\right|_{m=m_i}\frac{\partial m_i}{\partial K} + \frac{m_i^3}{3} \\
&= \frac{m_i^3}{3}.
\end{aligned}
\tag{3.20}
$$

Using the fact that $m_i, i = \{0,1,2\}$ are the stationary points of $\phi(\cdot)$, we have that $\dfrac{\partial m_i}{\partial K}$ satisfies

$$
\begin{aligned}
&\frac{1}{1-m_i^2}\frac{\partial m_i}{\partial K} - m_i^2 - 2Km_i\frac{\partial m_i}{\partial K} - J\frac{\partial m_i}{\partial K} = 0 \\
&\frac{\partial m_i}{\partial K}\left[\frac{1}{1-m_i^2} - 2Km_i - J\right] = m_i^2 \\
&\frac{\partial m_i}{\partial K} = -\frac{m_i^2}{\phi''(m_i)}
\end{aligned}
\tag{3.21}
$$

and similarly for $\dfrac{\partial m_i}{\partial J}$ one obtains

$$
\begin{aligned}
&\frac{1}{1-m_i^2}\frac{\partial m_i}{\partial J} - 2Km_i\frac{\partial m_i}{\partial J} - m_i - J\frac{\partial m_i}{\partial J} = 0 \\
&\frac{\partial m_i}{\partial J}\left[\frac{1}{1-m_i^2} - 2Km_i - J\right] = m_i \\
&\frac{\partial m_i}{\partial J} = -\frac{m_i}{\phi''(m_i)}
\end{aligned}
\tag{3.22}
$$

and this concludes the proof. $\qquad\square$

Remark 3.2.1. *Note that from (b) of Proposition 3.2.2, we can deduce that there are no degenerate maximum points of $\phi(m)$ for $K > 0$. Consequently, the only occurrence of a degenerate maximum arises for the critical point $(K_c, J_c) = (0,1)$, corresponding to a Curie-Weiss model, where the magnetisation takes the value $m_c = 0$.*

The critical point (K_c, J_c) is identified as the point (K, J) where $\phi(m)$ has a unique degenerate maximum point m_c, signifying that $\phi''(m_c)|_{(K_c,J_c)} = 0$. These critical values, m_c, K_c and J_c, can be determined analytically.

Recall from equation (3.11) that $\phi''(m) = 2Km + J - \frac{1}{1-m^2}$. Now, we define $\eta(m) = (1 - m^2)\phi''(m)$, leading to the expression:

$$\eta(m) = 2Km - 2Km^3 + J - Jm^2 - 1.$$

The magnetisation at the critical point, denoted as m_c, can be found as the root of $\eta'(m)$, while the coordinates of the critical point, represented by (K_c, J_c), can be obtained by simultaneously solving $\eta(m_c) = 0$ and $\eta'(m_c) = 0$.

Upon inspection, it is observed that $\eta'(m)$ has two roots that are not defined within the domain of m, i.e., $m \in (-1, 1)$, when $(K, J) \in (\mathbb{R}_+, \mathbb{R})$, and $m = 0$ when $K = 0$. Consequently, the magnetisation at the critical point for which $\phi''(m) = 0$ is $m = m_c = 0$. It is easy to check that solving $\eta(m_c)$ and $\eta'(m_c)$ results, $(K_c, J_c) = (0, 1)$.

3.2.2 Existence and uniqueness of phase transition

Under this section, we study which of the stationary points described by Proposition 3.2.1 is or are global maximisers of $\phi(m)$ and show the existence of phase transition. These stationary points are: $m_0(K, J), m_1(K, J)$, and $m_2(K, J)$. Let us start by recalling the result of Proposition 3.2.1:

- if $J < \Psi(K)$, then m_0 is the only global maximum point of ϕ,

- if $\Psi(K) < J < J_c$ then $\phi(m)$ has two local maximisers m_0 and m_1,

- if $J \geq J_c$ then m_2 is the only the global maximum point of $\phi(m)$.

To identify the coexistence of two global maximum points of $\phi(m)$ when $\Psi(K) < J < J_c$, consider the following function:

$$\Delta(K, J) = \phi(m_1, K, J) - \phi(m_0, K, J). \tag{3.23}$$

Notice that $\Delta(K, J)$ can be extended by continuity at $J = \Psi(K)$ and $J = J_c$. In the above equation we use $\phi(\cdot, K, J)$ to emphasis the dependence of ϕ on the parameters.

Proposition 3.2.3. *(Existence and uniqueness). For all $K > 0$ there exists a unique $J = \gamma(K) \in (\Psi(K), J_c)$ such that $\Delta(K, J) = 0$. Furthermore,*

$$\Delta(K, J) \begin{cases} < 0, & \text{if} \quad \Psi(K) \leq J < \gamma(K) \\ > 0, & \text{if} \quad \gamma(K) < J \leq J_c. \end{cases} \tag{3.24}$$

Proof. Let us start by observing that

- $\Delta(K, \Psi(K)) < 0$, since for $J = \Psi(K)$, m_0 is the only maximum point of $\phi(m, K, J)$.

- $\Delta(K, J_c) > 0$, since $\lim_{J \to 1^-} m_1(K, J) = m_2(K, 1)$ and $m_2(K, 1)$ is the only global maximum for $\phi(m, K, J)$.

Now, by continuity of $\phi(m)$ and m_1, we have that $J \mapsto \Delta(K, J)$ is a continuous function, and then the existence of the *wall* $J = \gamma(K)$ follows from the application of the intermediate value theorem. For the uniqueness part we observe that $J \mapsto \Delta(K, J)$ is strictly increasing. Indeed from Proposition 3.2.2 we know that $\phi(m_1), m_1$ are smooth functions and

$$\begin{aligned} \frac{\partial \Delta}{\partial J}(K, J) &= \frac{\partial}{\partial J}\phi(m_1) - \frac{\partial}{\partial J}\phi(m_0) \\ &= \frac{1}{2}m_1{}^2 - \frac{1}{2}m_0{}^2 \\ &= \frac{1}{2}m_1{}^2 > 0 \end{aligned} \tag{3.25}$$

for $J \in (\Psi(K), J_c)$. $\qquad\square$

Corollary 3.2.1. *The function $\phi(m)$ has a unique global maximum point $m^*(K, J)$ given by:*

$$m^*(K, J) := \begin{cases} m_0 = 0, & \text{if} \quad J < \gamma(K) \\ m_1(K, J), & \text{if} \quad \gamma(K) < J < J_c \\ m_2(K, J), & \text{if} \quad J \geq J_c \end{cases} \tag{3.26}$$

where the function $\gamma(K)$ is defined by Proposition 3.2.3 and $\phi''(m^*) < 0$.

Note that on the curve γ there are two global maximum points of $\phi(m)$. Let us define

$$\bar{\gamma}(K) := \begin{cases} \gamma(K), & \text{if} \quad K > 0 \\ J_c, & \text{if} \quad K = K_c = 0. \end{cases} \tag{3.27}$$

Therefore by Proposition 3.2.2 one can conclude that $m^*(K, J)$ is continuous on its domain $(\mathbb{R}_+ \times \mathbb{R}) \backslash \gamma$ and it is C^∞ on $(\mathbb{R}_+ \times \mathbb{R}) \backslash \overline{\gamma}$. Moreover the following properties holds:

Proposition 3.2.4. *(Regularity properties.) The function $\overline{\gamma}(K)$ is $C^\infty(\mathbb{R}_+ \backslash \{0\})$ and at least C^1 for $K = 0$. In particular,*

$$\gamma\,'(K) := -\frac{2}{3} m_1(K, \gamma(K)) \qquad \forall \quad K > 0 \tag{3.28}$$

and

$$\overline{\gamma}\,'(K_c) := -\frac{2}{3} m_c. \tag{3.29}$$

Proof. i. We begin by showing that $\gamma(K) \in C^\infty(\mathbb{R}_+)$. By Proposition 3.2.3, $J = \gamma(K)$ is a unique solution of the equation

$$\Delta(K, J) = 0,$$

where Δ is defined by equation (3.23) for $\Psi(K) \leq J < J_c$ and $K > 0$. Furthermore, observe that Δ is C^∞ in its domain by the smoothness of ϕ and m_1. Recall from the proof of Proposition 3.2.3 that

$$\frac{\partial}{\partial J} \Delta(K, J) \neq 0 \qquad \forall \quad (K, J)\,\text{s.t.}\ \ J = \gamma(K), \tag{3.30}$$

hence, by the implicit function theorem A.2.1 $\gamma(K) \in C^\infty(\mathbb{R}_+)$. Therefore

$$\Delta(K, \gamma(K)) \equiv 0 = \frac{d}{dK} \Delta(K, \gamma(K))$$
$$= \frac{\partial \Delta}{\partial J}(K, \gamma(K))\gamma'(K) + \frac{\partial \Delta}{\partial K}(K, \gamma(K)) \tag{3.31}$$
$$\implies \gamma\,'(K) = -\frac{\partial \Delta}{\partial K} \Big/ \frac{\partial \Delta}{\partial J}(K, \gamma(K)).$$

From equations (3.19) and (3.20), we have that,

$$\frac{\partial \Delta}{\partial K} = \frac{m_1^3}{3} - \frac{m_0^3}{3} \qquad \text{and} \qquad \frac{\partial \Delta}{\partial J} = \frac{m_1^2}{2} - \frac{m_0^2}{2},$$

hence

$$\gamma\,'(K) = -\frac{2}{3} m_1(K, \gamma(K)) \tag{3.32}$$

since $m_0(K, \gamma(K)) = 0$, $\forall K > 0$. Notice that, by (3.7), $m_1(K, \gamma(K)) \xrightarrow[K \to \infty]{} 1$ which implies that

$$\lim_{K \to \infty} \gamma\,'(K) = -\frac{2}{3}.$$

A consequence of this property is that also when $J < 0$ (antiferromagnetic case) and very large there is always going to be phase transition between a polarised and unpolarised state.

ii. Now we prove that the extended function $\overline{\gamma} \in C^1(\mathbb{R}_+)$. Recall that $\gamma(K) \in [\Psi(K), J_c]$ and observe that $\lim_{K \to K_c^+} \Psi(K) = J_c$ then

$$\lim_{K \to K_c^+} \gamma(K) = J_c$$

which implies that $\overline{\gamma}$ is continuous at K_c. Now we have that

$$\gamma'(K) = -\frac{2}{3}m_1(K, \gamma(K)) \xrightarrow[K \to K_c^+]{} -\frac{2}{3}m_c = 0 \tag{3.33}$$

which implies that $\overline{\gamma}'(K_c) = -\frac{2}{3}m_c = 0$ by the application of mean value theorem.

$\square$

3.2.3   Critical exponent

Proof of Proposition 3.1.3

Under this section we study the behaviour of the solutions of the mean-field equation (3.12) near the critical point $(K_c, J_c) = (0, 1)$.

Proof. Let us start with the case $\alpha \geq 0$. This implies from equation (3.8) that $J(K) \geq J_c = 1$ and then $m^*(K) \equiv m_2(K, J(K))$ where m_2 is the only positive solution of the consistency equation (3.12).

Clearly $m^*(K) \to 0$ as $K \to 0^+$, hence by Taylor's expansion we have that

$$m^*(K) = J(K)m^*(K) + Km^*(K)^2 - \frac{J(K)^3 m^*(K)^3}{3} + \mathcal{O}(m^*(K)^4)$$
$$= (1 + \alpha K)m^*(K) + Km^*(K)^2 - \frac{(1 + \alpha K)^3 m^*(K)^3}{3} + \mathcal{O}(m^*(K)^4). \tag{3.34}$$

Hence

$$\frac{(1 + \alpha^3 K^3 + 3\alpha^2 K^2 + 3\alpha K)m^*(K)^2}{3} - Km^*(K) - \alpha K = \mathcal{O}(m^*(K)^3).$$

From the above equation, neglecting higher order corrections we have

$$m^*(K) \sim \frac{3}{2}\left(K + \sqrt{K^2 + \frac{4}{3}\alpha K + 4\alpha^2 K^2}\right). \tag{3.35}$$

Now, if $\alpha > 0$ then

$$m^*(K) \sim \sqrt{3\alpha K}. \tag{3.36}$$

Otherwise if $\alpha = 0$, then

$$m^*(K) \sim \frac{3}{2}\left(K + \sqrt{K^2}\right) \sim 3K. \tag{3.37}$$

This implies that the behaviour of the magnetisation when approaching the critical point is linear in K.

Now, let's turn on the case $\alpha < 0$. From Proposition 3.2.4 we know that $\gamma(K)$ is at least C^1 at $K = 0$. Since $\lim_{K \to 0^+} \gamma'(K) = 0$ we know that if $J(K) < \gamma(K)$ for K small enough, then $m^*(K) \equiv m_0(K, J) = 0$.

$\square$

3.3   Fluctuations of the magnetisation

In this section, we delve into the study of the asymptotic distribution of the magnetisation $m_N(\sigma)$ for a given configuration σ of spins distributed according to the equation (3.2). Building upon the extensive research conducted in [23], which focuses on the mean-field Ising model with a p-spin $(p > 2)$ interaction, we adopt the formalism introduced in that work to investigate the fluctuation properties of the magnetisation density of the mean-field Ising model with both cubic and quadratic interactions. Specifically, we examine the limiting behaviour of the magnetisation $m_N(\sigma)$ in cases where $\phi(m)$ exhibits a unique global maximum, more than one global maximum point, and at the critical point.

For technical purposes, we consider slightly perturbed parameter values (K, J, h_N) in the proofs, where $h_N \xrightarrow[N \to \infty]{} h = 0$ for some yet-to-be-determined sequence. Additionally, it is essential to note that the partition function Z_N, which lacks a closed form, plays a crucial role in the probability mass function (3.2) of the magnetisation density $m_N(\sigma)$. Therefore, obtaining a precise approximation of Z_N is necessary to compute the limiting properties of $m_N(\sigma)$. The study of (3.12) allows us to identify the regions in the (K, J) plane where $\phi(m)$ has a unique global maximum point $m^*(K, J)$ and where it has multiple global maximum points. Figure 3.5 shows that, aside the open curve defined by the implicit equation $J = \gamma(K)$, the function $m^*(K, J)$ in (3.12) is unique and continuous in the (K, J) plane. Moreover, $m^*(K, J)$ is a smooth function outside of the curve $\gamma \cup (K_c, J_c)$.
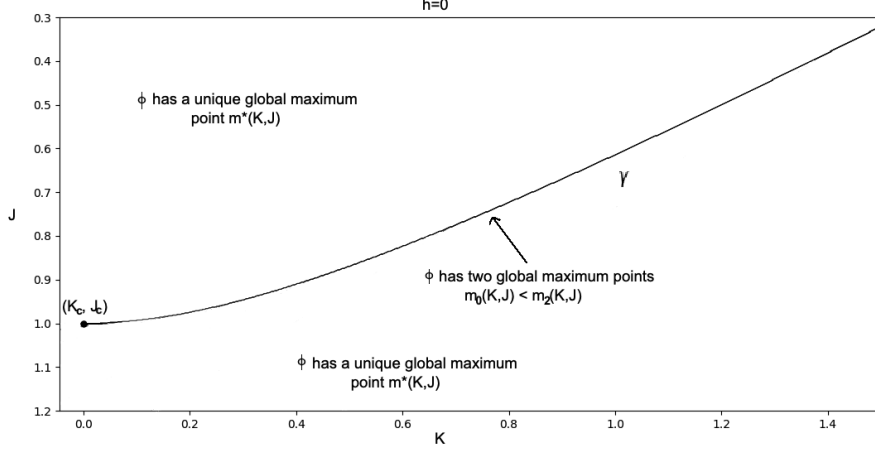
Figure 3.5: The coexistence curve γ and the critical point (K_c, J_c) in the (K, J) plane.

The following theorem presents the law of large numbers and the central limit theorem for the distribution of $m_N(\sigma)$ under the Boltzmann-Gibbs measure (3.2).

Theorem 3.3.1 (Asymptotic distribution of the magnetisation). *Consider the Hamiltonian in* (3.1)*, then the following holds:*

1. *For $(K, J) \in (\mathbb{R}_+ \times \mathbb{R}) \backslash (\gamma \cup (K_c, J_c))$ the function $\phi(m)$ in* (3.4) *has a unique global maximiser m^* such that $\phi''(m^*) < 0$ and*

$$m_N \xrightarrow[N \to \infty]{\mathcal{D}} \delta_{m^*}. \tag{3.38}$$

   Moreover,

$$N^{\frac{1}{2}}(m_N - m^*) \xrightarrow[N \to \infty]{\mathcal{D}} \mathcal{N}\left(0, -\frac{1}{\phi''(m^*)}\right). \tag{3.39}$$

2. *Given $(K, J) \in \gamma$ we denote by $m_0 < m_1$ the two global maximisers of $\phi(m)$. For $i \in \{0, 1\}$ we define the quantity*

$$\rho_i := \frac{[(m_i^2 - 1)\phi''(m_i)]^{-\frac{1}{2}}}{[(m_0^2 - 1)\phi''(m_0)]^{-\frac{1}{2}} + [(m_1^2 - 1)\phi''(m_1)]^{-\frac{1}{2}}}. \tag{3.40}$$

   Then we have that

$$m_N \xrightarrow[N \to \infty]{\mathcal{D}} \sum_{i \in \{0,1\}} \rho_i \delta_{m_i}. \tag{3.41}$$

Moreover let $A_i \subseteq [-1, 1]$ be an interval containing m_i in its interior such that $\phi(m_i) > \phi(m)$ for all $m \in cl(A_i)\backslash\{m_i\}$, then

$$N^{\frac{1}{2}}(m_N - m_i)\big|\{m_N \in A_i\} \xrightarrow[N\to\infty]{\mathcal{D}} \mathcal{N}\left(0, -\frac{1}{\phi''(m_i)}\right). \qquad (3.42)$$

3. At the critical point (K_c, J_c), we have that

$$m_N \xrightarrow[N\to\infty]{\mathcal{D}} \delta_0. \qquad (3.43)$$

Moreover,

$$N^{\frac{1}{4}} m_N \xrightarrow[N\to\infty]{\mathcal{D}} C \exp\left(\frac{\phi^{(4)}(0)}{24}x^4\right) dx = C \exp\left(\frac{-x^4}{12}\right) dx, \qquad (3.44)$$

where $\phi^{(4)}(0) = -2$ denote the fourth derivative of $\phi(m)$ evaluated at $m = 0$ and

$$C^{-1} = \int_{-\infty}^{\infty} \exp\left(\frac{-x^4}{12}\right) dx = \frac{\sqrt[4]{3}\,\Gamma(\frac{1}{4})}{\sqrt{2}}.$$

3.3.1   Asymptotic distribution of the magnetisation

In this section, we will present a detailed proof of Theorem 3.3.1, building upon the work in [23]. To do this we provide a brief description of what will be involved in the details of the proof based on the behaviour of ϕ with respect to its maximisers:

1. Uniqueness region ($\phi(m, K, J)$ has a unique global maximiser): We initiate the proof by establishing a concentration inequality for m_N in an asymptotically vanishing neighbourhood of m^*. In this case, the partition function is constrained to the spin configurations where m_N falls within a concentration neighbourhood of m^*. Subsequently, we derive an asymptotic approximation expansion of the partition function, which becomes instrumental in proving the central limit theorem.

2. Multiple maximisers of $\phi(m, K, J)$: We adopt a similar approach to prove the law of large numbers and the central limit theorem in scenarios where $\phi(m, K, J)$ has two global maximisers, denoted as m_i. For this case, we establish a conditional concentration inequality for m_N, considering its concentration at each of the maximisers m_i when m_N lies in a vanishing neighbourhood of m_i.

3. Critical point (K_c, J_c): At the critical point, where $\phi''(m_c, K_c, J_c) = 0$, we follow a similar approach as before, but with appropriate modifications to account for the critical behaviour.

It worth to mention that the proof of Theorem 3.3.1 will be attacked in three main parts, each corresponding to the nature of the solution of the consistency equation (3.12), just as mentioned above.

Throughout the analysis of the asymptotic distribution of m_N, we will refer to the general remark below, Remark 3.3.2, that will be used to facilitate our study.

Remark 3.3.2. *Consider a mean-field spin model with energy density g_N, namely*

$$H_N(\sigma) = -Ng_N(m_N(\sigma)), \ \ \sigma \in \{-1,1\}^N \tag{3.45}$$

where $m_N = \frac{1}{N}\sum_{i \leq N}\sigma_i$ is the magnetisation density. We assume that (g_N) is a sequence of continuous functions $g_N : [-1,1]^N \to \mathbb{R}$ converging uniformly to g. We assume also that g_N has bounded derivatives up to order 4 converging uniformly to g', g'', g''', g''''. We denote the law of the magnetisation under the Gibbs measure by

$$\mu_N(\sigma) = \frac{e^{-H_N(\sigma)}}{Z_N}. \tag{3.46}$$

The partition function Z_N can be written as

$$Z_N = \sum_{x \in R_N} A_N(x)e^{Ng_N(x)}, \tag{3.47}$$

where $R_N = \{-1 + \frac{2k}{N}, k = 0, \ldots, N\}$ and $A_N(x) = \text{card}\{\sigma \in \{-1,1\}^N : m_N(\sigma) = x\}$. Now, it follows from Lemma 2.2.1 that, for some universal constant L

$$\frac{1}{L\sqrt{N}}e^{-NI(x)} \leq A_N \leq e^{-NI(x)} \tag{3.48}$$

where $I(x)$ is defined in (3.6). Define the sequence ϕ_N as

$$\phi_N(x) = g_N(x) - I(x). \tag{3.49}$$

Notice the assumption on (g_N) that $\phi_N \to \phi = g - I$ uniformly on $(-1,1)$, as well as its derivarites up to order 4 on $(-1,1)$. Let observe that since there are $N-$spin particles, m_N can assume explicitly $N+1$ different values for $K > 0$ over the defined range R_N.

Lemma 3.3.1. *Let (g_N) be a sequence of continuous functions $g_N : [-1,1]^N \to \mathbb{R}$ converging uniformly to f. Suppose that g_N has bounded derivatives up to order 4 which converges uniformly to g', g'', g''', g''''. Then $\phi_N \to \phi$ uniformly.*

Proof. Note that for any generic function g_N, for a mean-field spin model of the type studied here, the map $x \mapsto g_N(x)$ is continuous for every N and uniformly bounded. For instance, in this work, (2.12) is uniformly bounded by $|\frac{K}{3} + \frac{J}{2} + h|$. Observe further that m_N is a closed and bounded, i.e., compact, subset of $\mathbb{R}$. Hence, it follows from Theorems 7.13 and 7.24 of [31] that g_N is equicontinuous. Now since g_N is uniformly bounded and equicontinuous, $g_N \to g$ uniformly. Hence, by extension, it follows from the convergence of g_N to g that $\phi_N \to \phi$ uniformly.

The convergence of g_N to its derivatives follows directly from Theorem 7.17 of [31]. □

Part 1: Uniqueness region

Suppose we are in the domain of (K, J) where $m^*(K, J)$ is the unique global maximiser of $\phi(m, K, J)$. Now, for a sequence $h_N = \frac{t}{\sqrt{N}}$ converging to 0 as $N \to \infty$, define $\phi_N(x) := \phi(x) + \frac{t}{\sqrt{N}}x$, where $\phi(x)$ has its usual representation as illustrated in (3.4). Suppose that $\phi_N(m)$ has a unique global maximiser m_N^* such that as $N \to \infty$, $m_N^* \to m^*(K, J)$ (see Lemma 3.3.2), we can define $B_{N,\alpha}$ for $\alpha \in (0, 1)$

$$B_{N,\alpha} = \left(m_N^* - N^{-\frac{1}{2}+\alpha}, m_N^* + N^{-\frac{1}{2}+\alpha} \right) \qquad (3.50)$$

where $m_N(\sigma)$ concentrates around m_N^* with respect to the Boltzmann Gibbs measure (3.2) at rate $N^{-\frac{1}{2}+\alpha}$.

The following lemma contains concentration properties of the magnetisation density m_N w.r.t. the Gibbs measure μ_N and asymptotic expansions of the partition function Z_N. For any $\alpha > 0$ and $y \in \mathbb{R}$ we denote by $B_{N,\alpha}(y)$ the open ball with center y and radius $N^{-1/2+\alpha}$ and by $B_{N,\alpha}^c(y)$ its complement.

Lemma 3.3.2. *Assume that $\phi(m)$ has a unique global maximiser $m^* \in (-1, 1)$ such that $\phi''(m^*) < 0$. Then for N large enough ϕ_N has a unique maximiser $m_N^* \to m^*$ such that $\phi_N''(m_N^*) < 0$. Moreover for $\alpha \in \left(0, \frac{1}{6}\right]$ and N large enough we have that*

$$\mu_N^{KJ}(m_N(\sigma) \in B_{N,\alpha}^c) = \exp\left\{ \frac{1}{2}N^{2\alpha}\phi''(m^*) \right\}\mathcal{O}(N^{\frac{3}{2}}), \qquad (3.51)$$

and the partition function (3.47) *can be expanded as,*

$$Z_N = \frac{e^{N\phi_N(m_N^*)}}{\sqrt{(m_N^{*2} - 1)\phi_N''(m_N^*)}} \left(1 + \mathcal{O}\left(N^{-\frac{1}{2} + \alpha}\right)\right). \tag{3.52}$$

Proof. Let m_N^* be any maximiser of ϕ_N which exists since $[-1, 1]$ is compact. Then there exists a subsequence $\{N_l\}_{l \geq 1}$ such that $m_{N_l}^*$ converges to some y. We know that $\phi_{N_l}(m_{N_l}^*) \geq \phi_{N_l}(m)$ for all $m \in [-1, 1]$, therefore by uniform convergence and taking $l \to \infty$ we obtain $\phi(y) \geq \phi(m)$ for all $m \in [-1, 1]$ and this implies that y is a global maximiser of $\phi(x)$. But m^* is the unique global maximiser of $\phi(m)$, hence $y = m^*$.

Since $\phi''(m^*) < 0$ one has, for ϵ small enough, $\phi(m) < 0$ for any $m \in [m^* - \epsilon, m^* + \epsilon]$. Let m_N and y_N be two global maximisers of ϕ_N. We already know that $m_N \to m^*$ and $y_N \to m^*$. Therefore for N large enough $m_N, y_N \in [m^* - \epsilon, m^* + \epsilon]$. Using the fact that ϕ_N'' converges uniformly to ϕ'' one can show that for N large enough ϕ_N is strongly convex on $[m^* - \epsilon, m^* + \epsilon]$ and therefore has unique maximiser which implies that $x_N = y_N$.

In order to lighten the notation set $B_{N,\alpha} = B_{N,\alpha}(m_N^*)$. From equations (3.46), (3.47) and (3.48) we have that,

$$\mu_N^{KJ}(m_N \in B_{N,\alpha}^c) = \frac{\sum_{m \in R_N \cap B_{N,\alpha}^c} A_N \exp\left\{N\left(\frac{K}{3}m^3 + \frac{J}{2}m^2 + h_N m\right)\right\}}{\sum_{m \in R_N} A_m \exp\left\{N\left(\frac{K}{3}m^3 + \frac{J}{2}m^2 + h_N m\right)\right\}}$$

$$\leq \frac{\sum_{m \in R_N \cap B_{N,\alpha}^c} \exp\left\{N\left(\frac{K}{3}m^3 + \frac{J}{2}m^2 + h_N m - I(m)\right)\right\}}{\sum_{m \in R_N} \frac{1}{L\sqrt{N}} \exp\left\{N\left(\frac{K}{3}m^3 + \frac{J}{2}m^2 + h_N m - I(m)\right)\right\}}$$

$$= \frac{L N^{\frac{1}{2}} \sup_{x \in B_{N,\alpha}^c} e^{N\phi_N(x)}}{\sup_{x \in [-1,1]} e^{N\phi_N(x)}}$$

$$= \exp\left\{N\left(\sup_{x \in B_{N,\alpha}^c} \phi_N(x) - \phi_N(m_N^*)\right)\right\} \mathcal{O}(N^{\frac{3}{2}}). \tag{3.53}$$

In the third equality, Laplace heuristic approximation of the sum is used leading to taking the supremum. Now, by Lemma B.11 of [23] it is known that for large N, and $x \in B_{N,\alpha}$, m_N^* is the unique maximiser of $\phi_N(x)$ and if $x \in B_{N,\alpha}^c$ then from (3.50), the maximiser of $\phi_N(x)$ is either $m_N^* - N^{-\frac{1}{2} + \alpha}$ or $m_N^* + N^{-\frac{1}{2} + \alpha}$ due to the

concaveness of $\phi_N(x)$. This implies that $\sup_{x \in B_{N,\alpha}^c} \phi_N(x)$ is either $\phi_N(m_N^* - N^{-\frac{1}{2}+\alpha})$ or $\phi_N(m_N^* + N^{-\frac{1}{2}+\alpha})$. Note that $\phi_N'(m_N^*) = 0$ since m_N^* is the maximiser and $\phi_N^{(3)}(m_N^*)$ is uniformly bounded on any closed interval in $(-1, 1)$. Hence by a second-order Taylor expansion of $\phi(m_N^* \pm N^{-\frac{1}{2}+\alpha})$ at the point m_N^*, we have that

$$\phi(m_N^* \pm N^{-\frac{1}{2}+\alpha}) = \phi_N(m_N^*) + \frac{1}{2}N^{-1+2\alpha}\phi_N''(m_N^*) + \mathcal{O}(N^{-\frac{3}{2}+3\alpha}). \qquad (3.54)$$

Notice that $\phi''(m_N^*) \xrightarrow[N \to \infty]{} \phi''(m^*) < 0$. This completes the first part of the proof of Lemma 3.3.2 following from equation (3.53).

To complete the proof of Lemma 3.3.2, let's start by observing that almost all the contribution to Z_N comes from spin configurations having magnetisation density in a vanishing neighbourhood of the maximiser m_N^*, i.e., $\mu_N^{KJ}(m_N(\sigma) \in B_{N,\alpha}) = 1 - \mathcal{O}(e^{-N^\alpha})$.

Let's observe that

$$\mu_N^{KJ}(m_N(\sigma) \in B_{N,\alpha}) = \frac{1}{Z_N} \sum_{m \in R_N \cap B_{N,\alpha}} \binom{N}{\frac{N(1+m)}{2}} \exp\left\{N\left(\frac{K}{3}m^3 + \frac{J}{2}m^2 + h_N m\right)\right\}. \qquad (3.55)$$

Hence,

$$Z_N = (1 + \mathcal{O}(e^{-N^\alpha})) \sum_{m \in R_N \cap B_{N,\alpha}} \underbrace{\binom{N}{\frac{N(1+m)}{2}} \exp\left\{N\left(\frac{K}{3}m^3 + \frac{J}{2}m^2 + h_N m\right)\right\}}_{=\zeta(m)} \qquad (3.56)$$

where $\zeta : [-1, 1] \to \mathbb{R}$. With this, one can accurately approximate the partition function over all configurations σ whose mean lies within a vanishing neighbourhood of m^* using standard approximation techniques.

We begin by applying the Laplace approximation of an integral over a shrinking interval $B_{N,\alpha}$ via the Riemann approximation of the sum in equation (3.56) with an integral and the binomial coefficient can be approximated by the Stirling's approximation method. Notice that by the Riemann approximation of the sum, we have that

$$\left| \int_{B_{N,\alpha}} \zeta(x)dx - \frac{2}{N} \sum_{m \in R_N \cap B_{N,\alpha}} \zeta(m) \right| \leq \frac{1}{2}(N^{-\frac{1}{2}+\alpha}) \cdot N^{-1} \sup_{x \in B_{N,\alpha}} |\zeta'(x)|$$

$$= \mathcal{O}(N^{-\frac{1}{2}+\alpha} \cdot N^{-1} \cdot N^{\frac{1}{2}+\alpha})\zeta(m_N^*) \qquad (3.57)$$

$$= \mathcal{O}(N^{-1+2\alpha})\zeta(m_N^*).$$

Observe that the binomial coefficient in (3.56) can be approximated by the Stirling's approximation method which gives

$$\binom{N}{\frac{N(1+m)}{2}} = \sqrt{\frac{2}{\pi N(1-m^2)}}\, e^{-NI(m)}\,(1+\mathcal{O}(N^{-1})) \tag{3.58}$$

and hence,

$$\zeta(m) = \sqrt{\frac{2}{\pi N(1-m^2)}}\, e^{N\phi_N(m)}\,(1+\mathcal{O}(N^{-1})). \tag{3.59}$$

It follows from equations (6.12), (3.58), (3.59) and the Laplace approximation of an integral over a shrinking interval $B_{N,\alpha}$ that:

$$\sum_{m\in R_N\cap B_{N,\alpha}} \zeta(m) = \frac{N}{2}\int_{B_{N,\alpha}} \zeta(x)dx + \mathcal{O}(N^{2\alpha})\zeta(m_N^*)$$

$$= \frac{N}{2}\int_{B_{N,\alpha}} \sqrt{\frac{2}{\pi N(1-x^2)}}\, e^{N\phi_N(x)}(1+\mathcal{O}(N^{-1}))dx$$

$$\quad + \mathcal{O}(N^{2\alpha})\cdot\left[\sqrt{\frac{2}{\pi N(1-m_N^{*2})}}\, e^{N\phi_N(m_N^*)}\,(1+\mathcal{O}(N^{-1}))\right]$$

$$= \frac{\sqrt{N}}{2}(1+\mathcal{O}(N^{-1}))\int_{B_{N,\alpha}} e^{N\phi_N(x)}\sqrt{\frac{2}{\pi(1-x^2)}}dx$$

$$\quad + \sqrt{\frac{2}{\pi N(1-m_N^{*2})}}\, e^{N\phi_N(m_N^*)}\,(1+\mathcal{O}(N^{-1}))\mathcal{O}(N^{2\alpha})$$

$$= \frac{\sqrt{N}}{2}\sqrt{\frac{2\pi}{N|\phi_N''(m_N^*)|}}\sqrt{\frac{2}{\pi(1-m_N^{*2})}}\, e^{N\phi_N(m_N^*)}\,(1+\mathcal{O}(N^{-\frac{1}{2}+3\alpha}))$$

$$\quad + \sqrt{\frac{2}{\pi N(1-m_N^{*2})}}\, e^{N\phi_N(m_N^*)}\,(1+\mathcal{O}(N^{-1}))\mathcal{O}(N^{2\alpha})$$

$$= \frac{e^{N\phi_N(m_N^*)}}{\sqrt{(m_N^{*2}-1)\phi_N''(m_N^*)}}\cdot(1+\mathcal{O}(N^{-\frac{1}{2}+3\alpha})).$$

$$\tag{3.60}$$

From equations (3.56) and (3.60), we have that

$$Z_N = (1+\mathcal{O}(e^{-N^\alpha}))\cdot(1+\mathcal{O}(N^{-\frac{1}{2}+3\alpha}))\cdot\frac{e^{N\phi_N(m_N^*)}}{\sqrt{(m_N^{*2}-1)\phi_N''(m_N^*)}}$$

$$= \frac{e^{N\phi_N(m_N^*)}}{\sqrt{(m_N^{*2}-1)\phi''(m_N^*)}}\cdot(1+\mathcal{O}(N^{-\frac{1}{2}+3\alpha}))$$

$$\tag{3.61}$$

This completes the proof of Lemma 3.3.2 and we use this results to prove the central limit theorem of $m_N(\sigma)$.   □

The following results make use of the arguments of Lemma 3.3.2 to proof the first part of Theorem 3.3.1, thus the law of large numbers and the central limit theorem of the distribution of m_N in the uniqueness regime of the consistency equation (3.12).

Proof. **CLT in the Uniqueness region**

By proposition 3.1.2 we know that if $(K, J) \in (\mathbb{R}_+ \times \mathbb{R}) \backslash (\gamma \cup (K_c, J_c))$ then $\phi(m)$ has a unique global maximiser m^* with $\phi''(m^*) < 0$. It's easy to check that $\phi(m)$ satisfies the hypothesis of Lemma 3.3.2, therefore (3.51) gives concentration inequality for m_N in a suitable neighbourhood of m^* under the probability measure (3.2). More precisely, for any $\alpha \in (0, \frac{1}{6}]$ and N large enough one has

$$\mu_N^{KJ}(m_N \in B_{N,\alpha}^c(m^*)) = \exp\left\{\frac{1}{2}N^{2\alpha}\phi''(m^*)\right\}\mathcal{O}(N^{\frac{3}{2}}) \qquad (3.62)$$

where $B_{N,\alpha}^c(m^*) = \{m \in \mathbb{R} : |m - m^*| \leq N^{-\frac{1}{2}+\alpha}\}$. Therefore the convergence in distribution (3.38) follows from (3.62) by standard approximation arguments.

Now, in order to obtain the central limit theorem of m_N, we will show that the moment generating function of $N^{\frac{1}{2}}(m_N - m^*)$ with respect to the measure μ_N converges pointwise to the moment generating function of the distribution $\mathcal{N}\left(0, -\frac{1}{\phi''(m^*)}\right)$. To obtain the central limit of m_N it is enough to compute the limit of the moment generating function of $N^{\frac{1}{2}}(m_N - m^*)$. For a fixed $t \in \mathbb{R}$, the moment generating function of $N^{\frac{1}{2}}(m_N - m^*)$ can be expressed as

$$\mathbb{E}\left[e^{tN^{\frac{1}{2}}(m_N - m^*)}\right] = e^{-tN^{\frac{1}{2}}m^*}\frac{\tilde{Z}_N(t)}{Z_N} \qquad (3.63)$$

where $\tilde{Z}_N(t)$ is a perturbed partition function associate to the Hamiltonian

$$\tilde{H}_N(\sigma) = H_N^{KJ}(\sigma) + \sqrt{N}\, t\, m_N(\sigma). \qquad (3.64)$$

We start by noticing that $\tilde{H}_N(\sigma) = Ng_N(m_N(\sigma))$ where $g_N(x) = \frac{K}{3}x^3 + \frac{J}{2}x^2 + \frac{t}{\sqrt{N}}x$ and then g_N together with all its derivatives tends uniformly to $g(x) = \frac{K}{3}x^3 + \frac{J}{2}x^2$ as introduced in Remark 3.3.2.

Observe that Lemma 3.3.2 provides the asymptotic expansion of Z_N and similar applies to $\tilde{Z}_N(t)$. Now, using the fact that $m_N^*(t) \to m^*$, the fractional term on the

right side of equation (3.63) as $N \to \infty$ can be rewritten as

$$\frac{\bar{Z}_N(t)}{Z_N} = e^{N\left(\phi_N(m_N^*(t)) - \phi(m^*)\right)} (1 + \mathcal{O}(N^{-\frac{1}{2}+3\alpha})), \tag{3.65}$$

where $\phi_N(x) = g_N(x) - I(x)$ and for N large enough $m_N^*(t)$ is its unique maximiser. Let's observe that $m_N^*(0) = m^*$ and $m_N^*(t)$ satisfies the equation

$$m_N^*(t) = \tanh\left(Km_N^*(t)^2 + Jm_N^*(t) + \frac{t}{\sqrt{N}}\right). \tag{3.66}$$

Hence, it's easy to check that $\frac{\partial m_N^*(t)}{\partial t}\big|_{t=0} = -\frac{1}{\sqrt{N}\phi''(m^*)}$ and $\frac{\partial^2 m_N^*(t)}{\partial t^2} = \mathcal{O}(N^{-1})$. Therefore the Taylor's expansion of $m_N^*(t)$ around $t = 0$ is

$$m_N^*(t) = m_N^*(0) - \frac{t}{\sqrt{N}\phi''(m^*)} + \mathcal{O}(N^{-1}). \tag{3.67}$$

Following from the definition of $\phi(m)$ in equation (3.4), one can easily check that $\phi_N(m_N^*(t)) = \phi(m_N^*(t)) + \frac{t}{\sqrt{N}}m_N^*(t)$. Hence,

$$\begin{aligned} N\left(\phi_N(m_N^*(t)) - \phi(m^*)\right) &= N\left(\phi(m_N^*(t)) + \frac{t}{\sqrt{N}}m_N^*(t) - \phi(m^*)\right) \\ &= N\left(\phi(m_N^*(t)) - \phi(m^*)\right) + t\sqrt{N}m_N^*(t) \end{aligned} \tag{3.68}$$

and a Taylor expansion of $\phi(m_N^*(t))$ around m^* gives

$$N\left(\phi(m_N^*(t) - \phi(m^*)\right) = \frac{N}{2}\left(m_N^*(t) - m^*\right)^2 \phi''(m^*) + o(1). \tag{3.69}$$

From (3.67) we know that

$$m_N^*(t) - m^* = -\frac{t}{N^{\frac{1}{2}}\phi''(m^*)} + \mathcal{O}(N^{-1}) \tag{3.70}$$

and consequently,

$$t\sqrt{N}m_N^*(t) = t\sqrt{N}m^*(K,J) - \frac{t^2}{\phi''(m^*)} + \mathcal{O}(N^{-1}). \tag{3.71}$$

Hence, it implies from (3.68) that,

$$N\left(\phi_N(m_N^*(t)) - \phi(m^*)\right) = t\sqrt{N}m^* - \frac{t^2}{2\phi''(m^*)} + \mathcal{O}(N^{-1}) \tag{3.72}$$

and by (3.65) the limiting moment generating function is given as

$$\lim_{N\to\infty} \mathbb{E}\left[e^{tN^{\frac{1}{2}}(m_N(\sigma) - m^*)}\right] = \exp\left\{-\frac{t^2}{2\phi''(m^*)}\right\}, \tag{3.73}$$

which implies (3.39) by noticing that the moment generating function of $\mathcal{N}(0, -\frac{1}{\phi(m^*)})$ evaluated at t is given by the constant in the limiting expectation (3.73). $\square$

Part 2: Multiple maximisers

Let's recall that on the coexistence curve γ, there are two global maximisers $m_i(K, J)$ of $\phi(m, K, J)$ for $i \in \{0, 1\}$. Similarly we consider a perturbed parameter $h_N = tN^{-\frac{1}{2}}$ converging to 0 as $N \to \infty$ and let's define $\phi_N(m_i) := \phi(m_i, h_N)$ such that $m_{i,N}$ is a local maximiser of $\phi_N(x)$ and $m_{i,N} \to m_i$ as N approach infinity, i.e., $N \to \infty$.

When there are more than one local maximiser, the Boltzmann-Gibbs probability distribution becomes multimodal and centered around each local maxima. Hence, the distribution has to be defined on clusters of spins around each local maxima or defined over subsets of the range of the magnetisation which contains each of the local maxima. Let's define A_i to be an open interval centered at one of the local maximisers, m_i, such that it is the global maximiser of $\phi(m, K, J)$. Now, let $m_{i,N}$ be a local maximiser for $\phi_N(m_{i,N})$ which converges to m_i as $N \to \infty$. We can condition our distribution for $m_N(\sigma) \in A_i$, such that for any open ball $B_{N,\alpha}$ with $\alpha \in (0, 1)$,

$$B_{N,\alpha}(m_{i,N}) = \left(m_{i,N} - N^{-\frac{1}{2}+\alpha}, m_{i,N} + N^{-\frac{1}{2}+\alpha} \right), \tag{3.74}$$

$m_N(\sigma)$ concentrates around m_i at rate of $N^{-\frac{1}{2}+\alpha}$. The following lemma details the conditional concentration inequality of the distribution for $m_N(\sigma)$ and shows that it concentrates around the local maximisers m_i when defined in a vanishing neighbourhood of the maximisers.

Lemma 3.3.3. *Suppose $\phi(m)$ has $S \in \mathbb{N}$ global maximisers m_i such that $\phi''(m_i) < 0$. For $i \leq S$, let $A_i \subset [-1, 1]$ be an interval such that $m_i \in int(A_i)$ is the unique maximiser of ϕ on $cl(A_i)$. Then for N large enough ϕ_N has a unique global maximiser $m_{i,N} \to m_i$ on A_i with $\phi_N''(m_{i,N}) < 0$ and for $\alpha \in \left(0, \frac{1}{6}\right]$, one has*

$$\mu_N^{KJ}(m_N \in B_{N,\alpha,S}^c) = \exp\left\{ \frac{1}{2}N^{2\alpha} \max_{i \leq S} \phi_N''(m_{i,N}) \right\} \mathcal{O}(N^{\frac{3}{2}}) \tag{3.75}$$

where $B_{N,\alpha,S} = \bigcup_{i \leq S} B_{N,\alpha}(m_{i,N})$, moreover the restricted partition function on A_i can be expanded as,

$$Z_N\big|_{A_i} = \frac{e^{N\phi_N(m_{i,N})}}{\sqrt{(m_{i,N}^2 - 1)\phi_N''(m_{i,N})}} \left(1 + \mathcal{O}\left(N^{-\frac{1}{2}+\alpha} \right) \right) \tag{3.76}$$

and the unrestricted partition function can be expanded as,

$$Z_N = \sum_{i \leq S} \frac{e^{N\phi_N(m_{i,N})}}{\sqrt{(m_{i,N}^2 - 1)\phi_N''(m_{i,N})}} \left(1 + \mathcal{O}\left(N^{-\frac{1}{2}+\alpha} \right) \right). \tag{3.77}$$

Note that, here, $int(A_i)$ and $cl(A_i)$ denote the interior and closure of A_i, respectively.

Proof. The fact that for N large enough ϕ_N has a unique maximiser $m_{i,N} \to m_i$ with $\phi''(m_{i,N}) < 0$ can be proved applying to the function ϕ_N restricted to $cl(A_i)$ and using the same argument of Lemma 3.3.2. Clearly, for N large enough, $B_{N,\alpha}(m_{i,N}) \subset A_i$ and

$$\mu_N^{KJ}(m_N(\sigma) \in B_{N,\alpha}^c(m_{i,N})|m_N(\sigma) \in A_i) = \exp\left\{ \frac{1}{2} N^{2\alpha} \phi_N''(m_{i,N}) \right\} \mathcal{O}(N^{\frac{3}{2}}) \tag{3.78}$$

following a step-by-step argument used to prove equation (3.51).

Now, for $i \leq S$ and N large enough, one has that $A_i \setminus B_{N,\alpha}(m_{i,N}) = A_i \setminus B_{N,\alpha,S}$ and then $\mu_N(m_N(\sigma) \in B_{N,\alpha}^c(m_{i,N})|m_N(\sigma) \in A_i) = \mu_N(m_N(\sigma) \in B_{N,\alpha,S}^c|m_N(\sigma) \in A_i)$. Therefore,

$$\begin{aligned} \mu_N^{KJ}(m_N(\sigma) \in B_{N,\alpha,S}^c) &= \sum_{1 \leq i \leq S} \mu_N^{KJ}(m_N(\sigma) \in B_{N,\alpha,S}^c|m_N(\sigma) \in A_i)\mu_N^{KJ}(m_N(\sigma) \in A_i) \\ &\leq \exp\left\{ \frac{1}{2} N^{2\alpha} \max_{1 \leq i \leq S} \phi''(m_i) \right\} \mathcal{O}(N^{\frac{3}{2}}) \sum_{1 \leq i \leq S} \mu_N^{KJ}(m_N(\sigma) \in A_i) \\ &= \exp\left\{ \frac{1}{2} N^{2\alpha} \max_{1 \leq i \leq S} \phi''(m_i) \right\} \mathcal{O}(N^{\frac{3}{2}}). \end{aligned}$$

$$\tag{3.79}$$

This completes the proof of equation (3.75) following from equation (3.79).

As observed from the proof above, the distribution of the magnetisation $m_{i,N}(\sigma)$ concentrates in a neighbourhood within which the local maximisers $m_i(K, J)$ are defined as N grows to infinity for $i \in \{0, 1\}$. Hence to prove the central limit theorem for $m_{i,N}(\sigma)$, we need to condition the partition function on the neighbourhood for each of the maximisers. After obtaining the conditional partition function on the neighbourhood of each maximiser, we then use the result to prove conditional central limit theorem of $m_{i,N}(\sigma)$. To do this, we need to find an approximation of the conditional partition function

$$Z_N|_{A_i} := \sum_{\sigma \in \Omega_N : m_{i,N}(\sigma) \in A_i} \exp\left\{ N\left(\frac{K}{3} m_{i,N}^3(\sigma) + \frac{J}{2} m_{i,N}^2(\sigma) + h_N m_{i,N} \right) \right\}$$

when $m_{i,N}(\sigma)$ concentrates around $m_i \in A_i$ and A_i is defined as in Lemma 3.3.3. The following lemma approximates the partition function.

The proof for (3.76) and (3.77) follows exactly the argument in the results of the previous Lemma 3.3.2. Note that for fixed $i \in \{0,1\}$ and $m_{i,N}(\sigma)$ concentrating around $m_i \in A_i$,

$$
\mu_N^{KJ}(m_N(\sigma) \in B_{N,\alpha}(m_{i,N})|m_{i,N}(\sigma) \in A_i)
$$
$$
= \frac{1}{Z_N|_{A_i}} \sum_{m \in R_N \cap B_{N,\alpha}} \binom{N}{\frac{N(1+m)}{2}} \exp\left\{ N\left(\frac{K}{3}m^3 + \frac{J}{2}m^2 + h_N m\right)\right\}.
$$
(3.80)

Now, following the exact computation and argument in Lemma 3.3.2, we have that the restricted partition function can be expanded as

$$
Z_N|_{A_i} = \sum_{m \in R_N \cap B_{N,\alpha}} \binom{N}{\frac{N(1+m)}{2}} \exp\left\{ N\left(\frac{K}{3}m^3 + \frac{J}{2}m^2 + h_N m\right)\right\}
$$
$$
= \frac{e^{N\phi_N(m_{i,N})}}{\sqrt{(m_{i,N}^2 - 1)\phi''(m_{i,N})}} \cdot (1 + \mathcal{O}(N^{-\frac{1}{2}+3\alpha}))
$$
(3.81)

and observe that, for each of the global maximisers m_i

$$
Z_N|_{A_i} = \frac{e^{N\phi_N(m_{i,N})}}{\sqrt{(m_{i,N}^2 - 1)\phi''(m_{i,N})}} \cdot (1 + \mathcal{O}(N^{-\frac{1}{2}+3\alpha})).
$$
(3.82)

Assuming that $m_N(\sigma)$ concentrates around the two global maximisers $m_{i,N}$ for $i \in \{0,1\}$ then, following from the proof of Lemma 3.3.3, equation (3.77) follows from (3.82). Hence, we have

$$
Z_N = \sum_{i \in \{0,1\}} Z_N|_{A_i}.
$$
(3.83)

$\square$

Proof. **CLT for multiple maximisers**

Let's recall that by Proposition 3.1.2 there exist two global maximisers m_i of $\phi(m)$ for $i \in \{0,1\}$ on γ. Moreover by point $b)$ of Proposition 3.2.2 we know that $\phi''(m_i) < 0$ for $i \in \{0,1\}$.

We can now use the results of Lemmas 3.3.3, specifically (3.75) and (3.76) as an argument to the convergence in distribution (3.41) and (3.40). To begin with,

let's define $B_{i,\epsilon} := (m_i - \epsilon, m_i + \epsilon)$ for $\epsilon > 0$ and $i \in \{0, 1\}$. Hence, for all $\epsilon > 0$, $\phi(m_i) > \phi(m)$ for all $m \in B_{i,\epsilon} \backslash \{m_i\}$. Observe that for $i \in \{0, 1\}$,

$$\mu_N^{KJ}(m_N(\sigma) \in B_{i,\epsilon}) = \frac{Z_N|_{B_{i,\epsilon}}}{Z_N}. \tag{3.84}$$

From equation (3.82) and (3.76)

$$Z_N|_{B_{i,\epsilon}} = \frac{e^{N \sup_{m \in [-1,1]} \phi(m)}}{\sqrt{(m_i^2 - 1)\phi''(m_i)}} \cdot (1 + o(1)) \tag{3.85}$$

and

$$Z_N = e^{N \sup_{m \in [0,1]} \phi(m)} \sum_{i \in \{-1,1\}} \frac{1}{\sqrt{(m_i^2 - 1)\phi''(m_i)}} \cdot (1 + o(1)). \tag{3.86}$$

Now, equation (3.41) is derived from the following equations (3.84), (3.85) and (3.86).

To obtain the local central limit theorem for m_N around the global maximisers m_i, we will show that the moment generating function of $N^{\frac{1}{2}}(m_N - m_i)|\{m_N \in A_i\}$ with respect to the measure μ_N converges pointwise in distribution to the moment generating function of $\mathcal{N}\left(0, -\frac{1}{\phi''(m_i)}\right)$. Here $A_i \subset [-1, 1]$ is such that m_i is the unique maximiser of $\phi(m)$ on its interior. The moment generating function of $N^{\frac{1}{2}}(m_N - m_i)|\{m_N \in A_i\}$ at a fixed $t \in \mathbb{R}$ is

$$\mathbb{E}\left[e^{tN^{\frac{1}{2}}(m_N - m_i)}\middle|\{m_N \in A_i\}\right] = e^{-tN^{\frac{1}{2}}m_i} \frac{\bar{Z}_N(t)|_{A_i}}{Z_N|_{A_i}} \tag{3.87}$$

where $\bar{Z}$ is the perturbed partition function. Following the asymptotic expansion of the partition function in (3.76) (see Lemma 3.3.3), the fraction on the right side of equation (3.87) reduces to

$$\frac{\bar{Z}_N(t)|_{A_i}}{Z_N|_{A_i}} \sim e^{N\left(\phi_N(m_{i,N}(t)) - \phi(m_i)\right)}. \tag{3.88}$$

Now, taking Taylor's expansion of $\phi_N(m_{i,N}(t))$ at m_i up to the second order, one can repeat the same arguments as in the unique maximum case, obtaining

$$\mathbb{E}\left[e^{tN^{\frac{1}{2}}(m_N - m_i)}\middle|\{m_N \in A_i\}\right] \xrightarrow[N \to \infty]{} \exp\left\{-\frac{t^2}{2\phi''(m_i)}\right\}. \tag{3.89}$$

This completes the proof of (3.42). $\square$

Part 3: Critical point

Notice that the critical point $(K_c, J_c) = (0, 1)$ is a degenerate maximum point for $\phi(m)$ in the sense that $\phi''(m^*(K, J))\big|_{(K,J)=(0,1)} = 0$. Notice again that $m^* = m_c$ and it is a unique maximiser of $\phi(m)$ at the critical point. This does not allow the use of the asymptotic expansions in Lemma 3.3.2. However, one can simply notice that the Hamiltonian H_N^{KJ} of the model at the critical point $(K_c, J_c) = (0, 1)$ coincides at any $N \in \mathbb{N}$ with the Hamiltonian function of the standard Curie-Weiss model at the critical temperature $J = 1$ and zero external field. Therefore (3.43) and (3.44) are well known results and their proof can be found in [21].

Under this section we study the asymptotic behaviour of the magnetisation $m_N(\sigma)$ at the critical point m_c. Recall from equation (3.11) that at the critical point $(K_c, J_c) = (0, 1)$, $\phi''(m_c, K_c, J_c) = 0$ where m_c is the unique maximiser of $\phi(m, K, J)$. Here the proof follows the same argument as before for the case with unique maximiser but taking into account the fact that $\phi''(m_c, K_c, J_c) = 0$ and this will require higher order Taylor expansion. Now, for a sequence $h_N = h + tN^{-\frac{3}{4}}$ converging to h, we define $\phi_N(m(K_N, J)) := \phi(m(K, J, h_N), K, J, h_N)$ and suppose that $m_N^*(h_N)$ is its unique global maximiser which converges to m_c as $N \to \infty$. In this case we consider that $m_N(\sigma)$ concentrates around m_N^* with respect to the Boltzmann Gibbs measure at the rate of $N^{-\frac{1}{4}+\alpha}$ for $\alpha > 0$ and define a concentration window as

$$B_{N,\alpha} = \left(m_N^* - N^{-\frac{1}{4}+\alpha}, m_N^* + N^{-\frac{1}{4}+\alpha} \right). \tag{3.90}$$

We use the following Lemma to show that $m_N(\sigma)$ concentrates around m_N^* at the rate of $N^{-\frac{1}{4}+\alpha}$ for $\alpha \in (0, \frac{1}{20}]$.

Lemma 3.3.4. *Suppose $\phi(m, K, J)$ has a unique global maximiser m_c. Then for $\alpha \in (0, \frac{1}{20}]$ and $B_{N,\alpha}$ as defined above in equation (3.90),*

$$\mu_N^{KJ}(m_N(\sigma) \in B_{N,\alpha}^c) = \exp\left\{ \frac{1}{24} N^{4\alpha} \phi^{(4)}(m_c)(1 + o(1)) \right\} \mathcal{O}(N^{\frac{3}{2}}). \tag{3.91}$$

Proof. Following the argument in the proof of Lemma 3.3.2

$$
\begin{aligned}
\mu_N^{KJ}&(m_N(\sigma) \in B_{N,\alpha}^c) \\
&= \exp\left\{ N\left(\sup_{x \in B_{N,\alpha}^c} \phi_N(x) - \phi_N(m_N^*) \right) \right\} \mathcal{O}(N^{\frac{3}{2}}) \\
&\leq \exp\left\{ N(\phi_N(m_N^* \pm N^{-\frac{1}{4}}) - \phi_N(m_N^*)) \right\} \mathcal{O}(N^{\frac{3}{2}}) \\
&= \exp\left\{ \frac{1}{6}N^{\frac{1}{4}+3\alpha}\phi_N^{(3)}(m_N^*) + \frac{1}{24}N^{4\alpha}\phi_N^{(4)}(m_N^*) + \mathcal{O}(N^{-\frac{1}{4}+5\alpha}) \right\} \mathcal{O}(N^{\frac{3}{2}}).
\end{aligned}
$$

(3.92)

Let's observe that $\phi^{(4)}(m,K,J) < 0$ for all $m \in [0,1]$ and $\phi_N^{(3)}(m_N^*) \to 0$ as $m_N^* \to m_c$. Hence using that $m_N^* \to m_c$ as $N \to \infty$,

$$
\frac{1}{6}N^{\frac{1}{4}+3\alpha}\phi_N^{(3)}(m_N^*) + \frac{1}{24}N^{4\alpha}\phi_N^{(4)}(m_N^*) = \frac{1}{24}N^{4\alpha}\phi^{(4)}(m_c)(1+o(1)).
$$

(3.93)

Lemma 3.3.4 now follows from equations (3.92) and (3.93).   □

We now need an approximation of the partition function at the critical point since Lemma 3.3.4 shows that when we reach the critical point $m_N(\sigma)$ concentrates in a vanishing neighbourhood of m_c.

Lemma 3.3.5. *Suppose $\phi(m,K,J)$ has a unique global maximiser $m_c(K,J)$ and let $h_N := h + tN^{-\frac{3}{4}}$ for $t \in \mathbb{R}$. Then for $\alpha \in (0, \frac{1}{20}]$ and N large enough the partition function can be expanded as,*

$$
Z_N = \frac{N^{\frac{1}{4}}e^{N\phi_N(m_N^*)}}{\sqrt{2\pi(1-m_N^{*2})}} \int_{-\infty}^{\infty} e^{\eta_t(y)} dy (1+o(1)),
$$

(3.94)

where $\eta_t(y) := ay^2 + by^3 + cy^4$, with

$$
a := \frac{(6t)^{\frac{2}{3}}(\phi^{(4)}(m_c))^{\frac{1}{3}}}{4}, \quad b := \frac{(6t)^{\frac{1}{3}}(\phi^{(4)}(m_c))^{\frac{2}{3}}}{6}, \quad and \ c := \frac{\phi^{(4)}(m_c)}{24}.
$$

(3.95)

Proof. We follow the same argument of in Lemma 3.3.2 for this proof. Let's note from Lemma 3.3.4 that

$$
Z_N = (1 + \mathcal{O}(e^{-N^\alpha})) \sum_{m \in R_N \cap B_{N,\alpha}} \zeta(m),
$$

(3.96)

where $\zeta(m)$ is as defined in Lemma 3.3.2 and $B_{N,\alpha}$ is defined in 3.90. Similarly, following Lemma 3.3.2, it's easy to show that

$$\left| \int_{B_{N,\alpha}} \zeta(x)dx - \frac{2}{N} \sum_{m \in R_N \cap B_{N,\alpha}} \zeta(m) \right| = \mathcal{O}(N^{-1+4\alpha})\zeta(m_N*). \qquad (3.97)$$

It follows from the above equation that (see Lemma A.5, B.6 and B.10 of [23])

$$\sum_{m \in R_N \cap B_{N,\alpha}} \zeta(m) = \frac{N}{2} \int_{B_{N,\alpha}} \zeta(x)dx + \mathcal{O}(N^{4\alpha})\zeta(m_N^*)$$

$$= \frac{\sqrt{N}}{2}(1 + \mathcal{O}(N^{-1})) \int_{B_{N,\alpha}} e^{N\phi_N(x)} \sqrt{\frac{2}{\pi(1-x^2)}} dx + \mathcal{O}(N^{4\alpha})\zeta(m_N^*)$$

$$= \frac{N^{\frac{1}{4}} e^{N\phi_N(m_N^*)}}{\sqrt{2\pi(1-m_N^{*2})}} \int_{-N^\alpha}^{N^\alpha} e^{\eta_t(y)} dy(1 + \mathcal{O}(N^{-\frac{1}{4}+5\alpha}))$$

$$+ \mathcal{O}(N^{4\alpha}) \cdot \left[\sqrt{\frac{2}{\pi(1-m_N^{*2})}} e^{N\phi_N(m_N^*)} (1 + \mathcal{O}(N^{-1})) \right]$$

$$= \frac{N^{\frac{1}{4}} e^{N\phi_N(m_N^*)}}{\sqrt{(m_N^{*2}-1)\phi_N''(m_N^*)}} \cdot \int_{-\infty}^{\infty} e^{\eta_t(y)} dy(1 + o(1)).$$

$$(3.98)$$

Now, from equations (3.96) and (3.98), we have that

$$Z_N = (1 + \mathcal{O}(e^{-N^\alpha})) \cdot (1 + o(1)) \cdot \frac{N^{\frac{1}{4}} e^{N\phi_N(m_N^*)}}{\sqrt{(m_N^{*2}-1)\phi_N''(m_N^*)}} \cdot \int_{-\infty}^{\infty} e^{\eta_t(y)} dy$$

$$= (1 + o(1)) \cdot \frac{N^{\frac{1}{4}} e^{N\phi_N(m_N^*)}}{\sqrt{(m_N^{*2}-1)\phi_N''(m_N^*)}} \cdot \int_{-\infty}^{\infty} e^{\eta_t(y)} dy$$

$$(3.99)$$

This completes the proof of Lemma 3.3.5 and we use this results to prove the central limit theorem of $m_N(\sigma)$. □

Proof. **CLT at the critical point**

To obtain the central limit theorem of $m_N(\sigma)$ at m_c we use the results of Lemma 3.3.5 and follow the argument used in the case of unique maximiser in section 3.3.1. For a fixed $t \in \mathbb{R}$, denote the moment generating function of $N^{\frac{1}{4}}(m_N(\sigma) - m_c)$ by

$$\mathbb{E}\left[e^{tN^{\frac{1}{4}}(m_N(\sigma) - m_c)} \right] = e^{-tN^{\frac{1}{4}}m_c} \frac{Z_N(K, J, h + tN^{-\frac{3}{4}})}{Z_N(K, J)}. \qquad (3.100)$$

Considering equation (3.99) and observing that $m_N^* \to m_c$ as $N \to \infty$, we have

$$\frac{Z_N(K, J, h + tN^{-\frac{3}{4}})}{Z_N(K, J)} \sim e^{N\{\phi_N(m_N^*(h + tN^{-\frac{3}{4}})) - \phi(m_c(K, J))\}}. \tag{3.101}$$

By the definition of the variational pressure in equation (3.4),

$$
\begin{aligned}
N\{\phi_N(m_N^*(h + tN^{-\frac{3}{4}}), K, J, h_N) - \phi(m_c(K, J), K, J)\} &= \\
= N\{\phi(m_N^*(h + tN^{-\frac{3}{4}})) + tN^{-\frac{3}{4}}m_N^*(h + tN^{-\frac{3}{4}}) - \phi(m_c(K, J))\} &\quad (3.102) \\
= N\{\phi(m_N^*(h + tN^{-\frac{3}{4}})) - \phi(m_c(K, J))\} + tN^{\frac{1}{4}}m_N^*(h + tN^{-\frac{3}{4}}).
\end{aligned}
$$

Applying Taylor expansion around the unique maximiser $m_c(K, J)$, we have that

$$
\begin{aligned}
N\{\phi(m_N^*(h + tN^{-\frac{1}{2}})) - \phi(m_c(K, J))\} &= \\
= \frac{N}{2}\{m_N^*(h + tN^{-\frac{1}{2}}) - m_c(K, J)\}^2\phi''(m_c(K, J)) \\
+ \frac{N}{6}\{m_N^*(h + tN^{-\frac{1}{2}}) - m_c(K, J)\}^3\phi^{(3)}(m_c(K, J)) &\quad (3.103) \\
+ \frac{N}{24}\{m_N^*(h + tN^{-\frac{1}{2}}) - m_c(K, J)\}^4\phi^{(4)}(m_c(K, J)) \\
+ \mathcal{O}(N\{m_N^*(h + tN^{-\frac{1}{2}}) - m_c(K, J)\}) + o(1).
\end{aligned}
$$

We apply a further Taylor expansion of $\phi'(m, K, J)$ around m_c and use the fact that $\phi'(m_c) = \phi''(m_c) = \phi^{(3)}(m_c) = 0$,

$$
\begin{aligned}
\phi'(m_N^*(h_N)) &= \phi'(m_c) + \{m_N^* - m_c\}\phi''(m_c) + \frac{\{m_N^* - m_c\}^2}{2}\phi^{(3)}(m_c) \\
&\quad + \frac{\{m_N^* - m_c\}^3}{6}\phi^{(4)}(m_c) + \mathcal{O}(N^{-\frac{1}{4}}) \\
&= \frac{\{m_N^* - m_c\}^3}{6}\phi^{(4)}(m_c) + \mathcal{O}(N^{-\frac{1}{4}}).
\end{aligned}
\tag{3.104}
$$

Which implies that,

$$\frac{6\phi'(m_N^*)}{\phi^{(4)}(m_c)} \sim (m_N^* - m_c)^3. \tag{3.105}$$

Let us recall that, m_N^* and m_c are the unique global maximisers of $\phi_N(m, K, J, h_N)$ and $\phi(m, K, J)$ respectively at the critical point (K_c, J_c) and observe further that by definition of $\phi(m_N^*(h_N))$ and $\phi_N(m_N^*(h_N))$,

$$
\begin{aligned}
\phi'(m_N^*) &= \phi'_N(m_N^*) - tN^{\frac{-3}{4}} = -tN^{\frac{-3}{4}} \\
\implies -\frac{6t}{\phi^{(4)}(m_c)} &= N^{\frac{3}{4}}(m_N^* - m_c)^3 + \mathcal{O}(N^{-\frac{1}{4}}).
\end{aligned}
$$

Notice that $m_N^* \to m_c$ as $N \to \infty$. Hence

$$(m_N^* - m_c) = -\left(\frac{6t}{\phi^{(4)}(m_c)}\right)^{\frac{1}{3}} \cdot N^{-\frac{1}{4}} + \mathcal{O}(N^{-\frac{1}{4}}) \tag{3.106}$$

and

$$N^{\frac{1}{4}}(m_N^* - m_c) = -\left(\frac{6t}{\phi^{(4)}(m_c)}\right)^{\frac{1}{3}} + \mathcal{O}(N^{-\frac{1}{4}}). \tag{3.107}$$

Therefore from (3.103), we have

$$N\{\phi(m_N^*(h + tN^{-\frac{1}{2}})) - \phi(m_c(K, J))\}$$
$$= \frac{N}{24}\left(-N^{-\frac{1}{4}} \cdot \left(\frac{6t}{\phi^{(4)}(m_c)}\right)^{\frac{1}{3}}\right)^4 \phi^{(4)}(m_c) + o(1) \tag{3.108}$$
$$= \frac{\phi^{(4)}(m_c)}{24}\left(\frac{6t}{\phi^{(4)}(m_c)}\right)^{\frac{4}{3}} + o(1).$$

Now, from (3.106),

$$tN^{\frac{1}{4}}m_N^*(h + tN^{-\frac{3}{4}}) = tN^{\frac{1}{4}}m_c(K, J) - t\left(\frac{6t}{\phi^{(4)}(m_c)}\right)^{\frac{1}{3}} + \mathcal{O}(N^{-\frac{3}{2}}) \tag{3.109}$$

Hence,

$$N\{\phi_N(m_N^*(h + tN^{-\frac{1}{2}})) - \phi(m_c(K, J))\} =$$
$$= \frac{\phi^{(4)}(m_c)}{24}\left(\frac{6t}{\phi^{(4)}(m_c)}\right)^{\frac{4}{3}} + tN^{\frac{1}{4}}m_c - t\left(\frac{6t}{\phi^{(4)}(m_c)}\right)^{\frac{1}{3}} + o(1). \tag{3.110}$$

Therefore, the limiting moment generation functions of $m_N(\sigma)$ at m_c becomes

$$\lim_{N \to \infty} \mathbb{E}\left[e^{tN^{\frac{1}{4}}(m_N(\sigma) - m_c)}\right] = \exp\left\{\frac{\phi^{(4)}(m_c)}{24}x^4 - tx\right\} \tag{3.111}$$

where $x = \left(\frac{6t}{\phi^{(4)}(m_c)}\right)^{\frac{1}{3}}$. $\square$

Chapter 4

Three-spin and an external field: the Kh Ising model

This chapter investigates the phase properties of the Ising model with three-spin interactions and an external magnetic field within the framework of mean-field approximation theory. The objective is to minimise the free energy using an appropriate variational principle, which allows for the calculation of the magnetic order parameter. The behaviour of the magnetic order parameter is then thoroughly analysed, specifically in relation to the interaction parameter and the external magnetic field. The investigation focuses on fundamental concepts and properties of the model, such as the existence and uniqueness of phase transitions as well as the properties of an order parameter that exhibits a critical point characterised by critical exponents. The results discussed in this chapter can be found in the reference list as [39].

4.1   The model and results

Starting from the Hamiltonian of a system with three-spin interactions and an external field, the following features are studied: the existence and properties of phase transitions, the properties of the magnetisation and its behaviour along phase boundaries, and the behaviour of the magnetisation near transition point of the system. In particular, this chapter uses the following specified Hamiltonian:

$$H_N^{Kh}(\sigma) = - \sum_{\langle i,j,k \rangle} K_{ijk} \sigma_i \sigma_j \sigma_k - \sum_i h_i \sigma_i, \qquad (4.1)$$

defined on $N-$spins with $\sigma = (\sigma_i)_{i \leq N} \in \{-1, +1\}^N = \Omega_N$. The first term in the Hamiltonian modulates the interactions between triplets of spins, while the second term represents the effect of an applied magnetic field on each spin. Hence, following the normalisation of the parameters K and h introduced in Chapter 2, (4.1) becomes:

$$H_N^{Kh}(\sigma) = -N\left(\frac{K}{3}m_N^3(\sigma) + hm_N(\sigma)\right) \tag{4.2}$$

where $m_N(\sigma)$ is the magnetisation density. Here, the model is expressed in terms of the magnetisation per particle, and it involves a cubic term and a linear term that depend on the values of K, h, and $m_N(\sigma)$. The Hamiltonian (4.2) is invariant if we reverse the direction of K and h and of all spins $\sigma_i \to -\sigma_i$ $(i = 1, ..., N)$, i.e., $H_N^{Kh}(\sigma; K, h) = H_N^{Kh}(-\sigma; -K, -h)$. The Boltzmann-Gibbs type probability measure related to the Hamiltonian (4.2) for a given configuration σ is

$$\mu_N^{Kh}(\sigma) = \frac{e^{-H_N^{Kh}(\sigma)}}{Z_N}, \tag{4.3}$$

where $Z_N = \sum_{\sigma \in \Omega_N} \exp\left(-H_N^{Kh}(\sigma)\right)$ is the normalisation factor, also called the partition function. The interest here is to study the limiting behaviour of $m_N(\sigma)$ as a function of K and h.

In the thermodynamic limit, the Hamiltonian in (4.2) can be described by its order parameter denoted as $m(K, h)$, which is the limiting expected value of $m_N(\sigma)$. The order parameter characterises the entire phase space of the model and can be identified among the solutions of the consistency equation

$$m = \tanh(Km^2 + h). \tag{4.4}$$

In the plane (K, h), the order parameter m is shown to have two distinct jumps or discontinuities in the phase space which is characterised by a curve implicitly defined as $h = \gamma(K)$. The curve $\gamma(K)$ is differentiable and smooth outside the critical point (K_c, h_c),

$$(K_c, h_c) = \left(\pm\frac{3\sqrt{3}}{4}, \ \text{arctanh}\left(\pm\frac{1}{\sqrt{3}}\right) - \frac{K_c}{3}\right), \tag{4.5}$$

and originates at

$$m_c = \pm\frac{1}{\sqrt{3}} \tag{4.6}$$

in the phase space. The order parameter $m(K, h)$ near the critical point is characterised by the critical exponents of the mean-field theory: 1 along the direction of γ and $1/2$ along any other direction of the plane (K_+, h) where K_+ refers to $K > 0$.

It is worth noting that the law of large numbers and the central limit theorem for the distribution of $m_N(\sigma)$ have been studied in [23] for $K > 0$ and therefore will not be discussed in this work. The limiting distribution of the magnetisation away from the curve γ was found to be Gaussian, with local Guassian fluctuations on the coexistence curve γ and non-Gaussian at (K_c, h_c) with rate $N^{1/4}$.

This chapter is organised as follows: Section 4.2 introduces the Gibbs free energy of the model and solves it via an appropriate variational principle. The properties of the order parameter describing the system in its steady-state equilibrium are also discussed in this section. These properties allow an analytical description of the phase diagram of the system and the calculation of the critical exponents. The conclusion and future prospects of the model are discussed in section 4.3.

4.2   Definitions and exact solution

The generating functional of the moments for the distribution (4.3), the thermodynamic pressure is defined as:

$$p_N = \frac{1}{N} \log Z_N \tag{4.7}$$

and its thermodynamic limit

$$p := \lim_{N \to \infty} p_N \tag{4.8}$$

can be computed by an application of the Varadhan's integral lemma [20, 25, 26]. The limiting pressure (4.8) admits the following variational representation:

$$p = \sup_{m \in [-1,1]} \phi(m), \tag{4.9}$$

where $\phi(m) = u(m) - I(m)$ with

$$u(m) = \frac{K}{3} m^3 + hm \tag{4.10}$$

is the energy contribution, and

$$I(m) = \frac{1-m}{2} \log\left(\frac{1-m}{2}\right) + \frac{1+m}{2} \log\left(\frac{1+m}{2}\right) \tag{4.11}$$

is the binary entropy contribution. The solutions of the variational principle (4.9) coincide with its stationary points which are obtained as the roots of the mean-field equation,

$$m = \tanh(Km^2 + h) \tag{4.12}$$

for fixed K and h. Figure 4.1 represents the solutions of (4.12) that realise the supremum of (4.9) and shows that the function $\phi(m)$ in (4.9) can have not more than two global maximisers in the interval $(-1, 1)$ for fixed (K, h).
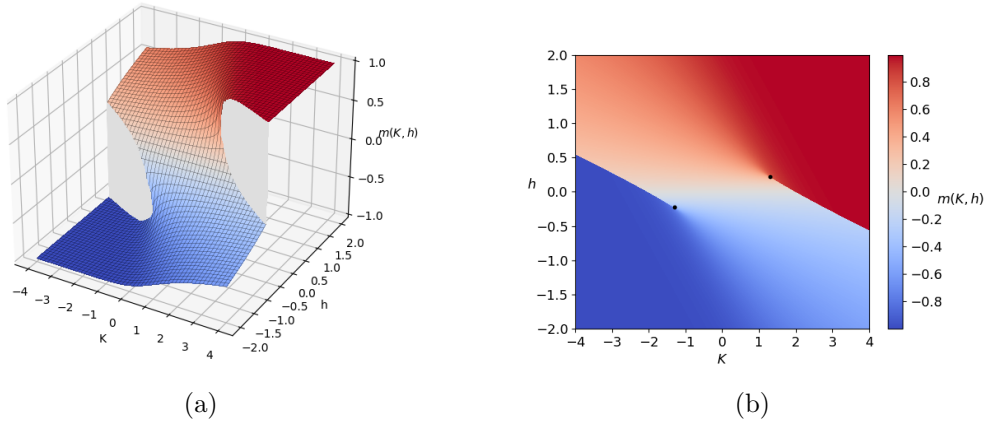

$$\text{(a)} \qquad\qquad\qquad\qquad\qquad\qquad \text{(b)}$$

Figure 4.1: Stable solutions of the mean-field equation as a function of K and h showing two discontinuous jumps or transitions with m varying smoothly for all h and $K \in \left(-\frac{3\sqrt{3}}{4}, \frac{3\sqrt{3}}{4}\right)$.

Due to the invariance property of (4.2) under spin reversal and transformation of the parameters K and h, one can study the model only for $K > 0$ without loss of generality. In what follows the parameter space will be restricted to $(K, h) \in \mathbb{R}_+ \times \mathbb{R}$ and the phase space is divided accordingly as:

Proposition 4.2.1 (Phase diagram). *For any $K > 0$, there exists $h = \gamma(K)$ such that the function $m \mapsto \phi(m)$ has a unique maximum point m^* for $(K, h) \in (\mathbb{R}_+ \times \mathbb{R}) \backslash \gamma$ and on the curve γ there are two global maximisers $m_1(K, h), m_2(K, h)$, such that the limit as $K \to K_c$ of $\gamma(K)$ identifies the critical point (K_c, h_c) at $m = m_c = \frac{1}{\sqrt{3}}$.*

The two global maximisers of Proposition 4.2.1 indicates the presence of two different thermodynamic equilibrium phases, while the curve γ represents the co-existence curve. Figure 4.2 displays numerical simulations of the phase diagram as described in Proposition 4.2.1.

The critical exponents of the model are computed to understand the limiting behaviour of the magnetisation approaching the critical point (K_c, h_c). The average value of the magnetisation in this case will be denoted by $m^*(K, h)$. The following
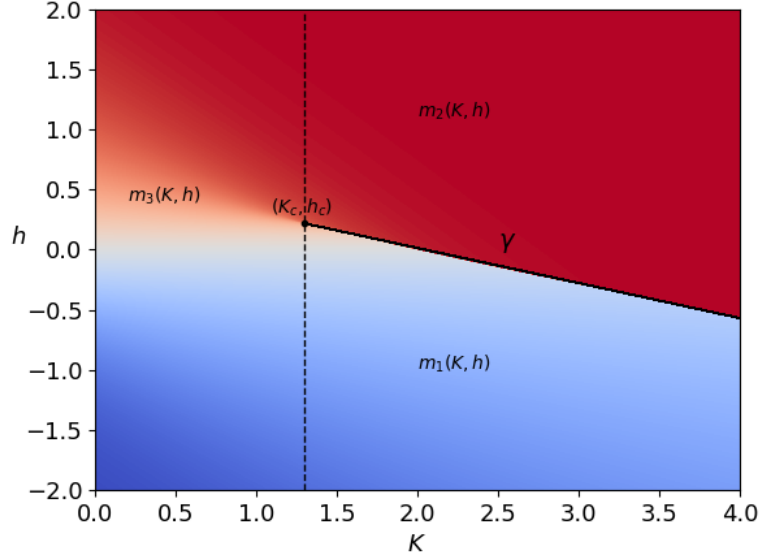
Figure 4.2: Phase diagram of the model with coexistence curve γ and the critical point (K_c, h_c) in the (K, h) plane for $K > 0$. The colormap has the same scale as used in Figure 4.1.

proposition describes the critical behaviour of $m^*(K, h)$ when $(K, h) \to (K_c, h_c)$ from various directions:

Proposition 4.2.2. *Let $m^*(K, h)$ be the unique global maximiser of $\phi(m)$ defined in Corollary 4.2.1. Given any curve $h = \tau(K)$ tangent to the wall $\gamma(K)$ at the critical point such that $\tau'(K_c) = -m_c^2$ and another not tangent to the critical point with $\tau'(K_c) \neq -m_c^2$. Then, as $(K, h) \to (K_c, h_c)$,*

$$m^*(K, h) - m_c \sim \begin{cases} \mathcal{C}(K - K_c), & \text{if } \tau'(K_c) = -m_c^2 \\ \mathcal{C}_1(K - K_c)^{1/2}, & \text{if } \tau'(K_c) \neq -m_c^2 \end{cases} \tag{4.13}$$

for all $K > K_c$, and $\mathcal{C}$ and $\mathcal{C}_1$ are constants.

In the sequel the proof of the above two propositions, Propositions 4.2.1 and 4.2.2, which characterises the phase of the model is given.

4.2.1 Proofs

The proofs of the results of this chapter are given in this section and organised as follows: an analysis of the properties of the function $\phi(m)$ appearing in the

variational problem (4.9) is given in this section and used as the proof of Proposition 4.2.1 and the critical exponents of the model are computed in section 4.2.1.

Proof of Proposition 4.2.1

The proof comes in several steps following from Lemma 4.2.1, Propositions 4.2.3, 4.2.4, 4.2.5 and 4.2.6 below. From the variational principle in (4.9), let us observe that the function $\phi(m)$ satisfies the following:

$$\begin{aligned} \frac{\partial}{\partial m}\phi(m) &= Km^2 + h - \operatorname{arctanh}(m) = 0 \quad \text{and} \\ \frac{\partial^2}{\partial m^2}\phi(m) &= 2Km - \frac{1}{1-m^2}. \end{aligned} \tag{4.14}$$

Note from (4.14) that, $\lim_{m \to -1^+} \phi'(m) = +\infty$ and $\lim_{m \to 1^-} \phi'(m) = -\infty$. Hence, there exists an interval $[-1, -1+\epsilon]$ such that $\phi(m)$ is strictly increasing and strictly decreasing on $[1-\epsilon, 1]$ for $\epsilon > 0$. It then follows that the local maximisers of $\phi(m)$ do not include the endpoints -1 and $+1$, since they are singular points of $\phi'(m)$. It is therefore obvious that the variational pressure $\phi(m)$ reaches its maximum in at least one point $m = m(K, h) \in (-1, 1)$ which satisfies the following condition:

$$\frac{\partial}{\partial m}\phi(m) = 0, \qquad \text{i.e.,} \quad m = \tanh\left(Km^2 + h\right). \tag{4.15}$$

Now there is a unique critical value for (K, h), denoted by (K_c, h_c), such that $\phi(m)$ has a unique degenerate maximum m_c, in the sense that $\phi''(m)\big|_{(K_c, h_c)} = 0$.

Lemma 4.2.1 (Critical values)**.** *The degenerate maximum points of $\phi(m)$ are obtained for $K_c = \pm\frac{3}{4}\sqrt{3}$ and $h_c = \operatorname{arctanh}\left(\pm\frac{1}{\sqrt{3}}\right) - \frac{K_c}{3}$. The magnetisation at the point (K_c, h_c) takes the value $m_c = \pm\frac{1}{\sqrt{3}}$.*

Proof. The critical values (K_c, h_c) and m_c can be determined analytically by first observing from (4.15) that $\underbrace{\tanh\left(Km^2 + h\right)}_{=y} - m = 0$ has a triple root m_c such that the following holds:

$$\begin{aligned} \tanh\left(K_c m_c^2 + h_c\right) - m_c &= 0 \\ \eta = \frac{\partial y}{\partial m}\bigg|_{(m_c, K_c, h_c)} - 1 &= 0 \\ \eta' = \frac{\partial^2 y}{\partial m^2}\bigg|_{(m_c, K_c, h_c)} &= 0. \end{aligned} \tag{4.16}$$

Notice that

$$\eta(m_c) = 2K_c m_c (1 - m_c^2) - 1 = 0$$

and

$$\eta'(m_c) = 2K_c - 6K_c m_c^2 = 0.$$

Solving η and η' simultaneously for K_c and m_c, we find that η' has two roots, $m_c := \pm\frac{1}{\sqrt{3}}$ and each of these roots is a local maximum point of η for $K_c := \pm\frac{3}{4}\sqrt{3}$. Knowing m_c and K_c, it follows that $h_c := \operatorname{arctanh}\left(\pm\frac{1}{\sqrt{3}}\right) - \frac{\sqrt{3}}{4}$.

Let $\bar{m} \in (-1, 1)$ be any solution of $\phi''(m) = \eta(m) = 0$. Observe that for all $m \leq 0$ and $K \geq 0$, $\eta(m) = \phi''(m) \leq -1$, which implies that $\bar{m}$ is a solution of $\phi''(m) = \eta(m) = 0$ if $\bar{m} \in (0, 1)$. We have already shown that the only positive solution (zeros) of $\eta'(m) = 0$, is $m = m_c = \frac{1}{\sqrt{3}}$ which occurs as a double root of $\eta(m_c) = 0$ at $K = K_c = \frac{3}{4}\sqrt{3}$. Therefore, it follows from Rolle's theorem that $\eta(m)$ evaluated at $K = K_c = \frac{3}{4}\sqrt{3}$, cannot have any positive root other than $\bar{m} = m_c = \frac{1}{\sqrt{3}}$ and hence it is the only root of $\phi''(m)$ if and only if $K = K_c = \frac{3}{4}\sqrt{3}$. Now, since $\phi''(m_c) = \eta(m_c) = \eta'(m_c) = 0$ for $K = K_c$, it is easy to see that if $h = h_c$ then $\phi'(m_c) = \phi^{(3)}(m_c) = 0$. Moreover, it is worth noting that for $K = K_c$ and $h = h_c$, $\phi'(m) > 0$ holds for all $m \in (-1, m_c)$ and $\phi'(m) \leq 0$ holds for $m \in [m_c, 1)$, which is a consequence of the fact that $\phi'(m) \xrightarrow[m \to -1^+]{} \infty$ and $\phi'(m) \xrightarrow[m \to 1^-]{} -\infty$. This implies that for $K = K_c > 0$ and $h = h_c > 0$, $\phi'(m)$ is decreasing, has a unique triple root at m_c and $\phi''(m) \leq 0$ on the domain $(-1, 1)$ for $0 \leq K \leq K_c$. Given this, it is clear that if $K > K_c$, there exists a $\epsilon > 0$ such that $\phi''(m) > 0$ on the domain $m \in (m_c - \epsilon, m_c + \epsilon)$ and hence has exactly two roots. Note further that $\phi''(m) = 0$ holds for $K = K_c$ if and only if $m = m_c$. Consequently, $m_c = \pm\frac{1}{\sqrt{3}}$ are the degenerate maximum points of $\phi(m)$ and that $\phi''(m)|_{\{m_c = \frac{1}{\sqrt{3}}\}} \geq \phi''(m)|_{\{m_c = -\frac{1}{\sqrt{3}}\}}$ with equality only at $K = K_c$. $\qquad\square$

In the rest of the work, due to the fact that the Hamiltonian (4.1) for the transformation of the direction of the cubic interaction parameter (K) and the external field parameter (h) is invariant under spin flip, the analysis of the model is restricted to the case where $K \geq 0$. The following proposition provides a complete classification of the stationary points of $\phi(m)$:

Proposition 4.2.3. *(Classification of stationary points) For all $K \geq 0$ and $h \in \mathbb{R}$, the roots of equation (4.15) are described as follows:*

1. *Define the following functions for $K > K_c$*

$$\psi_1(K) := \min_{m \in [-1,1]} g(m, K), \tag{4.17}$$

$$\psi_2(K) := \max_{m \in [-1,1]} g(m, K) \tag{4.18}$$

   where $g(m, K) := \operatorname{arctanh}(m) - Km^2$ and $\psi_1(K), \psi_2(K) < h_c$. Hence:

   a. *if $h = \psi_1(K)$, then $\phi'(m)$ has two solutions $m_1(K, h) < m_2(K, h)$. $m_1(K, h)$ is a local maximum point and $m_2(K, h)$ is an inflection point of $\phi(m)$.*

   b. *if $h < \psi_1(K)$, then $\phi'(m)$ has a unique solution $m_1(K, h)$ with the same sign of h such that it is the unique maximum point of $\phi(m)$.*

   c. *if $\psi_1(K) < h < \psi_2(K)$, then $\phi'(m)$ has three solutions $m_1(K, h) < \tilde{m}(K, h) < m_2(K, h)$. Where $m_1(K, h)$ and $m_2(K, h)$ are local maximum points while $\tilde{m}(K, h)$ is a local minimum point of $\phi(m)$.*

   d. *if $h = \psi_2(K)$, then $\phi'(m)$ has two solutions $m_1(K, h) < m_2(K, h)$. Here $m_1(K, h)$ is an inflection point of $\phi(m)$ while $m_2(K, h)$ is a local maximum point.*

   e. *if $h > \psi_2(K)$, then there exists a unique positive solution $m_2(K, h)$ of $\phi'(m)$ such that it is the only maximum point of $\phi(m)$.*

2. *Given that $0 \le K \le K_c$ and $h \in \mathbb{R}$, there exist a unique solution $m_3(K, h)$ of $\phi'(m)$ with the sign of h, which is zero if and only if $h = 0$, and it is the only maximal point of $\phi(m)$.*

Proof. It is easy to observe that $m = 0$ is always a solution of (4.15) and that $\phi''(0) < 0$ for all K. The mean-field equation (4.15) can be rewritten as follows

$$h = \underbrace{\left[\operatorname{arctanh}(m) - Km^2 \right]}_{=g(m,K)}. \tag{4.19}$$

The solutions of (4.15) follow from (4.19) as the intersections between h and the function $g(m, K)$. Let us now begin by examining some properties of the function $g(m, K)$ as defined in (4.19). Given that $g(m, K) := \operatorname{arctanh}(m) - Km^2$, then it's

first and second partial derivatives with respect to m are:

$$g'(m, K) = \left[\frac{1}{1 - m^2} - 2Km \right] \quad \text{and}$$

$$g''(m, K) = \left[\frac{2m}{(1 - m^2)^2} - 2K \right]. \tag{4.20}$$

Note that the function $g''(m, K)$ is strictly increasing on $(-1, 1)$ for all K, hence it has a unique solution. Furthermore, observe that,

$$\begin{cases} g'(0, K) = 1, & \forall\, K \\ g''(0, K) = -2K \leq 0, & \forall\, K \geq 0 \\ \lim_{m \to 1^-} g(m, K) = +\infty, \\ \lim_{m \to -1^+} g(m, K) = -\infty. \end{cases} \tag{4.21}$$

Now, let us notice from (4.17) and (4.18) that $\psi_1(K)$ and $\psi_2(K)$ denote the minimum and maximum values of $g(m, K)$ for $K > K_c$, respectively. In the following, $\psi_1(K)$ and $\psi_2(K)$ are used together with the properties of $g(m, K)$ in (4.21) to study the solutions of $\phi'(m) = 0$.

1. Notice that since the function $g(m, K) \to -\infty$ as $m \to -1^+$ and $g(m, K) \to \infty$ as $m \to 1^-$, any horizontal line tangent to $g(m, K)$ at $\psi_1(K)$ or $\psi_2(K)$ identifies two solutions of $\phi'(m)$. Thus, when $h = \psi_1(K)$, it is easy to see that $\phi'(m)$ has two solutions, one of which, namely $m_2(K, h)$, is a horizontal tangent point of the function $g(m, K)$ such that $g'(m_2, K) = 0$ and turns out to be an inflection point of $\phi(m)$, while the other, namely $m_1(K, h)$, is a maximum point of $\phi(m)$. Likewise, if $h = \psi_2(K)$, $\phi'(m)$ has two solutions where the one tangent to $\psi_2(K)$ is an inflection point of $\phi(m)$.

   Hence by definition, it is clear that if $h < \psi_1(K)$ then (4.15), $\phi'(m)$, has a unique solution $m_1(K, h)$ that has the same sign as h. On the other hand, if $\psi_1(K) < h < \psi_2(K)$, by continuity of $g(m, K)$ and the fact that for $m \to 1^-$, $g(m, K) \to +\infty$, imply that (4.15) has three solutions, namely $m_1(K, h) < \tilde{m}(K, h)$ and $m_2(K, h)$. Furthermore, when $h > \psi_2(K)$ clearly there is a unique solution $m_2(K, h)$ of (4.15).

2. Now, let us consider the case where $0 \leq K \leq K_c$. Since the function $\phi'(m)$ is decreasing and $\phi''(m) \leq 0$ on the domain $m \in (-1, 1)$, for $K \in [0, K_c]$ and $h \in \mathbb{R}$, this implies that $\phi'(m)$ can have only one solution namely $m_3(K, h)$.

Notice that $m_3(K, 0) = 0$ and has the same *sign* as h for $h \neq 0$ and $\phi''(m) = 0$ if $m_3(K_c, h_c) = m_c$. Since $m_3(K, h)$ is the unique solution of $\phi'(m)$ on the interval $0 \leq K \leq K_c$, it is the unique maximum point of $\phi(m)$ as $\phi''(m) \leq 0$ on the domain $m \in (-1, 1)$.

$\square$

The classification of the solutions of $\phi'(m)$ and their characterisations given by Proposition 4.2.3 are shown in Figures 4.3, 4.4 and 4.5.
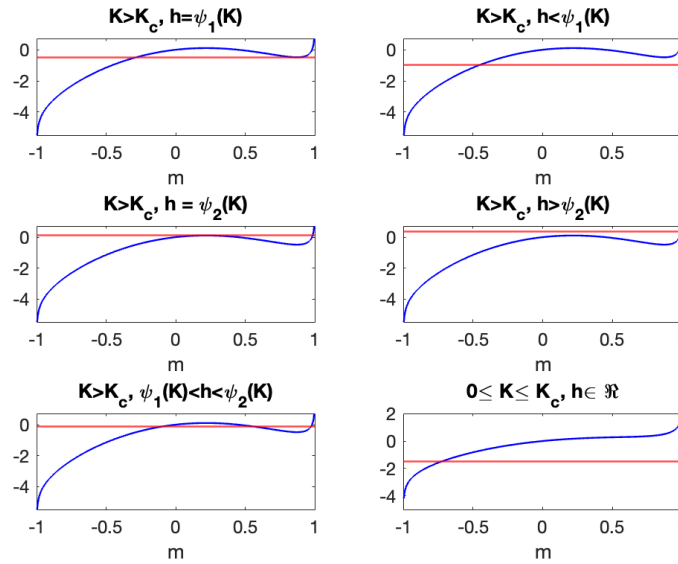
Figure 4.3: The intersections of the blue curve $g(m, K)$, as defined in (4.19), and the red solid horizontal line corresponding to h are the stationary points of $\phi(m)$. These intersection points represent the solutions of the consistency equation (4.15).

The following proposition examines the regularity properties of the solution(s) of the consistency equation (4.15) with respect to the parameters K, h.

Proposition 4.2.4. *(Regularity properties). Let $m_1(K, h), m_2(K, h)$ and $m_3(K, h)$ be the stationary points of $\phi(m)$ described in Proposition 4.2.3 and defined on their respective domains $D_1 := \{(K, h)|K > K_c, h \leq \psi_1(K)\}, D_2 := \{(K, h)|K > K_c, h \geq \psi_2(K)\}$ and $D_3 := \{(K, h)|0 \leq K \leq K_c, h \in \mathbb{R}\}$. Then the following properties hold:*

(a) *for any $i \in \{1, 2, 3\}$, $\phi''(m_i(K, h)) < 0$ on the interior of the respective domains D_i for $m_i(K, h)$,*

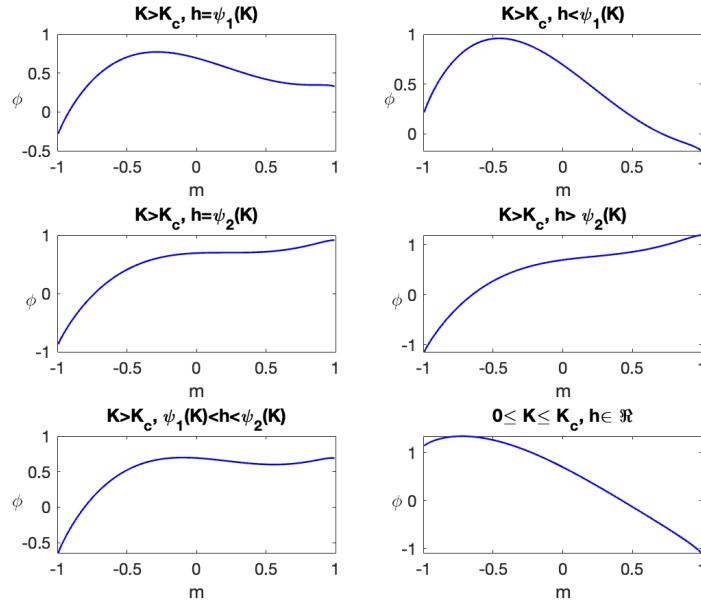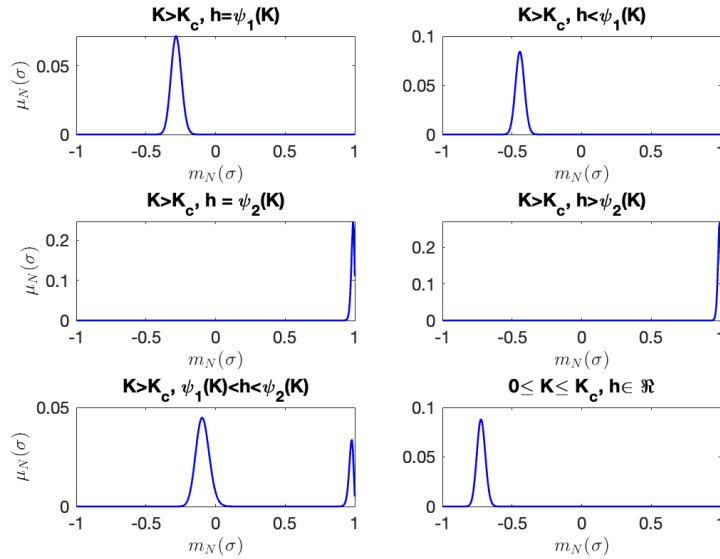Figure 4.4: The variational pressure as a function of the magnetisation.

Figure 4.5: Boltzmann-Gibbs distribution of the total magnetisation.

(b) $m_i(K, h)$ are continuous and C^∞ on the interior of their respective domains.

(c) For any $i \in \{1, 2, 3\}$

$$\frac{\partial}{\partial h}\phi(m_i) = m_i, \qquad \frac{\partial}{\partial K}\phi(m_i) = \frac{1}{3}m_i^3, \tag{4.22}$$

$$\frac{\partial m_i}{\partial h} = -\frac{1}{\phi''(m_i)}, \qquad \frac{\partial m_i}{\partial K} = -\frac{m_i^2}{\phi''(m_i)} \tag{4.23}$$

and

$$\frac{\partial^2 m_i}{\partial h^2} = -\frac{\phi^{(3)}(m_i)}{\left[\phi''(m_i)\right]^3}, \qquad \frac{\partial^2 m_i}{\partial K^2} = -\frac{m_i^4\phi^{(3)}(m_i)}{\left[\phi''(m_i)\right]^3} - \frac{2m_i^3}{\left[\phi''(m_i)\right]^2} \tag{4.24}$$

on the interior of D_i such that $\phi''(m_i(K,h)) \neq 0$.

Proof. (a) Let denote by $G(m) := \frac{\partial^2\phi(m)}{\partial m^2}$ and let us show that $G(m)\big|_{m_i(K,h)} < 0$ on the interior of the domains of $m_i(K,h)$. Note first, by the definition of the variational principle in (4.9), that the $m \in (-1,1)$ satisfying (4.9) are the maximisers of $\phi(m)$ and hence it is expected that $G(m)\big|_{m_i(K,h)} < 0$ on the interior of the respective domains of $m_i(K,h)$. Some properties of $G(m)$ are given below:

$$\frac{\partial G}{\partial m}(m) = 2K - \frac{2m}{(1-m^2)^2}$$
$$\frac{\partial^2 G}{\partial m^2}(m) = -\frac{2(3m^2+1)}{(1-m^2)^3} < 0 \qquad \text{for } m \in (-1,1)$$

and hence,

$$\begin{cases} G(0) = -1 < 0, \\ G'(0) = 2K \geq 0, \quad \forall\, K \geq 0 \\ G''(0) = -2 \\ \lim_{\substack{m \to 1^- \\ m \to -1^+}} G(m) = -\infty, \quad \forall\, K > 0. \end{cases} \tag{4.25}$$

From Lemma 4.2.1 it was discussed that for $K > K_c$ there exists an interval $(m_c - \epsilon, m_c + \epsilon)$ for which $G(m) > 0$. Together with the properties of G given in (4.25), this implies that $G(m) = 0$ can have at most two solutions. Recall from Proposition 4.2.3 that if $K > K_c$, then $\phi'(m) = 0$ can have at most three solutions and these solutions correspond to the turning points of $\phi(m)$. Similarly, $G(m) = 0$ has exactly two solutions identifying the turning points of $\phi'(m)$, which characterise the zeroes of $\phi'(m)$ as a local maximum or local minimum or an inflection point of $\phi(m)$. Note again that $\phi'(m)$ does not always decrease on the entire domain of m, for

$m \in (-1, 1)$, although $\phi'(m) \xrightarrow[m \to -1^+]{} \infty$ and $\phi'(m) \xrightarrow[m \to 1^-]{} -\infty$. The formal proof uses the above arguments as follows:

i. Consider the domain $D_1 := \{(K, h) | K > K_c, h \leq \psi_1(K)\}$. We want to show that $G(m_1(K, h)) < 0$ on the interior of D_1. From Proposition 4.2.3 it follows that for fixed $K > K_c$, $m_1(K, h)$ is the smallest solution of $\phi'(m) = 0$ and that it is unique on the interior of D_1. Since $G(m) = 0$ has exactly two roots for any $K > K_c$, $\phi'(m)$ has exactly two turning points, i.e., one is a global maximum point and the other a global minimum point of $\phi'(m)$. Hence, it is clear that the root of $\phi'(m) = 0$ on the interior of D_1 is smaller than all two roots of $G(m) = 0$, since $h < \psi_1(K)$. Considering the properties of $G(m)$ in (4.25), in particular $\lim_{\substack{m \to 1^- \\ m \to -1^+}} G(m) = -\infty \quad \forall K > 0$, and the fact that it is a continuous function implies that $G(m)\big|_{(m_1 - \epsilon, m_1 + \epsilon)} < 0$ for $\epsilon > 0$. Since $G(m) < 0$ holds in both the left and right neighbourhoods of $m_1(K, h)$ for $\epsilon > 0$, it follows that $G(m_1(K, h)) < 0$ holds on the interior of D_1. Therefore by extension and a direct application of the implicit function theorem A.2.2, since $G(m_1(K, h)) \neq 0$ and $\phi'(m) \in C^\infty$, then $G(m_1(K, h)) \in C^\infty$ on the interior of D_1.

Given that (K, h) is in the interior of D_2, it is known by point e. of the Proposition 4.2.3 that $m_2(K, h)$ is the unique solution of $\phi'(m) = 0$. Therefore, following similar argument as for the case of $m_1(K, h)$ proves that on the interior of the domain D_2, $G(m_2(K, h)) < 0$ and C^∞.

ii. On the interior of $D_3 := \{(K, h) | 0 \leq K \leq K_c, h \in \mathbb{R}\}$, $\phi'(m)$ has a unique solution $m_3(K, h)$. In Lemma 4.2.1 it was shown that $G(m) = 0$ when $m = m_c$ and $K = K_c$, but on the interior of D_3, $K \neq K_c$. Again, from the same lemma, it was also shown that for all $K < K_c$, $G(m) < 0$ and therefore on the interior of D_3, it follows that $G(m_3(K, h)) < 0$ and C^∞.

Now, since we have been able to show that $G(m_i(K, h)) < 0$ for $i = 1, 2, 3$, it can be concluded in addition that $m_i(K, h)$ are the maximum points of $\phi(m)$ on the interior of their respective domains.

(b) The proof follows directly from the discussion of the proof of point (a) above and an application of Berge's maximum theorem. It is evident from Proposition 4.2.3 and the proof of point (a) above that $m_1(K, h), m_2(K, h)$, and $m_3(K, h)$ are the unique maximum points of $\phi(m)\big|_{D_1}, \phi(m)\big|_{D_2}$, and $\phi(m)\big|_{D_3}$, respectively. Therefore,

by the application of Berge's maximum theorem (see [31,37]) and the continuity of $\phi(m)$ implies that $m_1(K,h), m_2(K,h)$, and $m_3(K,h)$ are continuous on the interior of their respective domains D_1, D_2 and D_3. Hence, the smoothness of $m_i(K,h)$ on the interior of its domain follows directly from noticing that $\phi(m) \in C^\infty$ and hence $\phi'(m) \in C^\infty$, i.e., $m_1(K,h), m_2(K,h)$, and $m_3(K,h)$ are C^∞ on the interior of their respective domains.

(c) It has already been established that for any $i \in \{1,2,3\}$, $\phi''(m_i) \neq 0$ for suitable K,h. Hence, a direct computation shows that:

$$
\begin{aligned}
\frac{\partial}{\partial h}\phi(m_i) &= \underbrace{\frac{\partial}{\partial m}\phi(m)\Big|_{m=m_i}}_{=0}\frac{\partial m_i}{\partial h} + \frac{\partial}{\partial h}\phi(m)\Big|_{m=m_i} \\
&= m_i
\end{aligned}
\tag{4.26}
$$

and similarly,

$$
\begin{aligned}
\frac{\partial}{\partial K}\phi(m_i) &= \frac{\partial}{\partial m}\phi(m)\Big|_{m=m_i}\frac{\partial m_i}{\partial K} + \frac{\partial}{\partial K}\phi(m)\Big|_{m=m_i} \\
&= \frac{m_i^3}{3}.
\end{aligned}
\tag{4.27}
$$

Recall that $m_i, i = \{1,2,3\}$ are the stationary points of $\phi(\cdot)$, and hence taking the first order partial derivative of $\operatorname{arctanh}(m_i) - Km_i^2 - h = 0$ with respect to K and h, $\dfrac{\partial m_i}{\partial K}$ satisfies

$$
\begin{aligned}
\frac{1}{1-m_i^2}\frac{\partial m_i}{\partial K} - m_i^2 - 2Km_i\frac{\partial m_i}{\partial K} &= 0 \\
\frac{\partial m_i}{\partial K}\underbrace{\left[\frac{1}{1-m_i^2} - 2Km_i\right]}_{=-\phi''(m_i)} &= m_i^2 \\
\frac{\partial m_i}{\partial K} &= -\frac{m_i^2}{\phi''(m_i)}
\end{aligned}
\tag{4.28}
$$

and similarly for $\dfrac{\partial m_i}{\partial h}$ one obtains

$$\frac{1}{1-m_i^2}\frac{\partial m_i}{\partial h} - 2Km_i\frac{\partial m_i}{\partial h} - 1 = 0$$

$$\frac{\partial m_i}{\partial h}\left[\frac{1}{1-m_i^2} - 2Km_i\right] = 1 \qquad (4.29)$$

$$\frac{\partial m_i}{\partial h} = -\frac{1}{\phi''(m_i)}.$$

Now, taking a second order partial derivative of $\operatorname{arctanh}(m_i) - Km_i^2 - h = 0$ with respect to K and h yields:

$$\frac{1}{1-m_i^2}\frac{\partial^2 m_i}{\partial h^2} + \left(\frac{\partial m_i}{\partial h}\right)^2\left(\frac{2m_i}{(1-m_i^2)^2}\right) - 2Km_i\frac{\partial^2 m_i}{\partial h^2} - 2K\left(\frac{\partial m_i}{\partial h}\right)^2 = 0$$

$$\frac{\partial^2 m_i}{\partial h^2}\left[\frac{1}{1-m_i^2} - 2Km_i\right] = \left(\frac{\partial m_i}{\partial h}\right)^2\underbrace{\left[2K - \frac{2m_i}{(1-m_i^2)^2}\right]}_{=\phi'''(m)} \qquad (4.30)$$

$$\frac{\partial^2 m_i}{\partial h^2} = -\frac{\phi'''(m_i)}{\left[\phi''(m_i)\right]^3}$$

and

$$\left(\frac{1}{1-m_i^2} - 2Km_i\right)\frac{\partial^2 m_i}{\partial K^2} + \left(\frac{\partial m_i}{\partial K}\right)^2\left(\frac{2m_i}{(1-m_i^2)^2} - 2K\right) - 2m_i\frac{\partial m_i}{\partial K} = 0$$

$$\frac{\partial^2 m_i}{\partial h^2}\left[\frac{1}{1-m_i^2} - 2Km_i\right] = \left(\frac{\partial m_i}{\partial K}\right)^2\left[2K - \frac{2m_i}{(1-m_i^2)^2}\right] + 2m_i\frac{\partial m_i}{\partial K} \qquad (4.31)$$

$$\frac{\partial^2 m_i}{\partial K^2} = -\frac{m_i^4\phi'''(m)}{\left[\phi''(m_i)\right]^3} + \frac{2m_i^3}{\left[\phi''(m_i)\right]^2}$$

and this concludes the proof. $\qquad\square$

In the following, the existence and uniqueness of the phase transition, i.e., the existence of two thermodynamic equilibrium phases for fixed (K,h) is proved, and its properties are also studied. Recall from the previous results of Proposition 4.2.3 that:

1. if $K > K_c$ and $h < \psi_1(K)$, then $m_1(K,h)$ is the only local maximum point of $\phi(m)$ and hence the global maximiser. $\phi(m)$ has two local maximisers $m_1(K,h)$ and $m_2(K,h)$ if $\psi_1(K) < h < \psi_2(K)$ while for $h > \psi_2(K)$, $m_2(K,h)$ is the only local maximiser and thus the global maximiser of $\phi(m)$.

2. if $0 \leq K \leq K_c$ and $h \in \mathbb{R}$ then $m_3(K,h)$ is the only local maximiser of $\phi(m)$, hence the global maximum point.

In the first observation above, there are two local maximisers $m_1(K,h)$ and $m_2(K,h)$ if $\psi_1(K) < h < \psi_2(K)$ while when we move out of that range of h only one survives. Now, the interest is to identify which one is the global maximiser by considering the sign of the following function:

$$\Delta(K,h) = \phi(m_2(K,h)) - \phi(m_1(K,h)) \tag{4.32}$$

for $K > K_c$ and $h \in \mathbb{R}$. The following proposition makes use of the intermediate value theorem to investigate the sign of $\Delta(K,h)$ on the given interval $\psi_1(K) \leq h \leq \psi_2(K)$.

Proposition 4.2.5. *(Existence and uniqueness). For all $K > K_c$, there exists a unique $h = \gamma(K) \in (\psi_1(K), \psi_2(K))$ such that $\Delta(K,h) = 0$. Furthermore,*

$$\Delta(K,h) \begin{cases} < 0, & \text{if} \quad \psi_1(K) \leq h < \gamma(K) \\ > 0, & \text{if} \quad \gamma(K) < h \leq \psi_2(K). \end{cases} \tag{4.33}$$

Proof. For $K > K_c$, observe that

1. $h \mapsto \Delta(K,h)$ is a continuous function, by continuity of $\phi(m), m_1(K,h)$ and $m_2(K,h)$. Hence the function $\Delta(K,h)$ can be extended by continuity at $h = \psi_1(K)$ and $h = \psi_2(K)$.

2. $\Delta(K, \psi_1(K)) < 0$, because if $h = \psi_1(K)$, $m_1(K,h)$ is the only maximum point while $m_2(K,h)$ is an inflection point of $\phi(m)$. Hence $m_1(K,h)$ is the global maximum point of $\phi(m, K, h)$.

3. $\Delta(K, \psi_2(K)) > 0$, since at $h = \psi_2(K)$ the only maximum point of $\phi(m)$ is given by $m_2(K,h)$. Hence it is the global maximum point of $\phi(m, K, J)$.

Since the function $\Delta(K,h)$ is continuous and changes sign from negative to positive on the interval $\psi_1(K) \leq h \leq \psi_2(K)$, a direct application of the intermediate value theorem implies that, there exist a coexistence curve $h = \gamma(K) \in (\psi_1(K), \psi_2(K))$ such that $\Delta(K, \gamma(K)) = 0$. The uniqueness of $\gamma(K)$ such that $\Delta(K, \gamma(K)) = 0$ follows from the fact that $h \mapsto \Delta(K,h)$ is strictly increasing on the domain $\psi_1(K) \leq h \leq \psi_2(K)$.

In fact, from Proposition 4.2.4, it has been shown that $\phi(m_i(K, h)), m_i(K, h)$, $i = 1, 2$ are smooth functions, and hence

$$\frac{\partial \Delta}{\partial h}(K, h) = \frac{\partial}{\partial h}\phi(m_2) - \frac{\partial}{\partial h}\phi(m_1)$$
$$= m_2(K, h) - m_1(K, h) > 0 \tag{4.34}$$

for $h \in (\psi_1(K), \psi_2(K))$. Furthermore, observe that $\Delta(K, h)$ is C^∞ by the smoothness of $\phi(m)$, $m_1(K, h)$ and $m_2(K, h)$ in its domain. Note from equation (4.34) that, since

$$\frac{\partial}{\partial h}\Delta(K, h) \neq 0 \tag{4.35}$$

on the domain $\{(K, h)|K > K_c, \psi_1(K) < h < \psi_2(K)\}$, then by the implicit function theorem it can be concluded that $\gamma(K) \in C^\infty((K_c, \infty))$.

Let us note that in the case $K < 0$ the above results hold due to the invariance property of the Hamiltonian under transformation of the sign of the parameters and the spin flip. This leads to the observation of two unique phase jumps (see Figure 4.1) and a smooth variation of the order parameter between the two critical points $m_c = \pm 1/\sqrt{3}$ in the phase space. $\qquad \square$

The following corollary summarises the result above:

Corollary 4.2.1. *Denote by $m^*(K, h)$ the unique global maximum point of $\phi(m)$. Then:*

$$m^*(K, h) := \begin{cases} m_1(K, h), & \text{if } K > K_c, \ h < \gamma(K) \\ m_2(K, h), & \text{if } K > K_c, \ h > \gamma(K), \\ m_3(K, h), & \text{if } 0 \leq K \leq K_c \ h \in \mathbb{R}, \end{cases} \tag{4.36}$$

where $\gamma(K)$ is defined by Proposition 4.2.5 and, by Proposition 4.2.4, $\phi''(m^*(K, h)) < 0$.

Note that $\gamma(K)$ represents the coexistence curve in which there exist two global maximum points of $\phi(m)$ and which is unique on the defined domain $(K, h) \in (\mathbb{R}_+ \setminus \{K_c\} \times \mathbb{R})$. Now, denote by

$$\bar{\gamma}(K) := \begin{cases} \gamma(K), & \text{if } K > K_c \\ h_c, & \text{if } K = K_c. \end{cases} \tag{4.37}$$

Hence it follows form Proposition 4.2.4 that $m^*(K, h)$ is continuous on its domain $(\mathbb{R}_+ \times \mathbb{R}) \backslash \gamma$ and it is C^∞ on $(\mathbb{R}_+ \times \mathbb{R}) \backslash \overline{\gamma}$. In the following proposition we study some properties of $\overline{\gamma}(K)$:

Proposition 4.2.6. *(Regularity properties.) The function $\overline{\gamma}(K)$ is $C^\infty(\mathbb{R}_+ \setminus \{K_c\})$ and at least C^1 for $K = K_c$. In particular if $K > K_c$, then*

$$\gamma'(K) := -\frac{1}{3}\left(m_2(K, \gamma(K))^2 + m_1(K, \gamma(K))m_2(K, \gamma(K)) + m_1(K, \gamma(K))^2 \right) \quad (4.38)$$

and

$$\overline{\gamma}'(K_c) := -m_c^2. \quad (4.39)$$

Proof. i. To lighten the notation for the maximisers, m_i will interchangeably be used to denote $m_i(K, \cdot)$ for $i = 1, 2$. It has been shown in Proposition 4.2.5 that $\gamma(K) \in C^\infty((K_c, \infty))$ and $h = \gamma(K)$ is the only solution of the equation

$$\Delta(K, h) = 0,$$

by an application of the intermediate value theorem, where $\Delta(K, h)$ is defined as equation (4.32) for $\psi_1(K) \le h \le \psi_2(K)$ and $K > K_c$. Therefore

$$\begin{aligned}
\Delta(K, \gamma(K)) \equiv 0 &= \frac{d}{dK}\Delta(K, \gamma(K)) \\
&= \frac{\partial \Delta}{\partial h}(K, \gamma(K))\gamma'(K) + \frac{\partial \Delta}{\partial K}(K, \gamma(K)) \quad (4.40) \\
\implies \gamma'(K) &= -\frac{\partial \Delta}{\partial K} \Big/ \frac{\partial \Delta}{\partial h}(K, \gamma(K)).
\end{aligned}$$

Now, it follows from equations (4.26), (4.27) and (4.34) that

$$\frac{\partial \Delta(K, h)}{\partial K} = \frac{m_2^3}{3} - \frac{m_1^3}{3} \qquad \text{and} \qquad \frac{\partial \Delta(K, h)}{\partial h} = m_2 - m_1.$$

Hence substituting the above into (4.40), yields,

$$\gamma'(K) = -\frac{1}{3}\big(m_2^2 + m_1 m_2 + m_1^2\big)(K, \gamma(K)). \quad (4.41)$$

ii. Now, let us consider the extended function $\overline{\gamma}$. Recall that $\gamma(K) \in [\psi_1(K), \psi_2(K)]$ and observe that $\lim_{K \to K_c^+} \psi_1(K) = \lim_{K \to K_c^+} \psi_2(K) = h_c$, hence

$$\lim_{K \to K_c^+} \gamma(K) = h_c.$$

This implies that $\gamma(K)$ is continuous at K_c. Now, observe further that for $i = 1, 2$

$$m_i(K, h) \xrightarrow[(K,h)\to(K_c,h_c)]{} m_c.$$

Therefore,

$$\gamma'(K) = -\frac{1}{3}\left(m_2^2 + m_1 m_2 + m_1^2\right)(K, \gamma(K)) \xrightarrow[K\to K_c^+]{} -m_c^2 = -\frac{1}{3} \qquad (4.42)$$

by continuity of $\gamma(K)$ and $m_i(K, h)$. Now, an application of the mean value theorem assures that $\overline{\gamma}'(K_c) = -m_c^2 = -\frac{1}{3}$. $\qquad\qquad\qquad\qquad\qquad\qquad\qquad\qquad\square$

Proof of Proposition 4.2.2

Proof. The aim of this section is to study the behaviour of the magnetisation near the critical point (K_c, h_c). It is worth noting that $m^*(K) - m_c \to 0$ as $K \to K_c$.

Let us define for any $K > K_c$ a curve $h = \tau(K)$ such that $\tau(K_c) = h_c$. Let us now consider the following cases: First, if the curve $\tau(K)$ is tangent to γ in K_c, then $\tau'(K_c) = \overline{\gamma}'(K_c) = -m_c^2$, and second, if it is not tangent to γ in the critical point, then $\tau'(K_c) \neq \overline{\gamma}'(K_c)$. Now the critical exponents are calculated using the above arguments.

From equation (4.15) define $\xi =: Km^2 + h$ and $\xi_c =: K_c m_c^2 + h_c$ such that $m \equiv m^*(K) = \tanh\left(\xi\right)$ and $m_c = \tanh\left(\xi_c\right)$. Now, observe that

$$\begin{aligned}
\xi - \xi_c &= Km^2 + h - K_c m_c^2 - h_c + Km_c^2 - Km_c^2 \\
&= K(m^2 - m_c^2) + (h - h_c) + m_c^2(K - K_c).
\end{aligned} \qquad (4.43)$$

(a) If $h = \tau(K)$ and $\tau'(K_c) = -m_c^2$ then a Taylor's expansion of $\tau(K)$ at K_c is given as

$$\begin{aligned}
\tau(K) &= \tau(K_c) + \tau'(K_c)(K - K_c) \\
h - h_c &= -m_c^2(K - K_c)
\end{aligned} \qquad (4.44)$$

and a Taylor's expansion of m as defined in equation (4.15) at ξ_c, gives,

$$\begin{aligned}
m &= \tanh\left(\xi_c\right) + \left[1 - \tanh^2\left(\xi_c\right)\right](\xi - \xi_c) \\
&\quad - \tanh\left(\xi_c\right)\left[1 - \tanh^2\left(\xi_c\right)\right](\xi - \xi_c)^2 + \mathcal{O}((\xi - \xi_c)^3) \\
&= m_c + (1 - m_c^2)(\xi - \xi_c) - m_c(1 - m_c^2)(\xi - \xi_c)^2 + \mathcal{O}((\xi - \xi_c)^3) \qquad (4.45) \\
&= m_c + K(1 - m_c^2)(m - m_c)(m + m_c) \\
&\quad - K^2 m_c(1 - m_c^2)(m - m_c)^2(m + m_c)^2 + \mathcal{O}((m^2 - m_c^2)^3).
\end{aligned}$$

This implies that,

$$
\begin{aligned}
1 =& K \underbrace{(1 - m_c^2)(m + m_c)}_{=\alpha} - \underbrace{K^2 m_c (1 - m_c^2)(m + m_c)^2}_{=\beta}(m - m_c) + \mathcal{O}\big((m - m_c)\big) \\
=& \alpha K - \beta(m - m_c) + \mathcal{O}\big((m - m_c)\big) \\
=& \alpha K - \alpha K_c + \alpha K_c - \beta(m - m_c) + \mathcal{O}\big((m - m_c)\big).
\end{aligned}
$$

and simplifies as

$$
(m - m_c) \sim \frac{\alpha}{\beta}(K - K_c) + \frac{\alpha}{\beta}K_c - \frac{1}{\beta}. \tag{4.46}
$$

Notice that as $K \to K_c$, $\frac{\alpha K_c}{\beta} - \frac{1}{\beta} \to 0$ and $\frac{\alpha}{\beta} \to \frac{1}{2K_c^2 m_c^2}$. Hence it follows that

$$
m - m_c \sim \frac{1}{2K_c^2 m_c^2}(K - K_c) \qquad \text{as} \quad K \to K_c. \tag{4.47}
$$

(b) Now, let's suppose that $h = \tau(K)$, $h_c = \tau(K_c)$ and $\tau'(K_c) = \kappa \neq -m_c^2$, then by a Taylor's expansion of $\tau(K)$ at K_c

$$
\begin{aligned}
\tau(K) =& \tau(K_c) + \tau'(K_c)(K - K_c) \\
\implies h - h_c =& \kappa(K - K_c).
\end{aligned} \tag{4.48}
$$

Using the same argument as before and following from (4.43) and (4.45),

$$
\begin{aligned}
\xi - \xi_c =& K(m^2 - m_c^2) + \kappa(K - K_c) + m_c^2(K - K_c) \\
=& K \underbrace{(m - m_c)}_{=\vartheta}(m + m_c) + (K - K_c)(\kappa + m_c^2)
\end{aligned} \tag{4.49}
$$

and

$$
\begin{aligned}
\vartheta =& (1 - m_c^2)\big[K\vartheta(m + m_c) + (K - K_c)(\kappa + m_c^2)\big] \\
& - m_c(1 - m_c^2)\big[K\vartheta(m + m_c) + (K - K_c)(\kappa + m_c^2)\big]^2 \\
& + \mathcal{O}\big(\big[K\vartheta(m + m_c) + (K - K_c)(\kappa + m_c^2)\big]^3\big).
\end{aligned} \tag{4.50}
$$

Therefore,

$$
\begin{aligned}
& K^2 m_c(1 - m_c^2)(m + m_c)^2 \vartheta^2 + \bigg(2K m_c(1 - m_c^2)(m + m_c)(\kappa + m_c^2)(K - K_c) \\
& - K(1 - m_c^2)(m + m_c) + 1\bigg)\vartheta + m_c(1 - m_c^2)(\kappa + m_c^2)^2(K - K_c)^2 \\
& - (1 - m_c^2)(\kappa + m_c^2)(K - K_c) \sim 0.
\end{aligned}
$$

$$
\tag{4.51}
$$

Notice that as $K \to K_c$, equation (4.51) can be rewritten as:

$$4K_c^2 m_c^3(1 - m_c^2)\vartheta^2 + \left(4K_c m_c^2(1 - m_c^2)(\kappa + m_c^2)(K - K_c) + \underbrace{1 - 2K_c m_c(1 - m_c^2)}_{=0} \right)\vartheta$$

$$+ \left[m_c(K - K_c)(\kappa + m_c^2) - 1 \right](1 - m_c^2)(\kappa + m_c^2)(K - K_c) \sim 0.$$

Now, the above equation is a quadratic equation in $\vartheta = (m - m_c)$ and can be solved using the quadratic formula. Hence, in the sequel, it will be used that $a = 4K_c^2 m_c^3(1 - m_c^2)$, $b = 4K_c m_c^2(1 - m_c^2)(\kappa + m_c^2)(K - K_c)$ and $c = \left[m_c(K - K_c)(\kappa + m_c^2) - 1 \right](1 - m_c^2)(\kappa + m_c^2)(K - K_c)$. The discriminant is then obtained as:

$$b^2 - 4ac = 16K_c^2 m_c^3(1 - m_c^2)^2(\alpha + m_c^2)(K - K_c). \tag{4.52}$$

This implies that

$$\vartheta \sim \frac{-4K_c m_c^2(1 - m_c)(\kappa + m_c^2)(K - K_c) \pm \sqrt{16K_c^2 m_c^2(1 - m_c^2)^2}\sqrt{m_c(\kappa + m_c^2)(K - K_c)}}{8K_c^2 m_c^3(1 - m_c^2)} \tag{4.53}$$

which simplifies to

$$\begin{aligned} m - m_c &\sim \frac{-m_c(\kappa + m_c^2)(K - K_c) \pm \sqrt{m_c(\kappa + m_c^2)(K - K_c)}}{2K_c m_c^2} \\ &\sim \frac{\pm\sqrt{m_c(\kappa + m_c^2)(K - K_c)}}{2K_c m_c^2} \end{aligned} \tag{4.54}$$

as $K \to K_c$.

$\square$

4.3 Conclusion

This chapter comprehensively characterises the equilibrium states and phase properties of the Ising model with three-spin interaction and an external field. The investigation covered various properties of the model, such as the existence and uniqueness of phase transitions as well as the properties of an order parameter that exhibits a critical point characterized by critical exponents, and excludes the asymptotic distribution of the magnetisation. This is because the asymptotic distribution of the magnetisation for this model has been examined in a previous work in [23] and can be replicated without significant modifications, specifically for $K > 0$.

The model exhibits two distinct second-order phase transitions in the order parameter, which are separated by a smooth transition with respect to the external

field. The critical exponents of the order parameter within the entire phase space have specific values: $\tilde{\beta} = 1$ in a direction tangential to the critical point, and $\tilde{\beta} = 1/2$ otherwise, following mean-field behaviour.

Chapter 5

The inverse problem beyond pairwise interaction

In this chapter we study the inverse problem for a class of mean-field models in statistical mechanics with cubic interaction as introduced in (2.1). The discussion follows from [40]. The direct problem of statistical mechanics is to compute macroscopic variables (i.e., the average values of magnetisations and correlations) when the couplings and fields are known. In the inverse problem the reverse is done: the couplings and fields are computed using the (statistical) datum of the macroscopic quantities. This is often achieved by a technique known as Boltzmann machine learning, a special case of learning in statistical inference theory [41, 42] when the probability measure is the Boltzmann-Gibbs one.

The system we consider here is made of Ising spins and, beside an homogeneous magnetic field and a constant two-body interaction, it contains a constant three-body term. One of the peculiarities of this model, which turns out to have a cubic Hamiltonian function, is that it lacks the standard convexity property of its quadratic version and its direct and inverse problems are therefore outside the general methods of convex optimisation problems. Taking into account the three-body term, we move from a generic graph (network) structure where we consider only dyadic or pairwise interactions into hypergraphs where faces are also considered [43–45]. This allows for the consideration of a large spectrum of applications that are closely related to real-world phenomena, such as team collaborations rather than collaborations between pairs (see [46]). According to [44, 46] the presence of higher-order interactions, such as three-or more-body interactions, may have significant impact also on the dynamics of interacting networked systems and potentially

lead to abrupt transitions between states [12]. Abrupt transitions are a prevalent phenomenon in nature that can be found in areas as diverse as social networks or biology [46, 47].

In recent years, studies in deep learning for artificial intelligence have been approached in terms of the inverse problem in statistical mechanics [48–50]. The techniques to study that case are of very different nature than those we treat in this work because the parameters to be identified are of very high dimension and the involved models concern the theory of disordered systems [51]. Although in this study we are only interested in computing three parameters, we believe that a robust understanding of the statistical mechanics low-dimensional of inverse problem may shed some light on the general Boltzmann machine learning problem due to the presence of phase transitions for very large systems.

A further reason of interest for the problem we deal with is that, in recent times, this method has attracted some attention due to it's ability to advance a useful novel approach for several applications like neural networks, protein structures, computer vision [52–56], and socio-economic sciences [57–65].

The model we consider is invariant under the permutation group but its extension to the case in which that symmetry is not present has already been considered in [35] for the two-populated case with the same perspectives of the multi-populated quadratic models [60, 66]. An intriguing feature of such model is that it shows a *discontinuous first-order phase transition* which is not present in the case of the standard quadratic mean-field model.

To solve the inverse problem we first compute, exploiting the exact solution of the model, the analytical formulas for the system's macroscopic variables in the thermodynamic limit where they provide explicit expressions for the interaction couplings (cubic and quadratic) and the magnetic field. It is worth noticing that since the number of necessary relations to compute the free parameters is three we need to make observations up to the third moment of the probability distribution. To relate the analytical inversion with the (statistical) observations we use the maximum likelihood criteria and we establish a link between estimated and theoretical values. Finally, we test how well the model's free parameters are reconstructed using the inversion formulas and how their robustness is affected by both the system size and the number of independent samples simulated from the model's equilibrium configuration.

The chapter is organised as follows. The cubic mean-field model is introduced

in Section 5.1 where it has been shown how to compute and test the robustness of the analytical inverse formulas using the maximum likelihood estimation procedure. Section 5.2 is devoted to the numerical testing of the robustness of the inversion formulas for unique stable solutions. In Section 5.3 the case of metastable or multiple solutions for finite-size systems is discussed. The final section, Section 5.4, provides a general conclusion and the model's future prospects.

5.1   Inverse problem for the cubic mean-field Ising model

The Hamiltonian to be considered for this chapter is given by:

$$H_N(\sigma) = -N \left(\frac{K}{3} m_N^3(\sigma) + \frac{J}{2} m_N^2(\sigma) + h m_N(\sigma) \right), \tag{5.1}$$

and the Boltzmann-Gibbs state on a configuration σ will be denoted by

$$P_{N,K,J,h}(\sigma) = \frac{e^{-H_N(\sigma)}}{Z_N}, \tag{5.2}$$

where Z_N is the usual normalisation constant and the pressure per particle associated with the thermodynamic system is given by (2.6). Recall from equation (2.5) that for a given observable $f(\sigma)$ the Boltzmann-Gibbs expectation is denoted by $\omega_N(f(\sigma))$. Notwithstanding, taking suitable derivatives of the pressure density function (2.6) one generates the moments of the system with respect to the Boltzmann-Gibbs measure (5.2). Hence, one obtains the following finite-size quantities:

$$\frac{\partial p_N}{\partial h} = \omega_N(m_N(\sigma)) = \frac{\sum_{\sigma \in \Omega_N} m_N(\sigma) e^{-H_N(\sigma)}}{\sum_{\sigma \in \Omega_N} e^{-H_N(\sigma)}}, \tag{5.3}$$

$$\frac{\partial^2 p_N}{\partial h^2} = \frac{N \sum_\sigma m_N^2 e^{-H_N(\sigma)} \cdot \sum_\sigma e^{-H_N(\sigma)} - N \sum_\sigma m_N e^{-H_N(\sigma)} \cdot \sum_\sigma m_N e^{-H_N(\sigma)}}{(\sum_\sigma e^{-H_N(\sigma)})^2}$$
$$= N[\omega(m_N^2(\sigma)) - \omega^2(m_N(\sigma))]$$
$$= \chi_N \tag{5.4}$$

and

$$
\begin{aligned}
\frac{\partial^3 p_N}{\partial h^3} &= \frac{\partial \chi_N}{\partial h} \\
&= N \frac{\partial}{\partial h} \left[\omega(m_N^2) - \omega^2(m_N) \right] \\
&= N \left[\frac{\partial}{\partial h} \left(\frac{\sum_{\sigma \in \Omega_N} m_N^2(\sigma) e^{-H_N(\sigma)}}{\sum_{\sigma \in \Omega_N} e^{-H_N(\sigma)}} \right) - \frac{\partial}{\partial h} \left(\frac{\sum_{\sigma \in \Omega_N} m_N(\sigma) e^{-H_N(\sigma)}}{\sum_{\sigma \in \Omega_N} e^{-H_N(\sigma)}} \right)^2 \right] \\
&= N \left[\frac{N \sum_\sigma m_N^3 e^{-H_N(\sigma)} \cdot \sum_\sigma e^{-H_N(\sigma)} - N \sum_\sigma m_N e^{-H_N(\sigma)} \cdot \sum_\sigma m_N^2 e^{-H_N(\sigma)}}{(\sum_\sigma e^{-H_N(\sigma)})^2} \right] \\
&\quad - 2\omega(m_N) N \left[\frac{N \sum_\sigma m_N^2 e^{-H_N(\sigma)} \cdot \sum_\sigma e^{-H_N(\sigma)} - N \sum_\sigma m_N e^{-H_N(\sigma)} \cdot \sum_\sigma m_N e^{-H_N(\sigma)}}{(\sum_\sigma e^{-H_N(\sigma)})^2} \right] \\
&= N^2 \left[\omega(m_N^3) - \omega(m_N)\omega(m_N^2) \right] - 2\omega(m_N) N^2 \left[\omega(m_N^2) - \omega^2(m_N) \right] \\
&= N^2 [\omega(m_N^3) - 3\omega(m_N)\omega(m_N^2) + 2\omega(m_N)\omega^2(m_N)] \\
&= \psi_N
\end{aligned}
$$

$$(5.5)$$

where $\omega_N(m_N(\sigma))$, χ_N and ψ_N are the finite-size average magnetisation, suscepti-bility and third moment respectively. In order to solve the inverse problem analyti-cally for a given configuration of spin particles, we first find the relation between the model parameters and the limiting pressure per particle: $p = \lim_{N \to \infty} p_N$ defined in (2.14). Observe that

$$\frac{\partial p}{\partial h} = Km^2 + Jm + h - \operatorname{arctanh}(m) = 0 \quad \text{i.e.} \quad m = \tanh(Km^2 + Jm + h). \quad (5.6)$$

The second and third partial derivatives are obtained as follows:

$$
\begin{aligned}
\frac{\partial^2 p}{\partial h^2} &= 2Km \frac{\partial m}{\partial h} + J \frac{\partial m}{\partial h} + 1 - \frac{1}{1-m^2} \frac{\partial m}{\partial h} = 0 \\
&= \frac{\partial m}{\partial h} \left[2Km + J - \frac{1}{1-m^2} \right] = -1 \\
&= \frac{\partial m}{\partial h} = -\frac{1}{\underbrace{\left[2Km + J - \dfrac{1}{1-m^2} \right]}_{=\phi''(m)}} \\
\chi &= \frac{\partial m}{\partial h} = \frac{(1-m^2)}{1 - (1-m^2)(J+2Km)}
\end{aligned}
$$

$$(5.7)$$
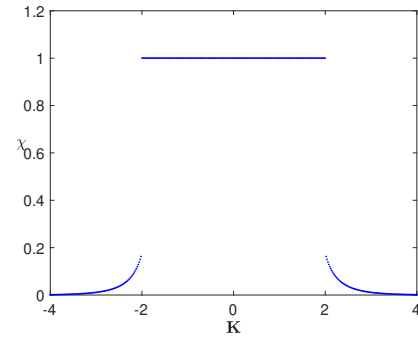
and

$$\frac{\partial^3 p}{\partial h^3} = \frac{\partial \chi}{\partial h} = 2Km\frac{\partial^2 m}{\partial h^2} + 2K\left(\frac{\partial m}{\partial h}\right)^2 + J\frac{\partial^2 m}{\partial h^2} - \frac{1}{1-m^2}\frac{\partial^2 m}{\partial h^2}$$

$$- \left(\frac{\partial m}{\partial h}\right)^2\left(\frac{2m}{(1-m^2)^2}\right) = 0$$

$$= \frac{\partial^2 m}{\partial h^2}\underbrace{\left[2Km + J - \frac{1}{1-m^2}\right]}_{=-\chi^{-1}} = \underbrace{-\left(\frac{\partial m}{\partial h}\right)^2}_{=-\chi^2}\left[2K - \frac{2m}{(1-m^2)^2}\right] \qquad (5.8)$$

$$\psi = \frac{\partial^2 m}{\partial h^2} = \chi^3\left(2K - \frac{2m}{(1-m^2)^2}\right).$$

In Figure 5.1 we illustrate an example of critical behaviour for the model with the presence of phase transitions occurring at $J = h = 0$ when K is varied.
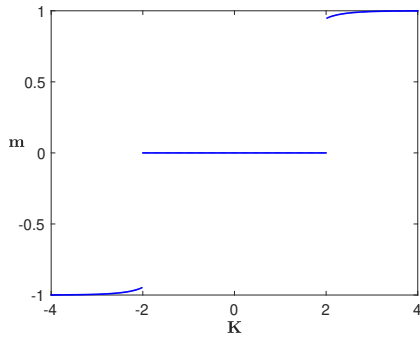
(a) magnetisation

(b) Magnetic Susceptibility
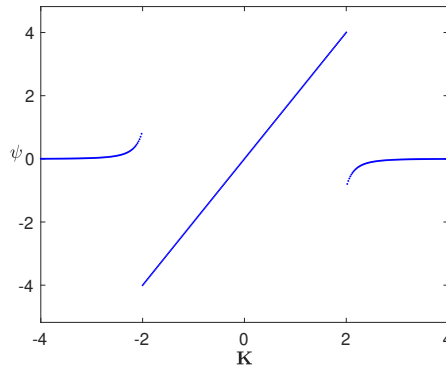
(c) Third moment

Figure 5.1: $J = 0$, $h = 0$. First three moments of the model as a function of K: In a the total magnetisation shows indications of phase transitions occurring at a critical point around ± 2. At the critical point the susceptibility as seen in b and the third moment in c has a jump to 1 and a jump to around ± 4 respectively.

The quantities, m, χ and ψ are the infinite-volume limit average magnetisation, susceptibility and third moment corresponding to the finite-size quantities ω_N, χ_N and ψ_N respectively in the thermodynamic limit. The system of equations (5.6), (5.7) and (5.8) has three unknowns K, J and h for which one can solve. Having knowledge of m, χ and ψ one can compute the parameters (i.e., K, J and h) of the model through the following equations:

$$K = \frac{m}{(1-m^2)^2} + \frac{\psi}{2\chi^3}, \tag{5.9}$$

$$J = \frac{1}{1-m^2} - \frac{1}{\chi} - 2Km \tag{5.10}$$

and the external magnetic field is then obtained from (2.25) as

$$h = \tanh^{-1}(m) - Km^2 - Jm. \tag{5.11}$$

Let us observe that, in the region of the parameter space where the consistency equation (2.25) has a unique stable solution the following holds:

$$\lim_{N \to \infty} \omega_N(m_N(\sigma)) = m. \tag{5.12}$$

In analogy to the behaviour of the quadratic case [67], the Boltzmann-Gibbs measure (5.2) may be multimodal for some (K, J, h) in the parameter space for both the finite-size system and in the thermodynamic limit. In this case equation (5.12) fails to hold. We will discuss later how to handle such a case, following the work done in [67, 68]. The procedure discussed so far deals with the analytical inverse problem.

Now let's focus on addressing the challenge posed by the intractability of the normalisation constant appearing in the probability measure (5.2) for large system size. Importantly, it worth observing that the Boltzmann-Gibbs measure (5.2) is defined for a configuration of spins, meanwhile the Hamiltonian (5.1) is of a mean-field nature such that the microstate of the spins configuration is replaced by its macrostate. In this case, to compute the probability for a given observation or for the system to be in a certain macrostate, one is first interested in answering the question: How many ways are there to split the total number of spins (N) into spins of $+1$ and -1 values, or how many microstates match a given macrostate $m_N(\sigma) = m$?

Let's notice that the answer to this question has been addressed in chapter 2 following equation (2.8). Now, recall from equations (2.8) and (2.7) that the

normalisation factor can be rewritten as:

$$Z_N = \sum_{x \in R_N} A_N(x) e^{-H_N(x)},$$

where $R_N = \{-1 + \frac{2k}{N}, k = 0, \ldots, N\}$ and

$$A_N(x) = \frac{N!}{\left(N \frac{(1+x)}{2}\right)! \left(N \frac{(1-x)}{2}\right)!}$$

with $x =: m_N(\sigma)$. Hence, (5.2) becomes:

$$P_{N,K,J,h}(m_N(\sigma) = x) = \frac{A_N \exp\left(N\left(\frac{K}{3}x^3 + \frac{J}{2}x^2 + hx\right)\right)}{\sum_{x \in R_N} A_N \exp\left(N\left(\frac{K}{3}x^3 + \frac{J}{2}x^2 + hx\right)\right)} \tag{5.13}$$

The remainder of this section will be devoted to the statistical procedure required to compute the estimators of K, J and h.

We start by generating M independent spin configurations $\sigma^{(1)}, \ldots, \sigma^{(M)}$ distributed according to (5.13) from the model's equilibrium configuration. Let's denote by m_l for $l = 1, \ldots, M$, the $M-$spin configuration means, for fixed (K, J, h):

$$m_l \sim P_{N,K,J,h}(m_N(\sigma) = m), \tag{5.14}$$

which will be used as observed data from which the parameters will be reconstructed. Notice that the analytical inverse formulas of K, J and h in equations (5.9), (5.10) and (5.11) respectively, are valid on the infinite volume limit of the observables, i.e., m, χ and ψ. Hence, to compute the estimates of the model parameters K, J and h, the maximum likelihood estimation procedure will be adopted having knowledge of real data. This procedure ensures that the estimated model parameters maximise the probability of getting the given sample of spin configurations from the distribution. Furthermore, the analytical inverse procedure requires statistical approximation of the infinite volume limit quantities (i.e., m, χ and ψ) which are substituted by their finite-size forms ω_N, χ_N and ψ_N. The likelihood function for the measure (5.2) is defined as

$$\begin{aligned}
L(K, J, h) &= P_{N,K,J,h}\{\sigma^{(1)}, \ldots, \sigma^{(M)}\} \\
&= \prod_{l=1}^{M} P_{N,K,J,h}\{\sigma^{(l)}\} \\
&= \prod_{l=1}^{M} \frac{A_N e^{-H_N(\sigma^{(l)})}}{\sum_{x \in R_N} A_N e^{-H_N(x)}}.
\end{aligned}$$

This procedure will enable defining the finite-size magnetisation $\omega_N(m_N(\sigma))$ in terms of the empirical average (i.e., m_N) for each of the M sampled spin configurations. Further, we have that

$$\ln L(K, J, h) = \sum_{l=1}^{M} \left[(-H_N(\sigma^{(l)}) - NI(m_l)) - \ln \sum_{x \in R_N} e^{-H_N(x)-NI(x)} \right]. \quad (5.15)$$

Requiring the derivatives with respect to the parameters K, J and h to vanish amounts to:

$$\frac{\partial}{\partial h} \ln L(K, J, h) = N \sum_{l=1}^{M} \left(m_N(\sigma^{(l)}) - \omega(m_N(\sigma)) \right)$$

$$\frac{\partial}{\partial J} \ln L(K, J, h) = \frac{N}{2} \sum_{l=1}^{M} \left(m_N^2(\sigma^{(l)}) - \omega(m_N^2(\sigma)) \right)$$

$$\frac{\partial}{\partial K} \ln L(K, J, h) = \frac{N}{3} \sum_{l=1}^{M} \left(m_N^3(\sigma^{(l)}) - \omega(m_N^3(\sigma)) \right)$$

and they vanish when

$$\omega_N(m_N(\sigma)) = \frac{1}{M} \sum_{l=1}^{M} m_N(\sigma^{(l)})$$

$$\omega_N(m_N^2(\sigma)) = \frac{1}{M} \sum_{l=1}^{M} m_N^2(\sigma^{(l)}) \quad (5.16)$$

$$\omega_N(m_N^3(\sigma)) = \frac{1}{M} \sum_{l=1}^{M} m_N^3(\sigma^{(l)}).$$

The function $L(K, J, h)$ is at its stationary points when the first, second and third moments of the magnetisation in equation (5.16) are obtained. It is worth noticing that

$$m_N(\sigma^{(l)}) = \frac{1}{N} \sum_{i=1}^{N} \sigma_i^{(l)} \qquad \text{for} \quad l = 1, \dots, M \quad (5.17)$$

are the total magnetisations of the M sample spin configurations. Let's note that $L(K, J, h)$ and its derivatives are only used to solve the forward problem, but not the inverse problem. Now, the inverse problem can be solved when we make use of (5.9), (5.10), (5.11) and (5.16). The maximum likelihood procedure computes the estimators of the infinite-volume quantities m, χ and ψ, from a sample data set through the following:

$$\widehat{m} = \frac{1}{M} \sum_{l=1}^{M} m_N(\sigma^{(l)}), \quad (5.18)$$

$$\widehat{\chi} = N\left(\frac{1}{M}\sum_{l=1}^{M} m_N^2(\sigma^{(l)}) - \widehat{m}^2\right) \tag{5.19}$$

and

$$\widehat{\psi} = N^2\left(\frac{1}{M}\sum_{l=1}^{M} m_N^3(\sigma^{(l)}) - 3\widehat{m}\frac{1}{M}\sum_{l=1}^{M} m_N^2(\sigma^{(l)}) + 2\widehat{m}^3\right). \tag{5.20}$$

We now define the estimators of the three parameters of the cubic mean-field model using the statistical estimators for the magnetisation, susceptibility and third moment (5.18), (5.19) and (5.20) in the infinite-volume limit relations among those quantities (5.9), (5.10) and (5.11)

$$\widehat{K} = \frac{\widehat{m}}{(1 - \widehat{m}^2)^2} + \frac{\widehat{\psi}}{2\widehat{\chi}^3}, \tag{5.21}$$

$$\widehat{J} = \frac{1}{1 - \widehat{m}^2} - \frac{1}{\widehat{\chi}} - 2\widehat{K}\widehat{m}, \tag{5.22}$$

and

$$\widehat{h} = \tanh^{-1}(\widehat{m}) - \widehat{K}\widehat{m}^2 - \widehat{J}\widehat{m}. \tag{5.23}$$

At the critical point $(K, J, h) = (0, 1, 0)$ where all the three phases of the model meet (see Figure 3.1) the magnetisation is zero and the infinite-volume magnetic susceptibility χ and the third moment ψ defined by equations (5.7) and (5.8) respectively diverge. Hence, the inversion formulas (5.9), (5.10) and (5.11) do not hold as it will be illustrated at the end of the next section. We do not include the inversion formulas at the critical point in this work but the problem will be considered in future work.

5.2   Test for the case of unique solution

In this section we are going to examine how the inversion equations perform for different and increasing choices of N and M, respectively the number of particles and sampled configurations. The specific case we consider is the inversion problem for those values of the triple (K, J, h) where there is a unique stable solution of (2.25). In this case, the Boltzmann-Gibbs distribution of the total magnetisation has a unique peak always centered around the analytic solution m: some examples are shown in Figure 5.2 for fixed N. The accuracy of the estimation increases as N and M increase.

The parameters K, J and h are obtained from the computation of the finite-size quantities m_N, χ_N and ψ_N using configurations extracted from the Boltzmann-Gibbs distribution of the data. Estimation of m_N, χ_N and ψ_N for fixed triples of
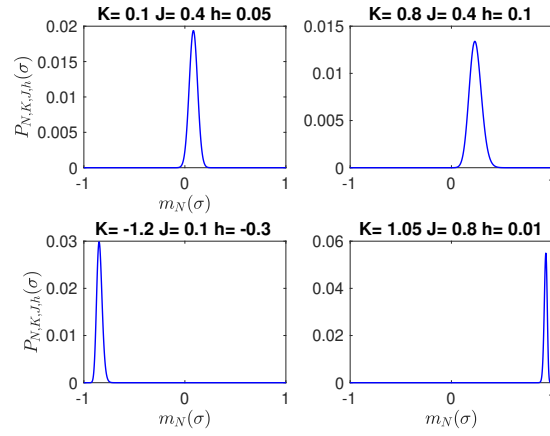
Figure 5.2: Boltzmann Gibbs distribution of the total magnetisation for $N = 1000$ and different sets of triples (K, J, h).

the parameters (K, J, h) and varying $N \in [500, 10000]$ are shown in Figure 5.3. In the same figure, the thermodynamic limits of those quantities are also shown.
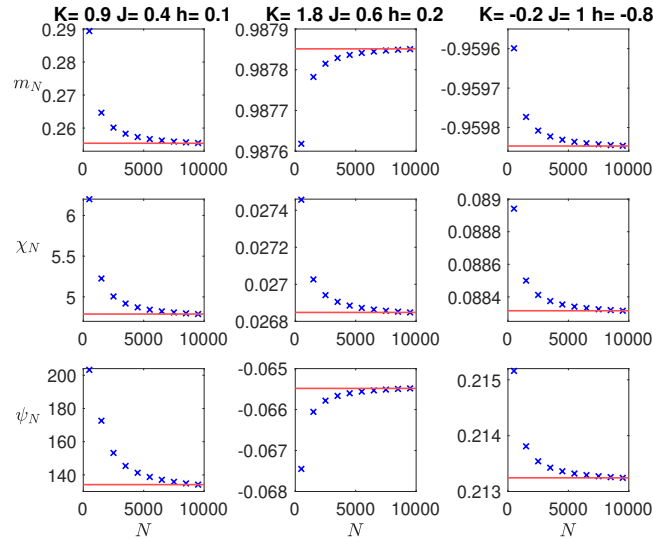
Figure 5.3: Finite-size average magnetisation m_N, susceptibility χ_N and third moment ψ_N as functions of N for three different set of triples (K, J, h). Blue crosses represent the values of m_N (upper panels), χ_N (middle panels) and ψ_N (lower panels) for varying N. As N increases m_N, χ_N and ψ_N approach their true values in the thermodynamic limit given as the red horizontal lines for the chosen values of K, J and h.

From Figure 5.3 we can observe the monotonic behaviour of m_N, χ_N and ψ_N as N increases. In Figure 5.4 we study the relationship between the absolute difference of the finite-size quantities and their corresponding thermodynamic values as a function of the system size N. We find evidence that the finite-size quantities m_N, χ_N and ψ_N converge to their true values with a power law behaviour as N increases. The obtained results indicate that using $N = 10000$ one can estimate the infinite-volume magnetisation, susceptibility and the third moment with vanishing error. We will proceed to use $N = 10000$ as the size for each of the M independent spin configurations $\sigma^{(1)}, ..., \sigma^{(M)}$. Further numerical tests will be performed to determine a suitable number of sample configurations M that can be used for reconstructing the model parameters using the inversion formulas.
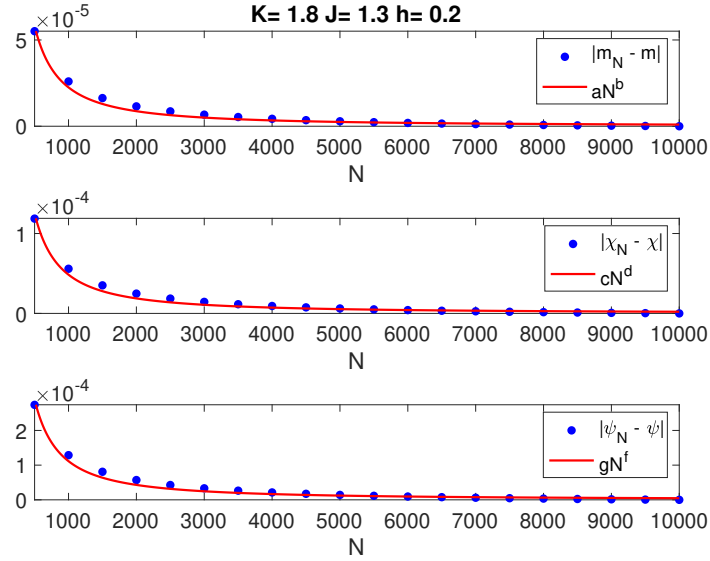
Figure 5.4: Absolute error of the finite size quantities m_N, χ_N and Ψ_N as functions of N together with the best power law fits. In the upper panel, $|m_N - m|$ is shown as a function of N together with the best fit aN^b, where $a = 0.28 \in (0.06, 0.50)$ and $b = -1.37 \in (-1.49, -1.25)$ with a goodness of fit $R^2 = 0.9829$. The middle panel displays $|\chi_N - \chi|$ as a function of N together with its corresponding best fit cN^d, with $c = 0.62 \in (0.14, 1.09)$, $d = -1.37 \in (-1.49, -1.25)$ and $R^2 = 0.9830$ as goodness of fit. The lower panel represents $|\psi_N - \psi|$ as a function of N together with its corresponding best fit gN^f, with $g = 1.47 \in (0.32, 2.62)$, $f = -1.37 \in (-1.49, -1.25)$ and a goodness of fit $R^2 = 0.9826$.

To obtain the statistics associated to the reconstruction of the estimators, we simulate from the model's equilibrium configuration 50 different instances of the M − iid sample configurations, i.e., $(\sigma^{(1)}, \dots, \sigma^{(M)})$, apply the maximum likelihood estimation procedure to each of them separately, solve the inverse problem using (5.21), (5.22) and (5.23) and then average the inferred values over the 50 different M-samples. The mean value of the estimators $\widehat{m}, \widehat{\chi}, \widehat{\psi}$, and $(\widehat{K}, \widehat{J}, \widehat{h})$ over the 50 different M-samples of spin configurations are denoted by $\overline{\widehat{m}}, \overline{\widehat{\chi}}, \overline{\widehat{\psi}}$, and $(\overline{\widehat{K}}, \overline{\widehat{J}}, \overline{\widehat{h}})$ respectively. The results are shown in Figures 5.5 and 5.6.
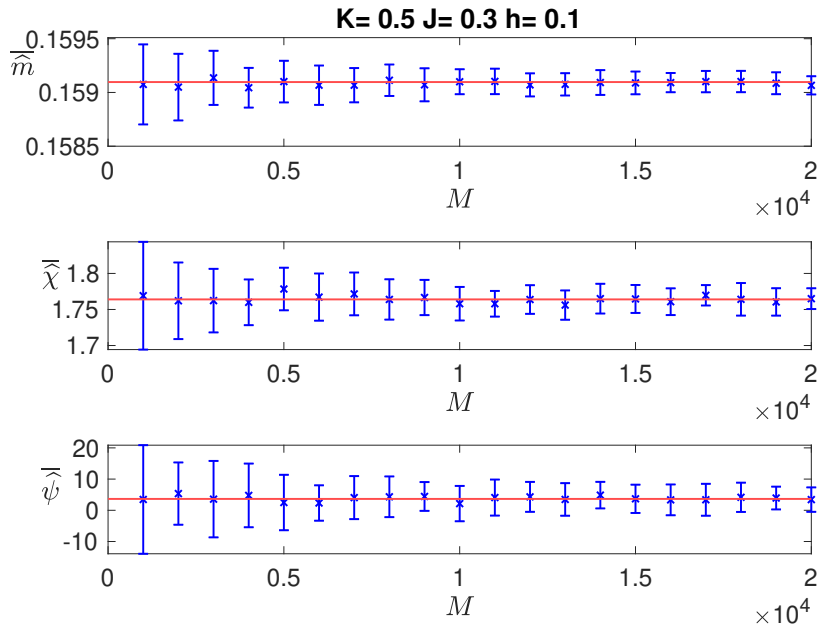

Figure 5.5: Reconstructed average magnetisation $\overline{\widehat{m}}$, susceptibility $\overline{\widehat{\chi}}$ and third moment $\overline{\widehat{\psi}}$ (given as blue crosses in each panel) as a function of M with standard deviation on 50 different M-sample and $N = 10000$. The continuous red line corresponds to m, χ and ψ in the thermodynamic limit.
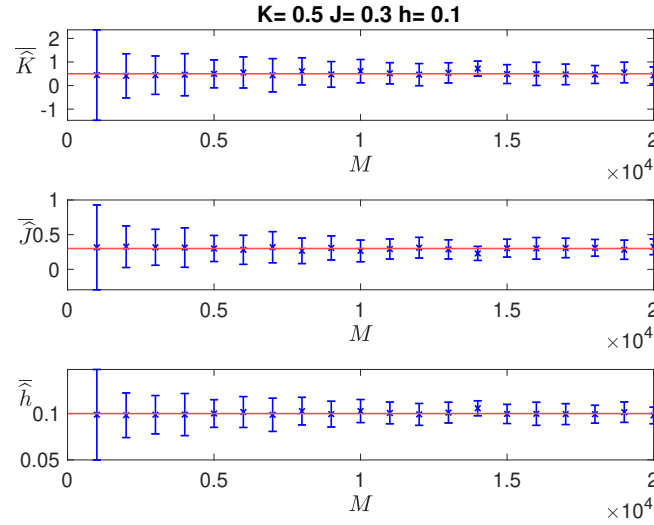
Figure 5.6: $\widehat{\overline{K}}, \widehat{\overline{J}}$ and $\overline{\overline{h}}$ as a function of M for $N = 10000$. The blue crosses are the estimation of $\widehat{\overline{K}}, \widehat{\overline{J}}$ and $\overline{\overline{h}}$ with standard deviations on 50 different M-samples of configurations of the same system. The horizontal red line in each panel corresponds to the exact values of K, J and h.

Figures 5.5 and 5.6 illustrate that at $M = 20000$ we get smaller error bounds for the reconstruction as compared to lesser values of M.

In the sequel, we study the behaviour of the reconstructed parameter for fixed values of J and h and varying K (Figures 5.7 and 5.8) and also for fixed values of K and h and varying J (Figures 5.9 and 5.10). The simulations are performed using $M = 20000$, $N = 10000$ and error bars are standard deviations on 50 different M-samples of the same system. We find all the reconstructed parameter values in good agreement with the exact ones. We can observe that as the intensity of the cubic and quadratic coupling increases the error bars associated to the reconstructed parameters grow, as we can expect since in that region of the parameter space the system is more disordered due to the presence of multiple local stable states and the fluctuations are greater.

Figure 5.7: $\overline{\widehat{K}}$ as a function of K for $N = 10000$ and $M = 20000$. $J = 0.3, h = 0.1$ in left panel and $J = 0.4, h = -0.3$ in the right panel. The estimations of $\overline{\widehat{K}}$ are given as the blue crosses in both panels with standard deviations on 50 different M-samples of configurations of the same system. The red continuous line represents $\overline{\widehat{K}} = K$.
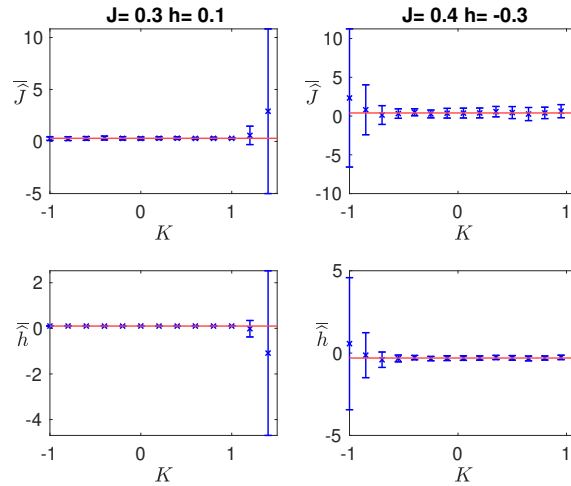
Figure 5.8: $\overline{\widehat{J}}$ and $\overline{\widehat{h}}$ as a function of K for $N = 10000$ and $M = 20000$. $J = 0.3, h = 0.1$ in the left panels and $J = 0.4, h = -0.3$ in the right panels. The estimates of $\overline{\widehat{J}}$ and $\overline{\widehat{h}}$ are given as the blue crosses in all the panels with standard deviations on 50 different M-samples of configurations of the same system. The red continuous lines represent the exact values of J and h.
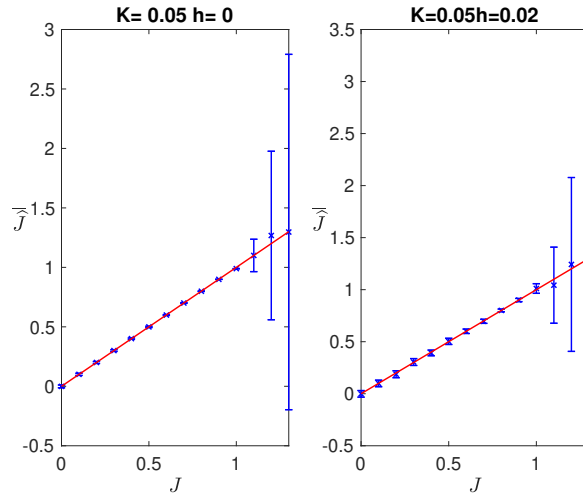
Figure 5.9: $\overline{\widehat{J}}$ as a function of J for $N = 10000$ and $M = 20000$. $K = 0.05, h = 0$ in the left panel and $K = 0.05, h = -0.02$ in the right panel. The blue crosses are the reconstructed values of J in both panels with standard deviations on 50 different M-samples of configurations of the same system. The red continuous line represents the exact value $\overline{\widehat{J}} = J$.
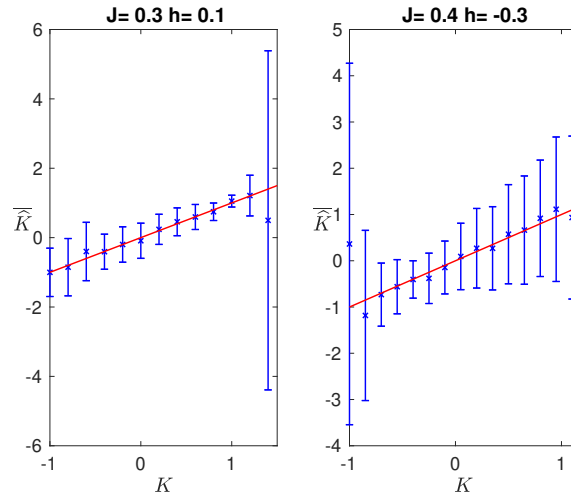

Figure 5.10: $\overline{\widehat{K}}$ and $\overline{\widehat{h}}$ as a function of J for $N = 10000$ and $M = 20000$. $K = 0.05, h = 0$ in the left panels and $K = 0.05, h = 0.02$ in the right panels. The estimate of $\overline{\widehat{K}}$ and $\overline{\widehat{h}}$ are given as the blue crosses in all the panels with standard deviations on 50 different M-samples of configurations of the same system. The red continuous lines represent the exact values of K and h.
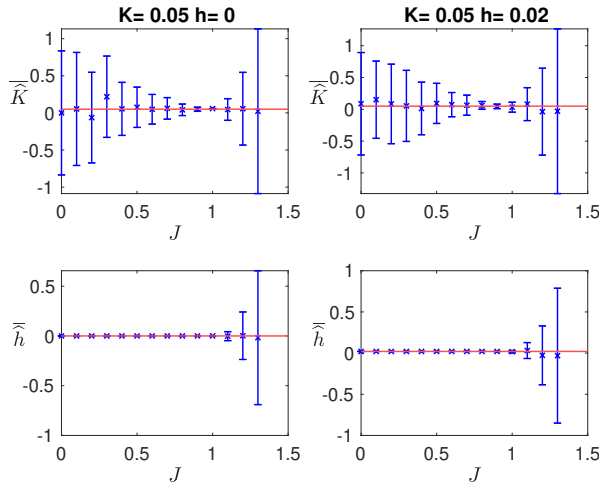
Furthermore, Figure 5.11 show the reconstructed parameters as a function of N at the critical point $(K = 0, J = 1, h = 0)$. It can be noticed that the reconstruction at the critical point for K and h agrees with their exact values with only a small percentage of error and that of J is underestimated.
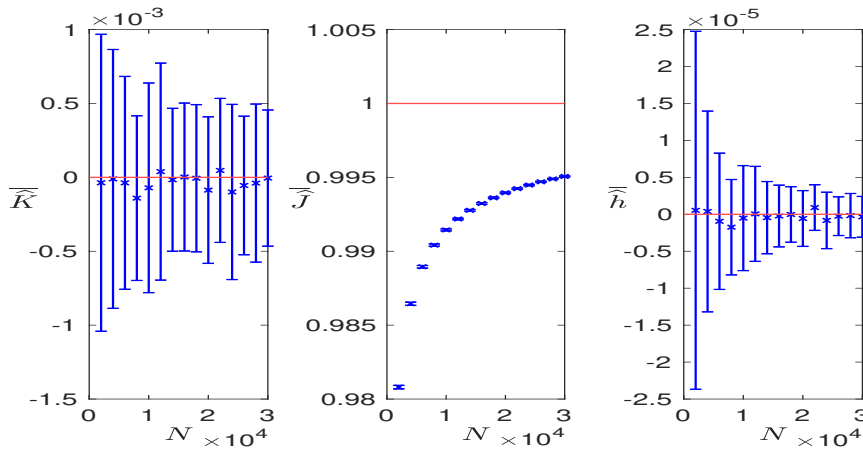
Figure 5.11: $\widehat{\overline{K}}, \widehat{\overline{J}}$ and $\widehat{\overline{h}}$ as a function of N for $M = 20000$. The reconstructed estimates of K, J and h are given as the blue crosses on statistical error bars of 50 different $M-$samples. The red continuous line is the exact value of the parameters K, J and h in the respective panels.

It worth observing that when $K = h = 0$ and $J > 1$ the consistency equation (2.25) has two stable solutions. In this case, for the finite-size system and in the thermodynamic limit, the Boltzmann-Gibbs distribution of the total magnetisation presents two peaks each centered around one of the stable solutions. In such a case the inverse problem procedure discussed in Section 5.1 cannot be used for the reconstruction of the model parameters. We refer readers to [66] where this case has been studied using the spin flip approach due to symmetry of the solution in both finite-size and infinite-volume systems for the quadratic mean-field model. The clustering algorithm to be outlined in the next section provides a more general approach to handle the reconstruction of the model parameters when the phase space has multiple locally stable solution.

5.3   Clustering algorithm for metastable state solutions

Here, we focus on cases where equation (5.6) has a metastable solution. This corresponds to the case where there is more than one locally stable solution of the consistency equation (5.6). For this model, equation (5.6) can have at most three solutions and ϕ has at most two local maxima for fixed (K, J, h). The existence of the metastable solution in the infinite-volume limit is represented at finite N by the occurrence of an extra peak in the distribution. Therefore, while in the thermo-dynamic limit the Boltzmann-Gibbs distribution of the magnetisation is unimodal with the peak corresponding to the stable solution, in the finite-size case also the peak corresponding to the metastable one is present and the distribution is bimodal. Hence, in this case, the inversion problem cannot be studied globally, as done in the previous section. Instead, the procedure has to be applied locally, that is to each subset of configurations clustered around the two local maxima. Given M spin configurations, $\sigma^{(1)}, ..., \sigma^{(M)}$, we perform the reconstruction by first partition-ing the M configurations in clusters according to their local densities around each local maximum. More precisely, using the clustering algorithm discussed in [68–72] we divide the M configurations into different clusters using the mutual distances between their magnetisations of each configuration. Configurations form a cluster if the magnetisation distances are less than a fixed threshold d_c. The choice of the optimal threshold is obviously crucial: a too small threshold will produce too many clusters, while a too large one will give only one cluster. Given d_c, for each configuration l the algorithm computes two quantities: the local density ρ_l, defined as the number of magnetisations within the given distance d_c to the magnetisation of $\sigma^{(l)}$, and the minimum distance δ_l between the magnetisation of configuration l and any other configuration with a higher density.

The algorithm is based on the assumptions that the cluster centers are sur-rounded by points with a lower density, and that the centers are at a relatively large distance from each other. For each configuration, plotting the minimum dis-tance δ as a function of the local density ρ provides a decision graph that gives the cluster centers: the cluster centers are the outliers in the graph. Finally, each remaining configuration is assigned to the same cluster of its nearest neighbour of higher density. In this study, we identify two clusters C_k, $k = 1, 2$, using the optimal threshold $d_c = 0.001$. Notice that it is not possible to observe three clusters in the inverse problem due to the analytical properties of the consistency equation (5.6).

Then, for each cluster C_k, $k = 1, 2$ we compute the estimates of the finite-size

quantities, $\widehat{m}$, $\widehat{\chi}$ and $\widehat{\psi}$, and the corresponding $\widehat{K}, \widehat{J}, \widehat{h}$. More precisely, we can define the estimators of the finite-size quantities with reference to the clusters as follows:

$$\widehat{m}_{C_k} = \frac{1}{M_k} \sum_{l \in C_k} m_N(\sigma^{(l)}), \tag{5.24}$$

$$\widehat{\chi}_{C_k} = N \left(\frac{1}{M_k} \sum_{l \in C_k} m_N^2(\sigma^{(l)}) - \widehat{m}_{C_k}^2 \right) \tag{5.25}$$

and

$$\widehat{\psi}_{C_k} = N^2 \left(\frac{1}{M_k} \sum_{l \in C_k} m_N^3(\sigma^{(l)}) - 3\widehat{m}_{C_k} \frac{1}{M_k} \sum_{l \in C_k} m_N^2(\sigma^{(l)}) + 2\widehat{m}_{C_k}^3 \right), \tag{5.26}$$

where M_k is the size of the cluster C_k, $k = 1, 2$ such that $M_1 + M_2 = M$. After obtaining the quantities above, we now compute the estimated values, $\widehat{K}_{C_k}, \widehat{J}_{C_k}, \widehat{h}_{C_k}$, using equations (5.21), (5.22) and (5.23) for each cluster and compute the final estimates of the parameters K, J and h as the weighted averages:

$$\widehat{K} = \frac{1}{M} \sum_{k=1}^{2} M_k \widehat{K}_{C_k}, \tag{5.27}$$

$$\widehat{J} = \frac{1}{M} \sum_{k=1}^{2} M_k \widehat{J}_{C_k} \tag{5.28}$$

and

$$\widehat{h} = \frac{1}{M} \sum_{k=1}^{2} M_k \widehat{h}_{C_k}. \tag{5.29}$$

Observe that if a point (K, J, h) in the parameter space corresponds to a metastable solution (at finite-volume) and it is sufficiently distant from the coexistence curve, we can expect a better reconstruction of the parameters by applying equations (5.21), (5.22) and (5.23) to the configurations in the largest cluster. However, if the point (K, J, h) is close to the coexistence curve, a better reconstruction can be expected using the density clustering algorithm, i.e., by using (5.27), (5.28) and (5.29).

Figure 5.12 illustrates how the Boltzmann-Gibbs measure of the magnetisation is changing with varying K, J and h in each column starting from the left respectively.
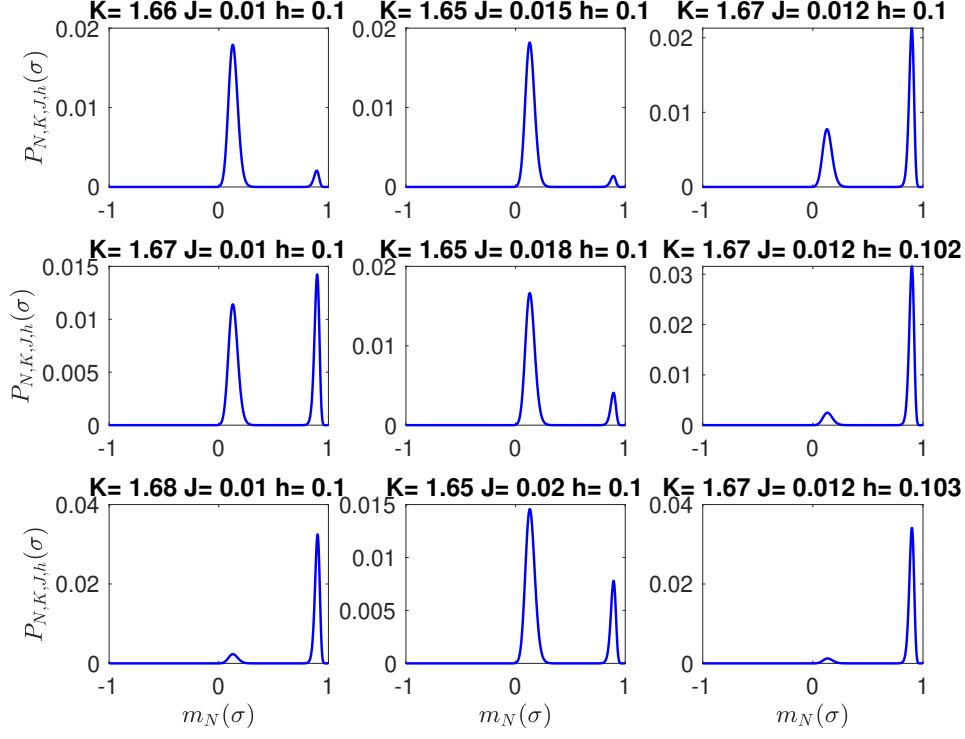
Figure 5.12:   Boltzmann-Gibbs distribution of the total magnetisation with metastable states for fixed K, J, h at $N = 1000$. The peaks of the distribution are centered around the two solutions of the consistency equation.

5.3.1   Test for metastable state solutions

The inverse problem is solved using the density clustering algorithm as discussed and identifying a suitable number of samples M for better reconstruction of the model parameters. The test is performed with $M = 20000$ and standard deviations are computed over 50 different M-samples from the same distribution. As an example, consider the reconstruction of the parameter values $(K, J, h) = (1.67, 0.01, 0.1)$ for $M = 20000$ and $N = 3000$. The distribution of the magnetisation at this point is given as the blue dashed curve in Figure 5.13, where the two peaks are centered around $m_1 = 0.1311$ and $m_2 = 0.8973$, the stable solution and the metastable solution of the consistency equation (5.6), respectively.

As is evident from Figure 5.13, the cluster centered around m_1 (i.e., C_1) has more configurations as compared to the other cluster centered around m_2 (i.e., C_2). We get the following reconstructed estimates for the parameter values by applying
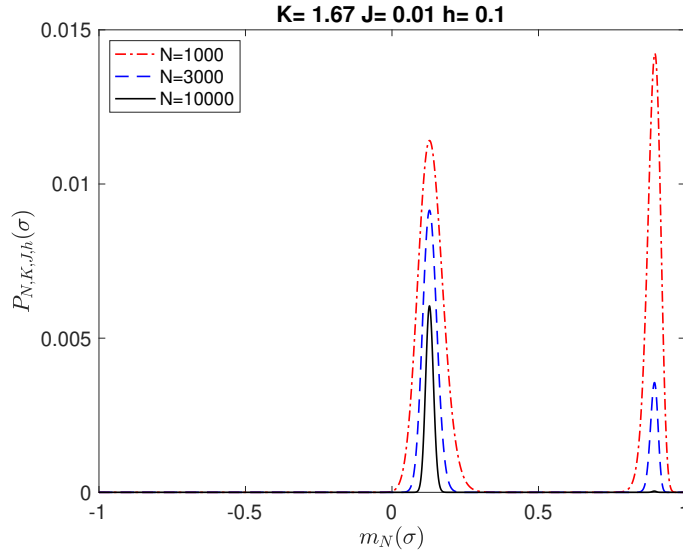
Figure 5.13: Boltzmann-Gibbs distribution of the total magnetisation at fixed values of N. The peaks of the distribution are centered around the two solutions of the equation (5.6), with $m_1 = 0.1311$ being the stable solution and $m_2 = 0.8973$ the metastable solution. We can observe that the probability of the metastable solution vanishes to 0 as N goes to infinity (black continuous curve). The red dot-dashed line corresponds to the distribution for $N = 1000$, blue dashed line corresponds to the distribution for $N = 3000$ and the black continuous line for the distribution with $N = 10000$.

equations (5.21), (5.22) and (5.23) to the setups in both clusters (i.e., C_1 and C_2) according to formulas (5.27), (5.28) and (5.29):

$$(\overline{\overline{\widehat{K}}}, \overline{\overline{\widehat{J}}}, \overline{\overline{\widehat{h}}}) = (1.76 \pm 0.67, -0.11 \pm 1.11, 0.15 \pm 0.49).$$

Instead, we obtain the following reconstructed parameter values by applying equations (5.21), (5.22) and (5.23) just to the configurations in the more dense cluster C_1:

$$(\overline{\overline{\widehat{K}}}, \overline{\overline{\widehat{J}}}, \overline{\overline{\widehat{h}}}) = (1.69 \pm 0.23, 0.01 \pm 0.06, 0.10 \pm 0.004).$$

Note that, the reconstructed parameters using only the configurations in the more dense cluster are in better agreement with the exact ones when compared to the reconstructed parameters on both clusters. This is an indication that the point $(K, J, h) = (1.67, 0.01, 0.1)$ is sufficiently distant from the coexistence curve. Ob-

serve that if two clusters have the same density, we do not choose between them and the clustering algorithm provides an optimal reconstruction.

Now, we perform reconstruction of the parameters using the cluster with largest size for fixed values of the model parameters and observe its performance for varying M in Figure 5.14. It can be observed that the reconstructed parameters are in good agreement to their corresponding exact values.
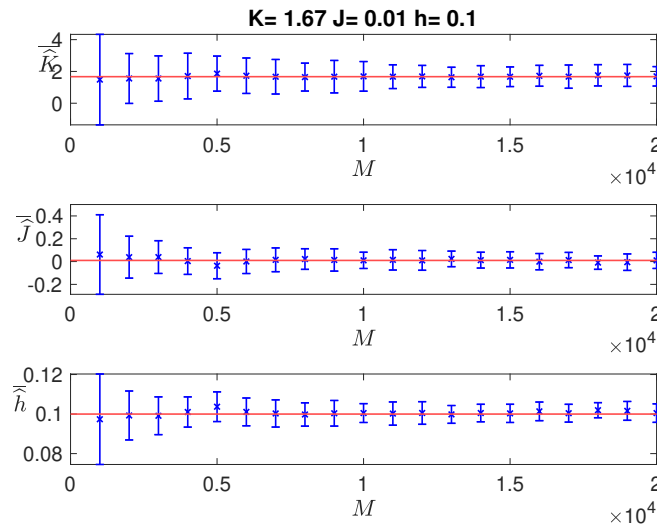
Figure 5.14: $K = 1.67, J = 0.01$ and $h = 0.1$. $\widehat{\overline{K}}, \widehat{\overline{J}}$ and $\widehat{\overline{h}}$ as a function of M using the largest cluster and $N = 3000$. The reconstructed estimates, $\widehat{\overline{K}}, \widehat{\overline{J}}$ and $\widehat{\overline{h}}$, are blue crosses on statistical error bars on 50 different M-samples of configurations of the same system. The horizontal red lines in each panel correspond to the exact values of K, J and h.

As a last remark, note that, given a point (K, J, h) in a neighbourhood of the coexistence curve, one can observe a metastable state when the number of particles N is not large enough. In this case, the clustering algorithm is useful to reconstruct the parameters, but it has a high computational cost. This is easily overcome by using large number of particles, which cause the metastable state to vanish (see Figure 5.13) and the inversion formulas in equations (5.21), (5.22), (5.23) become efficient.

5.4   Conclusion

In this chapter, we solved the inverse problem for a mean-field statistical me-
chanics model with three-body interaction displaying a first order phase transition.
We studied the inverse problem and tested the statistical robustness of the inversion
method and formulas. We numerically tested the inversion method for cases where
the consistency equation (5.6) has a unique stable solution as well as more than
one locally stable solution. For the case where the consistency equation (5.6) has
multiple locally stable solution, we used the clustering algorithm to reconstruct the
model parameters.

Robustness was tested for different values of the number of particles N and
samples M and reached the precision of a few percent for $M = 2 \times 10^4$.

Chapter 6

Multi-populated cubic mean-field Ising model

This chapter introduces a multi-populated version of the Ising model with three-spin interactions discussed in Chapter 2. The spins are partitioned into blocks with their total sum being equal to the total spins of the system and interactions among spins are governed by block membership. The limiting properties of the model is studied via methods of large deviations. The fluctuations for vector of block magnetisations, is shown to be approximated by a multivariate Gaussian distribution when the maximisers of the limiting pressure per particle is unique, while there is a local multivariate Gaussian distribution fluctuations when the limiting pressure has multiple maximisers. The model is then used as a minimal mathematical tool to simulate a Human-AI ecosystem.

6.1   The model

Let us consider a system made up of $N \in \mathbb{N}$ spin particles that interact with each other and an external field as described by (2.1). Now, let's suppose that the system is partitioned in $r \in \mathbb{N}$ blocks identified by $B_1, B_2, ..., B_r \subset \{1, 2, ..., N\}$ such that $B_i \cap B_j = \emptyset$ for $i \neq j$ and $|B_l| = N_l$. This implies that $\sum_{l=1}^{r} |B_l| = N$. Let's denote by $\gamma_N^{(l)} = \frac{N_l}{N} \in (0,1)$ the relative size of block l and $m^{(l)}(\sigma) = \frac{1}{N_l} \sum_{i \in B_l} \sigma_i$ the magnetisation per particle of block B_l, for $l = 1, ..., r$. Figure 6.1 below gives a schematic representation of the interaction network.
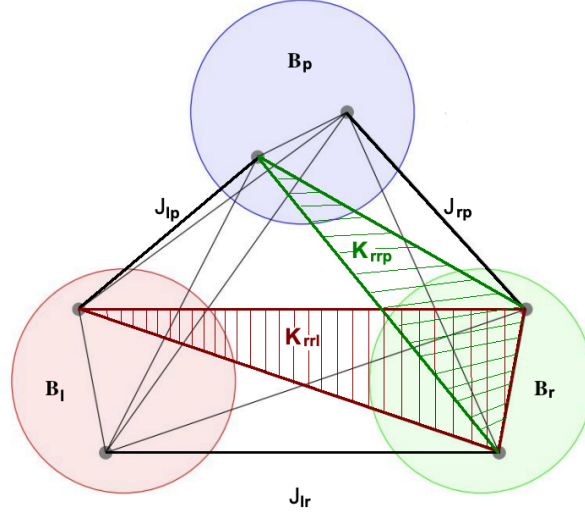
Figure 6.1: Schematic interacting network for the multi-populated Ising model.

To lighten notations in some cases the block magnetisation $m^{(l)}(\sigma)$ will be denoted by $m^{(l)}$. Observe that, since the system is partitioned into blocks, interactions is based on block membership and hence, (2.1) can be written as:

$$
\begin{aligned}
H_N(\sigma) = & -\frac{1}{3N^2} \sum_{l=1}^{r} \sum_{s=1}^{r} \sum_{q=1}^{r} \left(\sum_{i \in B_l} \sum_{j \in B_s} \sum_{k \in B_q} K_{ijk} \sigma_i \sigma_l \sigma_k \right) \\
& -\frac{1}{2N} \sum_{l=1}^{r} \sum_{s=1}^{r} \left(\sum_{i \in B_l} \sum_{l \in B_l} J_{il} \sigma_i \sigma_l \right) - \sum_{l=1}^{r} \sum_{i \in B_l} h_i \sigma_i \\
= & -N \sum_{l,s,q=1}^{r} \frac{K_{lsq}}{3} \gamma_N^{(l)} \gamma_N^{(s)} \gamma_N^{(q)} m^{(l)} m^{(s)} m^{(q)} - N \sum_{l,s=1}^{r} \frac{J_{ls}}{2} \gamma_N^{(l)} \gamma_N^{(s)} m^{(l)} m^{(s)} \\
& -N \sum_{l=1}^{r} h_l \gamma_N^{(l)} m^{(l)} \\
= & -N(U_N(\mathbf{m}))
\end{aligned}
$$

$$(6.1)$$

where $\mathbf{m} = (m^{(1)}, ..., m^{(r)})$ and

$$
U_N(\mathbf{m}) := \sum_{l,s,q=1}^{r} \frac{K_{lsq}}{3} \gamma_N^{(l)} \gamma_N^{(s)} \gamma_N^{(q)} m^{(l)} m^{(s)} m^{(q)} + \sum_{l,s=1}^{r} \frac{J_{ls}}{2} \gamma_N^{(l)} \gamma_N^{(s)} m^{(l)} m^{(s)} + \sum_{l=1}^{r} h_l \gamma_N^{(l)} m^{(l)}.
$$

In this model, the invariance of the Hamiltonian with respect to permutations among sites is replaced by a weaker one that takes into account the existence of

different species of spins. This setting is particularly useful in social science applications [35,64,73,74]. The joint distribution of σ is governed by a the same Boltzmann-Gibbs type measure (2.4) discussed in previous chapters where the Hamiltonian has the form in (6.1).

The mean-field approximation involved in the study of some finite-dimensional lattices provides a natural emergence of the multi-populated models. It is well known, for instance, that a system on a simple cubic lattice [75,76] with ferromagnetic and antiferromagnetic couplings has a factorized equilibrium measure that corresponds to a two-populated mean-field model. Similarly, it has been shown in [15] that on a regular square lattice, a system with cubic interaction has a product state equilibrium described by a two-populated mean-field model, while on a regular triangular lattice [14], by a three-populated mean-field model. This chapter presents a more general r-populated mean-field model where interactions among three species of particles within or across block are taking into consideration.

6.2   Existence of thermodynamic limit

In this section, the existence of thermodynamic limit of the pressure per particle is shown using methods from large deviation theory leveraging on the extreme value distribution (i.e., tail estimation) and combinatorial methods which rely on Stirling's approximation to compute a bound on the pressure per particle as done in Section 2.2. A version of the Varadhan's integral lemma introduced in [26] can be used to study the large deviation properties of a vector of empirical means, where the fractions of the subgroups (i.e., partitions of the system) are of unequal sizes, and can likewise verify the results obtained here.

Now, let us observe that the pressure per particle associated to the multi-populated system introduced here has the same form as (2.6). The limiting properties of the pressure per particle, enables the description of the system in its equilibrium state(s). In the sequel, the large N behaviour of the system is studied using modifications of the methods already introduced in Chapter 3.

Let's notice that for a given configuration $\sigma^{(l)}$ of spins in B_l, the magnetisation per particle $m^{(l)}$ has the following spectrum: $S_{m^{(l)}} = \{-1 + \frac{2n}{N_l}, n = 0, \ldots, N_l\}$, with $|S_{m^{(l)}}| = (N_l + 1)$. Now, considering that the Hamiltonian is expressed as a function of the magnetisation per particle of the blocks, the partition function can

be written as

$$Z_N = \sum_{y \in S_{\mathbf{m}}} \prod_{l=1}^{r} A_{y_l} \exp\left(-H_N(\sigma)\right), \tag{6.2}$$

where $y = (y_l)_{l \le r} \in \mathbb{R}^r$ and the sum is over all possible values of the random vector $\mathbf{m} = (m^{(l)}(\sigma))_{l \le r} \in \mathbb{R}^r$. Similarly, for each block $l \in \{1, ..., r\}$,

$$A_{y_l} := \text{card}\left\{\sigma^{(l)} \in \{-1, 1\}^{N_l} : m^{(l)}(\sigma) = y_l\right\} = \binom{N_l}{\frac{N_l(1+y_l)}{2}}. \tag{6.3}$$

Here, A_{y_l} counts the number of all possible configurations of $\sigma^{(l)}$ that share the same magnetisation $m^{(l)} = y_l \in S_{m^{(l)}}$. If $m^{(l)} = y_l$, then the configuration $\sigma^{(l)}$ has exactly, $\frac{N_l(1+y_l)}{2}$ number of $+1$ spins and $\frac{N_l(1-y_l)}{2}$ of -1 spins.

Lemma 6.2.1. *Let $\Omega_l = \{+1, -1\}^{N_l}$ denote the set of all possible configurations, $\sigma^{(l)}$, of the block B_l. Then for $A_{y_l} \in \mathbb{N}$ the following inequality holds:*

$$\frac{1}{L\sqrt{N_l}} e^{-N_l I(y_l)} \le A_{y_l} \le e^{-N_l I(y_l)}$$

where L is a universal constant and,

$$I(y_l) = \frac{1 - y_l}{2} \log\left(\frac{1 - y_l}{2}\right) + \frac{1 + y_l}{2} \log\left(\frac{1 + y_l}{2}\right)$$

Proof. Notice that the bounds of A_{y_l} are large deviation approximations of the block magnetisation $m^{(l)}$ that can be obtained using Stirling's approximation of factorial and exploiting the tail distribution of the block magnetisations. This same technique was illustrated in Section (2.2.1), and the sequel relies on the same approach.

Now, let's consider the case when $N_l(1 + y_l)$ is even for a given block l, we can apply Stirling's formula to approximate the combinatorial appearing in (6.3). We have that, for each block $l = 1, ...r$, $N_l! = N_l^{N_l} e^{-N_l}\sqrt{2\pi N_l}(1 + \mathcal{O}(N_l^{-1}))$, hence:

$$\binom{N_l}{\frac{N_l(1+y_l)}{2}} = \frac{N_l!}{\frac{N_l(1+y_l)}{2}!(\frac{N_l(1-y_l)}{2})!}$$

$$= \frac{N_l^{N_l}\sqrt{2}}{\left[\left(\frac{N_l(1+y_l)}{2}\right)^{\left(\frac{N_l(1+y_l)}{2}\right)}\left(\frac{N_l(1-y_l)}{2}\right)^{\left(\frac{N_l(1-y_l)}{2}\right)}\sqrt{\pi N_l(1-y_l^2)}\right]} \cdot (1+\mathcal{O}(N_l^{-1}))$$

$$= \sqrt{\frac{2}{\pi N_l(1-y_l^2)}} \cdot$$

$$\cdot \frac{1}{\exp \ln\left[\left(\frac{(1+y_l)}{2}\right)^{\left(\frac{N_l(1+y_l)}{2}\right)}\left(\frac{(1-y_l)}{2}\right)^{\left(\frac{N_l(1-y_l)}{2}\right)}\right]} \cdot (1+\mathcal{O}(N_l^{-1}))$$

$$= \sqrt{\frac{2}{\pi N_l(1-y_l^2)}} \cdot$$

$$\cdot \exp\left(-N_l\left(\frac{1-y_l}{2}\ln\left(\frac{1-y_l}{2}\right) + \frac{1+y_l}{2}\ln\left(\frac{1+y_l}{2}\right)\right)\right) \cdot (1+\mathcal{O}(N_l^{-1}))$$

The lower bound follows from the last equality, where

$$I(y_l) = \left(\frac{1-y_l}{2}\ln\left(\frac{1-y_l}{2}\right) + \frac{1+y_l}{2}\ln\left(\frac{1+y_l}{2}\right)\right).$$

Now, exploiting the tails, we first suppose that the spins σ_i are independent such that $\Pr(\sigma_i = +1) = \Pr(\sigma_i = -1) = 1/2$ for $\sigma_i \in B_l$ and $l = 1,...r$. Then for all $\sigma_i \in B_l$ all configurations $\sigma^{(l)} \in \Omega_l$, have equal probability of having the magnetisation y_l and thus,

$$\Pr(m^{(l)} = y_l) = \sum_{\sigma^{(l)} \in \{-1,1\}^{N_l}:m^{(l)}=y_l} \Pr(\sigma^{(l)}) \tag{6.4}$$

where $\Pr(\sigma^{(l)})$ is the joint distribution of i.i.d. random variables distributed in the set $\{-1,1\}^{N_l}$ with equal probability and the sum is over all possible configurations of $\sigma^{(l)}$ that yield a block magnetisation $m^{(l)} = y_l$. Observe that (6.4) gives the large deviation principles for the block magnetisation, given that the spin variables are independent and identically distributed. This will be discussed in the next section. Therefore, it follows that,

$$A_{y_l} = 2^{N_l}\Pr(m^{(l)} = y_l) \leq 2^{N_l}\Pr\left(\sum_{i \in B_l}\sigma_i \geq N_l y_l\right).$$

The last inequality above follows from the definition of the block magnetisation and leads to the use of tail estimation approach of $m^{(l)}$. Since σ_i is a random variable

belonging to a block which is assumed to be independent and distributed according to ρ, then for any $\lambda > 0$,

$$
\Pr\left(\sum_{i \in B_l} \sigma_i \geq N_l y_l\right) \leq \exp\left(-\lambda\, y_l N_l\right) \prod_{i=1}^{N_l} \mathbb{E}_\rho \exp\left(\lambda\, \sigma_i\right) \tag{6.5}
$$

$$
= \exp\left(N_l(-\lambda\, y_l + \ln\cosh\left(\lambda\right))\right).
$$

We can obtain λ by optimising (6.5) over all possible λ:

$$
\lambda = \operatorname{arctanh}\left(y_l\right) = \frac{1}{2}\ln\left(\frac{1 + y_l}{1 - y_l}\right)
$$

and it follows that since $1/\cosh^2\left(y\right) = 1 - \tanh^2\left(y\right)$, then $\ln\cosh\left(\lambda\right) = -1/2 \ln\left(1 - y_l^2\right)$. Substituting this observation into (6.5), we have that

$$
A_{y_l} \leq \exp\left(-N_l I(y_l)\right).
$$

$\square$

Using the result of Lemma 6.2.1, we can obtain a bound on the partition function and use it to compute the pressure per particle. Notice that the sum in the partition function has $N_l + 1$ terms and we are interested on behaviour on the exponential scale, hence we keep only the dominating terms;

$$
\frac{1}{L}\prod_{l=1}^{r}\frac{1}{\sqrt{N_l}}\exp\left(N(\max_y f_N(y))\right) \leq Z_N \leq \prod_{l=1}^{r}(N_l + 1)\exp\left(N(\max_y f_N(y))\right) \tag{6.6}
$$

where, $y = (y_1, ..., y_r)$ and

$$
f_N(y) = U_N(y) - \langle\gamma_N, I(y)\rangle \tag{6.7}
$$

where $I(y)$ is a vector of entropy associated to the block magnetisation and $\gamma_N = (\gamma_N^{(l)})_{l \leq r}$. Therefore, we obtain the following bound for the pressure function,

$$
-\frac{1}{N}\left(\ln L + \frac{1}{2}\sum_{l=1}^{r}\ln N_l\right) + \max_y f_N(x) \leq p_N \leq \frac{1}{N}\sum_{l=1}^{r}\ln(N_l + 1) + \max_y f_N(y).
$$

Now, the limiting pressure per particle is obtained as:

$$
\lim_{N\to\infty} p_N = p = \max_{y \in \mathbb{R}^k} f(y),
$$

were,

$$
f = U(y) - \langle\gamma, I(y)\rangle \tag{6.8}
$$

is derived by taking the limit as $N \to \infty$ of p_N. Therefore,

$$p = \max_{y \in [-1,1]^k} \left\{ U(y) - \langle \gamma, I(y) \rangle \right\} \tag{6.9}$$

and it has been used that, $\lim_{N \to \infty} U_N(y) = U(y)$ with $\lim_{N \to \infty} \gamma_N^{(l)} = \gamma^{(l)}$ and $\gamma = (\gamma^{(l)})_{l \leq r}$. The limiting behaviour of the block spin model with three-spin interaction is determined by properties of p. Observe that p is obtained at the supremum of $f(y)$ on the support of $y \in \mathbb{R}^r$. The following stationarity condition holds for f:

$$x_l = \tanh \left(h_l + \sum_{s=1}^{r} \gamma^{(s)} J_{ls} x_s + \sum_{s,q=1}^{r} \gamma^{(s)} \gamma^{(q)} K_{lsq} x_s x_q \right) \quad \text{for} \quad l = 1, ..., r. \tag{6.10}$$

The solutions of the fixed point equation (6.10), i.e., mean-field equation, identify the stationary points of f among which we are interested in the ones that reach the supremum. We denote by $\mu = (\mu^{(d)})_{d \in \mathbb{N}}$ a vector of all the global maximum points of f on the support of the vector of block magnetisaton $m = (m^{(l)})_{l \leq r} \in [-1, 1]^r$. Notice that since (6.10) is a fixed point equation of a tangent hyperbolic function for all l, there exist regions of the parameter space $(\mathbf{K}, \mathbf{J}, \mathbf{h}, \gamma)$, for $\mathbf{K} = (K_{l,s,q})_{l,s,q \leq r}$, $\mathbf{J} = (J_{l,s})_{l,s \leq r}$, and $\mathbf{h} = (h_l)_{l \leq r}$, where f has a unique or multiple maximisers.

The next section discusses the aysmptotic properties of the vector of block magnetisation when f has a unique global maximiser and multiple local maximisers.

6.3 Fluctuation of the block magnetisation

To study the fluctuations of the vector of random variables $\mathbf{m} = (m^{(l)})_{l \leq r}$, we are interested in approximating the distribution of the amount the rescaled random vector of block magentization is away form μ. To do this we first compute an asymptotic expansion of the partition function relying on some standard approximation techniques to be discussed in the next section.

6.3.1 Asymptotic expansion of Z_N

It is essential to note that the partition function Z_N, which lacks a closed form, plays a crucial role in the probability mass function of the magnetization density $m^{(l)}$. Hence, obtaining a precise approximation of Z_N is necessary to understand the asymptotic properties of the statistical estimator $\mathbf{m} = (m^{(l)})_{l \leq r}$, i.e., the vector of block magnetization. We will use the results obtained from Lemma 6.2.1 over

all configurations $\sigma^{(l)} \in \Omega_l$ to obtain an asymptotic expansion of the partition function. Notice from the expansion of the combinatorial factor A_{y_l} using the Stirling's formula, the partition function becomes:

$$
\begin{aligned}
Z_N &= \sum_y \prod_{l=1}^r \sqrt{\frac{2}{\pi N_l(1-y_l^2)}}\, e^{(-N_l I(y_l))} e^{(NU_N(y))}\, (1+\mathcal{O}(N_l^{-1})) \\
&= \sum_y \underbrace{\sqrt{\frac{2^r}{\pi^r \prod_{l=1}^r N_l(1-y_l^2)}}\, e^{Nf_N(y)} \left[1 + \mathcal{O}\!\left(\prod_{l=1}^r N_l^{-1}\right)\right]}_{=\zeta}
\end{aligned}
\tag{6.11}
$$

where f_N is defined in (6.7) and the sum is over all possible vector of the random vector $\mathbf{m} = (m^{(l)})_{l\le r}$. Leveraging on the approximation methods employed in [23, 34], we an asymptotic expansion of partition function using the Reimann approximation of the sum by an integral A.1.3 and Laplace approximation of the integral A.1.4.

Now, from Lemma 6.3.1, let's suppose that x_N is a random vector in $(-1,1)^r$ such that $\nabla f_N(x_N) = \mathbf{0}$ and the Hessian of $f_N(x_N)$ is negative definite, i.e., $\mathcal{H}_{f_N}(x_N) < 0$. Again, suppose that x_N is a unique vector of global maximizers of f_N converging uniformly to μ. Let's denote by $G_{N,\alpha}$ an open ball centered around x_N with radius $N^{-\frac{1}{2}+\alpha}$ in $\mathbb{R}^r$ as:

$$
G_{N,\alpha} = \{x \in \mathbb{R}^r \mid \|x - x_N\| < N^{-\frac{1}{2}+\alpha}\}.
$$

Here, $\|\cdot\|$ denotes the Euclidean norm. The open ball consists of all vectors y whose Euclidean distance from x_N is less than $N^{-\frac{1}{2}+\alpha}$ for $\alpha \in (0, 1/6]$ [34]. The set $G_{N,\alpha}$ is essentially a neighborhood around x_N in $\mathbb{R}^r$. Following the same argument as in Chapter 3, we approximate the sum in (6.11) by an integral using Lemma A.1.3 over the set $G_{N,\alpha}$ with shrinking interval containing the unique vector of global maximizer of f_N which are elements of $S_{\mathbf{m}}$:

$$
\begin{aligned}
\left|\int_{G_{N,\alpha}} \zeta(x)dx - \frac{2^r}{\prod_{l=1}^r N_l} \sum_{x \in S_{\mathbf{m}} \cap G_{N,\alpha}} \zeta(x)\right| &\le \frac{1}{2}\left(\prod_{l=1}^r N_l^{-\frac{1}{2}+\alpha}\right)\cdot \prod_{l=1}^r N_l^{-1} \sup_{x\in G_{N,\alpha}} |\zeta'(x)| \\
&= \mathcal{O}\!\left(\prod_{l=1}^r N_l^{-\frac{1}{2}+\alpha} \cdot \prod_{l=1}^r N_l^{-1} \cdot \prod_{l=1}^r N_l^{\frac{1}{2}+\alpha}\right) \zeta(x_N) \\
&= \mathcal{O}\!\left(\prod_{l=1}^r N_l^{-1+2\alpha}\right) \zeta(x_N). \quad (6.12)
\end{aligned}
$$

Now, following from (6.12) and applying the results of Lemma A.1.4 to approximate the integral, we have that:

$$
\sum_{x \in S_{\mathbf{m}} \cap G_{N,\alpha}} \zeta(x) = \frac{\prod_{l=1}^{r} N_l}{2^r} \int_{G_{N,\alpha}} \zeta(x) dx + \mathcal{O}\left(\prod_{l=1}^{r} N_l^{2\alpha}\right) \zeta(x_N)
$$

$$
= \frac{\prod_{l=1}^{r} N_l}{2^r} \int_{G_{N,\alpha}} \sqrt{\frac{2^r}{\pi^r \prod_{l=1}^{r} N_l(1 - x_l^2)}} \, e^{N f_N(x)} \left[1 + \mathcal{O}\left(\prod_{l=1}^{r} N_l^{-1}\right)\right] dx
$$

$$
+ \mathcal{O}\left(\prod_{l=1}^{r} N_l^{2\alpha}\right) \sqrt{\frac{2^r}{\pi^r \prod_{l=1}^{r} N_l(1 - x_N^2)}} \, e^{N f_N(x_N)} \left[1 + \mathcal{O}\left(\prod_{l=1}^{r} N_l^{-1}\right)\right]
$$

$$
= \frac{\prod_{l=1}^{r} N_l}{2^r} \sqrt{\frac{2^r}{\pi^r \prod_{l=1}^{r} N_l(1 - x_N(l)^2)}} \sqrt{\frac{(2\pi)^r}{\prod_{l=1}^{r} N_l \det\left(-\mathcal{H}_{\mathbf{f}_N}(x_N)\right)}} e^{N f_N(x_N)}
$$

$$
\cdot \left(1 + \mathcal{O}\left(\mathbf{N}^{\alpha - 1/2}\right)\right)
$$

$$
= \frac{e^{N f_N(x_N)}}{\sqrt{\det\left(-\mathcal{H}_{\mathbf{f}_N}(x_N)\right) \prod_{l=1}^{r}(1 - x_N(l)^2)}} \cdot \left(1 + \mathcal{O}\left(\mathbf{N}^{\alpha - 1/2}\right)\right).
$$

$$(6.13)$$

Hence, the partition function becomes:

$$
Z_N = \frac{e^{N f_N(x_N)}}{\sqrt{\det\left(-\mathcal{H}_{\mathbf{f}_N}(x_N)\right) \prod_{l=1}^{r}(1 - x_N(l)^2)}} \cdot \left(1 + \mathcal{O}\left(\mathbf{N}^{\alpha - 1/2}\right)\right). \qquad (6.14)
$$

where $\alpha \in (0, 1/6]$ [34]. With this form of the partition function, we can now study the fluctuations of the magnetization. The following lemma contains useful results that will aid in later computations and arguments.

Lemma 6.3.1. *Let's suppose $\mu = (\mu_1, ..., \mu_r) \in (-1, 1)^r$ is a vector of unique global maximum points of $f(x)$ for some fixed parameters, defined in (6.8), such that the Hessian $\mathcal{H}_f(\mu)$ is negative definite, i.e., $\mathcal{H}_f(\mu) < 0$. Again, suppose that $f_N(x)$ is continuous and differentiable sequence of functions, converging uniformly to f, with bounded partial derivatives up to order four converging uniformly to those of f for very large N. Then $f_N(x)$ has a unique maximizer $\hat{x}_N \to \mu$ for N large enough and $\mathcal{H}_{f_N}(\hat{x}_N) < 0$.*

Proof. Let suppose that $\{\hat{x}_N\}$ is a sequence of any maximizer of f_N which exists since it is defined over the compact set $[-1, 1]^r$. Then there exists a subsequence $\{N_n\}_{n \geq 1}$ such that $\{\hat{x}_{N_n}\}$ converges to some $\{\hat{x}\}$. This imples that $f_{N_n}(\hat{x}_{N_n}) \geq$

$f_{N_n}(x)$ for all $x \in [-1, 1]^r$. Therefore by uniform convergence and taking the limit as $n \to \infty$, we obtain that $f(\hat{x}) \geq f(x)$ for all $x \in [-1, 1]^r$. This implies that $\hat{x}$ is a vector of the global maximizers of $f(x)$. But we know that μ is the unique vector of global maximizers of $f(x)$, hence $\hat{x} = \mu$.

Note that the map $x \mapsto f_N(x)$ is continuous for every N and uniformly bounded. Observe further that x is a closed and bounded, i.e., compact, subset of $\mathbb{R}^r$. Hence, it follows from Theorems 7.13 and 7.24 of [31] that f_N is equicontinuous. Now since f_N is uniformly bounded and equicontinuous, $f_N \to f$ uniformly. Hence, by extension, it follows from the convergence of f_N to f that $\hat{x}_N \to \mu$ uniformly. While, the convergence of f_N to its derivatives follows directly from Theorem 7.17 of [31]. Since the Hessian $\mathcal{H}_f(\mu)$ characterises the curvature of the pressure per particle (4.7), which is related to its second partial derivative with respect to the vector $x \in [-1, 1]^r$ at the point of global maximizer μ, it follows immediately that it is negative definite. It consequently follows that the Hessian of f_N, $\mathcal{H}_{f_N}$, evaluated at $\hat{x}_N$ is negative definite given that $\hat{x}_N \to \mu$ for N large enough.

Now, since $\mathcal{H}_f(\mu) < 0$, it's obvious that for any $x \in [\mu - \epsilon, \mu + \epsilon]$, $f(x) < 0$ for all $\epsilon > 0$. Let's suppose that $\{\hat{x}_N\}$ and $\{\hat{w}_N\}$ are sequence of any two vectors of global maximizers of f_N. Then it is obvious that their components $\hat{x}_N^{(l)} \to \mu_l$ and $\hat{w}_N^{(l)} \to \mu_l$ for $l = 1, ..., r$. Therefore for N large enough $\hat{x}_N^{(l)}, \hat{w}_N^{(l)} \in [\mu_l - \epsilon, \mu_l + \epsilon]$. It is easy to verify that for N large enough f_N is strongly convex on $[\mu_l - \epsilon, \mu_l + \epsilon]$ following from the assumption that $\mathcal{H}_{f_N}$ converges uniformly to $\mathcal{H}_f$. Therefore, f_N has a unique maximizer which implies that $\hat{x}_N = \hat{w}_N$. $\square$

Corollary 6.3.1. *Consider the mean-field Hamiltonian $H_N = -N U_N(m^{(1)}, ..., m^{(r)})$ defined in (6.1). Let $\mu = (\mu_1, ..., \mu_r)$ be the unique vector of global maximisers of f. Then the asymptotic behaviour of the vector*

$$S(\sigma) = (\sqrt{N_1}(m^{(1)} - \mu_1), ..., \sqrt{N_r}(m^{(r)} - \mu_r))$$

as $N_1 \to \infty, ..., N_r \to \infty$ for fixed $\gamma^{(1)}, ..., \gamma^{(r)}$ is given by a multivariate normal distribution with covariance matrix $\chi = -\frac{1}{\mathcal{H}_f(\mu)}$:

$$\chi = \begin{bmatrix} \left(-\frac{\partial^2 f}{\partial \mu_1^2}\right)^{-1} & \left(-\sqrt{\frac{\partial^2 f}{\partial \mu_1^2}\frac{\partial^2 f}{\partial \mu_2^2}}\right)^{-1} & \cdots & \left(-\sqrt{\frac{\partial^2 f}{\partial \mu_1^2}\frac{\partial^2 f}{\partial \mu_k^2}}\right)^{-1} \\ \left(-\sqrt{\frac{\partial^2 f}{\partial \mu_1^2}\frac{\partial^2 f}{\partial \mu_2^2}}\right)^{-1} & \left(-\frac{\partial^2 f}{\partial \mu_2^2}\right)^{-1} & \cdots & \left(-\sqrt{\frac{\partial^2 f}{\partial \mu_2^2}\frac{\partial^2 f}{\partial \mu_k^2}}\right)^{-1} \\ \vdots & & \vdots & \vdots \\ \left(-\sqrt{\frac{\partial^2 f}{\partial \mu_1^2}\frac{\partial^2 f}{\partial \mu_k^2}}\right)^{-1} & \left(-\sqrt{\frac{\partial^2 f}{\partial \mu_2^2}\frac{\partial^2 f}{\partial \mu_r^2}}\right)^{-1} & \cdots & \left(-\frac{\partial^2 f}{\partial \mu_r^2}\right)^{-1} \end{bmatrix}.$$

Proof. In order to approximate the distribution of the scaled difference between the block magnetization and the limiting global maximizers, we will compute the limiting moment generating function of $\mathbf{m} = (m^{(l)})_{l \leq r}$ for some $t \in \mathbb{R}^r$ using the expanded form of the partition function in (6.14):

$$\mathbb{E}\left[e^{\langle t^T \sqrt{\mathbf{N}}, (\mathbf{m}-\mu) \rangle}\right] = e^{-\langle t^T \sqrt{\mathbf{N}}, \mu \rangle} e^{\langle t^T \sqrt{\mathbf{N}}, \mathbf{m} \rangle} \int_{\mathbb{R}^r} \mu_N(\mathbf{m}) d\mathbf{m} = e^{-\langle t^T \sqrt{\mathbf{N}}, \mu \rangle} \frac{Z_N(t)}{Z_N},$$

where $\mu_N(\mathbf{m})$ denotes the Gibbs measure of the block magnetization $\mathbf{m}$ related to the Hamiltonian (6.1) and $\mathbf{N} = (N_1, ..., N_r)$ denotes a vector of the partition of $N \in \mathbb{N}$ particles into r-blocks. From the above equality:

$$\frac{Z_N(t)}{Z_N} \sim \frac{\exp\left(N \max_{\mathbf{m}}\left[f_N(\mathbf{m}) + \langle t^T \sqrt{\mathbf{N}}, \mathbf{m} \rangle\right]\right)}{\exp\left(N \max_{\mathbf{m}} f_N(\mathbf{m})\right)}$$

$$= \exp\left(N[f_N(\hat{x}_{N,t}) - f_N(\hat{y}_N)] + \langle t^T \sqrt{\mathbf{N}}, \hat{x}_{N,t} \rangle\right). \tag{6.15}$$

In the first equality above, it has been used that, $\hat{x}_{N,t}$ and $\hat{y}_N$ are unique vectors of global maximizers of $f_N(x) + \langle t^T \sqrt{\mathbf{N}}, x \rangle$ and $f_N(x)$ for all $x \in (-1, 1)^r$ respectively.

Since $\hat{x}_{N,t}$ is a vector of unique global maximizers of $f_N(x) + \langle t^T \sqrt{\mathbf{N}}, x \rangle$, its components satisfy the following stationarity condition:

$$\hat{x}_{N,t}^{(l)} = \tanh\left(\sum_{s,q=1}^{r} \gamma_N^{(s)} \gamma_N^{(q)} K_{lsq} \hat{x}_{N,t}^{(s)} \hat{x}_{N,t}^{(q)} + \sum_{s=1}^{r} \gamma_N^{(s)} J_{ls} \hat{x}_{N,t}^{(s)} + h_l + \frac{t_l}{\sqrt{N_l}}\right), \quad \text{for} \quad l = 1, ..., r.$$

From the fixed point equation above, notice that $\hat{x}_{N,0}^{(l)} = \hat{y}_N^{(l)}$ and it can be verified for all $l = 1, ..., r$ that:

$$\frac{\partial \hat{x}_{N,t}^{(l)}}{\partial t_l}\Big|_{t=\mathbf{0}} = -\frac{1}{\sqrt{N_l} \nabla^2 f_N(\hat{y}_N^{(l)})} \quad \text{and} \quad \frac{\partial^2 \hat{x}_{N,t}^{(l)}}{\partial t_l^2} = \mathcal{O}(N_l^{-1}).$$

Now, taking Taylor's expansion of $\hat{x}_{N,t}^{(l)}$ around $t = \mathbf{0}$, we have that

$$\hat{x}_{N,t}^{(l)} = \hat{x}_{N,0}^{(l)} - \frac{t_l}{\sqrt{N_l} \nabla^2 f_N(\hat{y}_N^{(l)})} + \mathcal{O}(N_l^{-1}) \tag{6.16}$$

and hence,

$$t_l \sqrt{N_l} \, \hat{x}_{N,t}^{(l)} = t_l \sqrt{N_l} \, \hat{y}_N^{(l)} - \frac{t_l^2}{\nabla^2 f_N(\hat{y}_N^{(l)})} + \mathcal{O}(N_l^{-1/2}).$$

Now, observe from (6.15) that we need to obtain the following in order to make inference about the distribution: $f_N(\hat{x}_{N,t}) - f_N(\hat{y}_N)$ and $\langle t^T \sqrt{\mathbf{N}}, \hat{x}_{N,t} \rangle$. Again, taking Taylor's expansion of $f_N(\hat{x}_{N,t})$ at $\hat{y}_N$ to the second order, we have that:

$$f_N(\hat{x}_{N,t}) - f_N(\hat{y}_N) = \frac{1}{2}\langle \mathcal{H}_{f_N}(\hat{y}_N)(\hat{x}_{N,t} - \hat{y}_N), (\hat{x}_{N,t} - \hat{y}_N)\rangle + \mathcal{O}(||(\hat{x}_{N,t} - \hat{y}_N)^3||).$$
(6.17)

Consequently, from (6.16) and (6.17),

$$\hat{x}_{N,t} - \hat{y}_N = \frac{-t}{\langle \sqrt{\mathbf{N}}, \mathcal{H}_{f_N}(\hat{y}_N)\rangle} + \mathcal{O}(\mathbf{N}^{-1/2})$$

such that

$$\langle t^T \sqrt{\mathbf{N}}, \hat{x}_{N,t}\rangle = \langle t^T \sqrt{\mathbf{N}}, \hat{y}_N\rangle - \frac{\langle t^T, t\rangle}{\mathcal{H}_{f_N}(\hat{y}_N)} + \mathcal{O}(\mathbf{N}^{-1/2})$$

and

$$\begin{aligned}
N(f_N(\hat{x}_{N,t}) - f_N(\hat{y}_N)) &= \frac{N}{2}\left\langle \mathcal{H}_{f_N}(\hat{y}_N)\frac{t^T}{\langle \sqrt{\mathbf{N}}, \mathcal{H}_{f_N}(\hat{y}_N)\rangle}, \frac{t}{\langle \sqrt{\mathbf{N}}, \mathcal{H}_{f_N}(\hat{y}_N)\rangle}\right\rangle + o(1) \\
&= \frac{\langle t^T, t\rangle}{2\mathcal{H}_{f_N}(\hat{y}_N)} + o(1).
\end{aligned}$$

This implies that

$$\begin{aligned}
N(f_N(\hat{x}_{N,t}) &- f_N(\hat{y}_N)) + \langle t^T \sqrt{\mathbf{N}}, \hat{x}_{N,t}\rangle \\
&= \frac{\langle t^T, t\rangle}{2\mathcal{H}_{f_N}(\hat{y}_N)} + \langle t\sqrt{\mathbf{N}}, \hat{y}_N\rangle - \frac{\langle t^T, t\rangle}{\mathcal{H}_{f_N}(\hat{y}_N)} + \mathcal{O}(\mathbf{N}^{-1/2}) + o(1).
\end{aligned}$$

Therefore,

$$\mathbb{E}\left[e^{\langle t^T \sqrt{\mathbf{N}}, (\mathbf{m}-\mu)\rangle}\right] \sim e^{-\langle t^T \sqrt{\mathbf{N}}, \mu\rangle} \cdot e^{\langle t^T \sqrt{\mathbf{N}}, \hat{y}_N\rangle} \cdot e^{-\frac{\langle t^T, t\rangle}{2\mathcal{H}_{f_N}(\hat{y}_N)}}.$$
(6.18)

Now, following the arguments of Lemma 6.3.1,

$$\begin{aligned}
\lim_{N\to\infty} \mathbb{E}\left[e^{\langle t^T \sqrt{N}, (\mathbf{m}-\mu)\rangle}\right] &= e^{-\langle t^T \sqrt{N}, \mu\rangle} \cdot e^{\langle t^T \sqrt{N}, \mu\rangle} \cdot e^{-\frac{\langle t^T, t\rangle}{2\mathcal{H}_f(\mu)}} \\
&= \exp\left(-\frac{\langle t^T, t\rangle}{2\mathcal{H}_f(\mu)}\right).
\end{aligned}$$
(6.19)

The proof of Corollary 6.3.1 follows by setting $\chi = \frac{-1}{\mathcal{H}_f(\mu)}$. Around the stationary points of the pressure function, fluctuations in the magnetization are related to its curvature. Notice that since the Hessian $\mathcal{H}_f(\mu)$ is negative definite, hence, χ is positive definite and denotes the covariance matrix. $\qquad\square$

Corollary 6.3.2. *Given $H_N = -NU_N(m^{(1)}, ..., m^{(r)})$ defined in (6.1), let's suppose that $\mu = (\mu_1, ..., \mu_r)$ is a vector of nonunique global maximum point of f. Let's define η to be the minimum distance between all distinct pair of global maximum points of the function f. Then for any $d \in (0, \eta)$ when the random vector of the block magnetisations $\boldsymbol{m} = (m^{(l)})_{l \leq k}$ is inside the ball $\boldsymbol{B}(\mu, d)$ centered around the components of μ with radius d, the asymptotic behaviour of the vector*

$$S(\sigma) = \left(\sqrt{N_1}(m^{(1)} - \mu_1)|\{m^{(1)} \in \boldsymbol{B}(\mu_1, d)\}, ..., \sqrt{N_r}(m^{(r)} - \mu_r)|\{m^{(r)} \in \boldsymbol{B}(\mu_r, d)\} \right)$$

as $N_1 \to \infty, ..., N_r \to \infty$ for fixed $\gamma^{(1)}, ..., \gamma^{(r)}$ is given by a local multivariate normal distribution with covariance matrix $\chi_{|\boldsymbol{B}} = -\frac{1}{\mathcal{H}_f(\mu|\{\boldsymbol{B}\})}$.

Proof. The proof follows the same arguments as in Corollary 6.3.1 with respect to the ball $\mathbf{B}(\mu, d)$ such that for a given vector of block magnetisation $\mathbf{m}$, the measure:

$$\mu_N(\mathbf{m} \in \mathbf{B}(\mu, d)) := \frac{e^{-H_N(\sigma)}}{Z_{N|\mathbf{B}}} \prod_{i=1}^{N} d\rho(\sigma_i) \to 1 \qquad (6.20)$$

for $N \to \infty$. Observe that the partition function $Z_{N|\mathbf{B}}$, can be obtained using the same arguements of (6.14) with respect to the ball $\mathbf{B}$ such that $m^{(l)}$ concentrates uniquely around a single point of μ_l, since η is the minimum distance between all distinct pairs of maximisers. Hence, $\mathbf{B}$ contains a unique vector of local maximiser of μ based on the defined radius d. This yields local multivariate Gaussian fluctuations for the vector of block magnetisation around the multiple maximisers. $\qquad \square$

6.4   Case Study: Two-component model

Now, let us consider the case where the system is partitioned into only two blocks, consisting of two kinds of agents, i.e., a heterogeneous system, Humans (H) and Artificial Intelligence (AI) agents. The interactions that will be taken into account are the binary, quadratic ones (H-H, H-AI and AI-AI), the triplet or cubic (AI-AI-AI, AI-AI-H, AI-H-H, H-H-H) while the higher order ones (quartic, etc.) will be ignored. Furthermore, we consider the state (or opinion) variables of the agents as binary having in mind a task with possible binary outcome, like should a patient be operated or not. The nature of the interaction is that two or more agents in contact may like (or dislike) each others "opinion" and they change their state variables such that the system finds a stationary state. We assume that all agents

are in contact with each other, i.e., they sit on the nodes of a complete graph - an assumption needed for the analytical solvability of the system.

To this end, we investigate the two-block version of the model in equation (6.1), which we call henceforth the two-component cubic mean-field model, described as follows: Let partition the system of N agents into two subsystems AI and H of sizes N_1 and N_2 respectively, such that AI $\cap$ H $= \emptyset$ and $N_1 + N_2 = N$. Let $m_S(\sigma) = \frac{1}{|S|} \sum_{i \in S} \sigma_i$ be the average opinion of agents in a subsystem S and denote m_1 and m_2 as the average opinion for the subsystems AI and H respectively. Further, we define as the relative sizes of AI and H agents $\alpha_1 = \frac{N_1}{N}$ and $\alpha_2 = \frac{N_2}{N}$ respectively. The two-component cubic mean-field model has the following energy contribution:

$$
\begin{aligned}
\frac{H_N(\sigma)}{N} = &- \frac{1}{3} \left[K_{111} \alpha_{N_1}^3 m_{N_1}^3 + 3 K_{112} \alpha_{N_1}^2 \alpha_{N_2} m_{N_1}^2 m_{N_2} + 3 K_{122} \alpha_{N_1} \alpha_{N_2}^2 m_{N_1} m_{N_2}^2 \right] \\
&- \frac{1}{3} K_{222} \alpha_{N_2}^3 m_{N_2}^3 - \frac{1}{2} \left[J_{11} \alpha_{N_1}^2 m_{N_1}^2 + 2 J_{12} \alpha_{N_1} \alpha_{N_2} m_{N_1} m_{N_2} + J_{22} \alpha_{N_2}^2 m_{N_2}^2 \right] \\
&- h_1 \alpha_{N_1} m_{N_1} - h_2 \alpha_{N_2} m_{N_2}
\end{aligned}
$$

(6.21)

and the energy contribution of the model is given as:

$$
\begin{aligned}
U(m_1, m_2) = &\frac{1}{3} \left[K_{111} \alpha_1^3 m_1^3 + 3 K_{112} \alpha_1^2 \alpha_2 m_1^2 m_2 + 3 K_{122} \alpha_1 \alpha_2^2 m_1 m_2^2 + K_{222} \alpha_2^3 m_2^3 \right] \\
&+ \frac{1}{2} \left[J_{11} \alpha_1^2 m_1^2 + 2 J_{12} \alpha_1 \alpha_2 m_1 m_2 + J_{22} \alpha_2^2 m_2^2 \right] + \left[h_1 \alpha_1 m_1 + h_2 \alpha_2 m_2 \right].
\end{aligned}
$$

(6.22)

The variational form of the large number limit of the generating functional associated to (6.22) is:

$$
\sup_{m \in [-1,1]^2} \Phi(m) = \sup_{m \in [-1,1]^2} \left[U(m_1, m_2) - (\alpha_1 I(m_1) + \alpha_2 I(m_2)) \right]
$$

(6.23)

where $I(m_1)$ and $I(m_2)$ are the entropy associated to the average opinions of the subsystems and they sum up to the total number of configurations as a product of the individual ones. Therefore,

$$
p(\mathbf{K}, \mathbf{J}, \mathbf{h}) = \sup_{m \in \mathcal{X}} \Phi(m)
$$

(6.24)

Here $\mathbf{K}$, $\mathbf{J}$ and $\mathbf{h}$ denotes the vectors of model parameters $(K_{111}, K_{112}, K_{122}, K_{222})$, (J_{11}, J_{12}, J_{22}) and (h_1, h_2) respectively. The stationary solutions $\overline{m}$ of Φ are as follows

$$
\overline{m}_l = \tanh \left(h_l + \sum_{p,q=1}^{2} \alpha_p (J_{lp} + \alpha_q K_{lpq} \overline{m}_q) \overline{m}_p \right) \qquad \text{for} \qquad l = 1, 2, \quad (6.25)
$$

from which the global stable ones are to be selected. In the rest of this work, we assign $\alpha = \alpha_1$ and $(1 - \alpha) = \alpha_2$ then $\alpha \in [0, 1]$ and the total average opinion $\overline{m} = \alpha\overline{m}_1 + (1 - \alpha)\overline{m}_2$ will be used as combined order parameter. It is worth recalling that, when $\alpha = 0$ then there are only Human agents in the population and when $\alpha = 1$ there are only AI agents in the population. For the rest of the work, we adopt the re-parameterisation of h_1 and h_2 found in [77]. In this sense, the parameters h_1 and h_2 are thought of as dependent on the internal average opinion (given by m_1^* and m_2^*) and interaction within each subsystem without interaction with the other agents. Hence following the fixed point equation (6.25), we define h_1 and h_2 as

$$
\begin{aligned}
h_1 &= \operatorname{arctanh}(m_1^*) - K_{111}m_1^{*2} - J_{11}m_1^* \\
h_2 &= \operatorname{arctanh}(m_2^*) - K_{222}m_2^{*2} - J_{22}m_2^*
\end{aligned}
\tag{6.26}
$$

Surfaces of the solution of (6.25) that gives rise to the global maxima of Φ in equation (6.23), with respect to the free parameters α and $K_{112} = K_{122} = K$ for fixed values of the other parameters are shown as Figure 6.2.

When cross cubic interactions (i.e., $K_{112} = K_{122} = K$) are fixed, as observed in panels **(b), (c)** and **(d)** of Figure 6.2, there are jumps in the average opinion of the agents depending on their relative fractions. Smaller values of α (i.e., more Human agents), may lead to an inclination of the minus opinion while positive opinion inclination may result from larger values of α (i.e., more AI agents). Hence, a larger proportion of the AI agent population may lead to abrupt changes in behaviour of the ecosystem.

AI machines are made to assist and work with humans, therefore they are assumed to interact with humans. Figure 6.3 gives the scenario of an interacting system where only Humans or only AI agents are not interacting among themselves (see panel **(a)**) and when we assume that the cubic interaction among humans and AI agents are equal (see panel **(b)**). In both cases we observe transitions for large enough fraction of the AI agents in the order parameter when interaction bias and mutual interaction are absent.

6.4.1 Exploration of the effect of the composition

In this section we present phase diagrams of the model relating the parameter α and one among the interacting ones. The black continuous line is used to separate the opinion phases and in particular it emphasises the first order phase transitions,
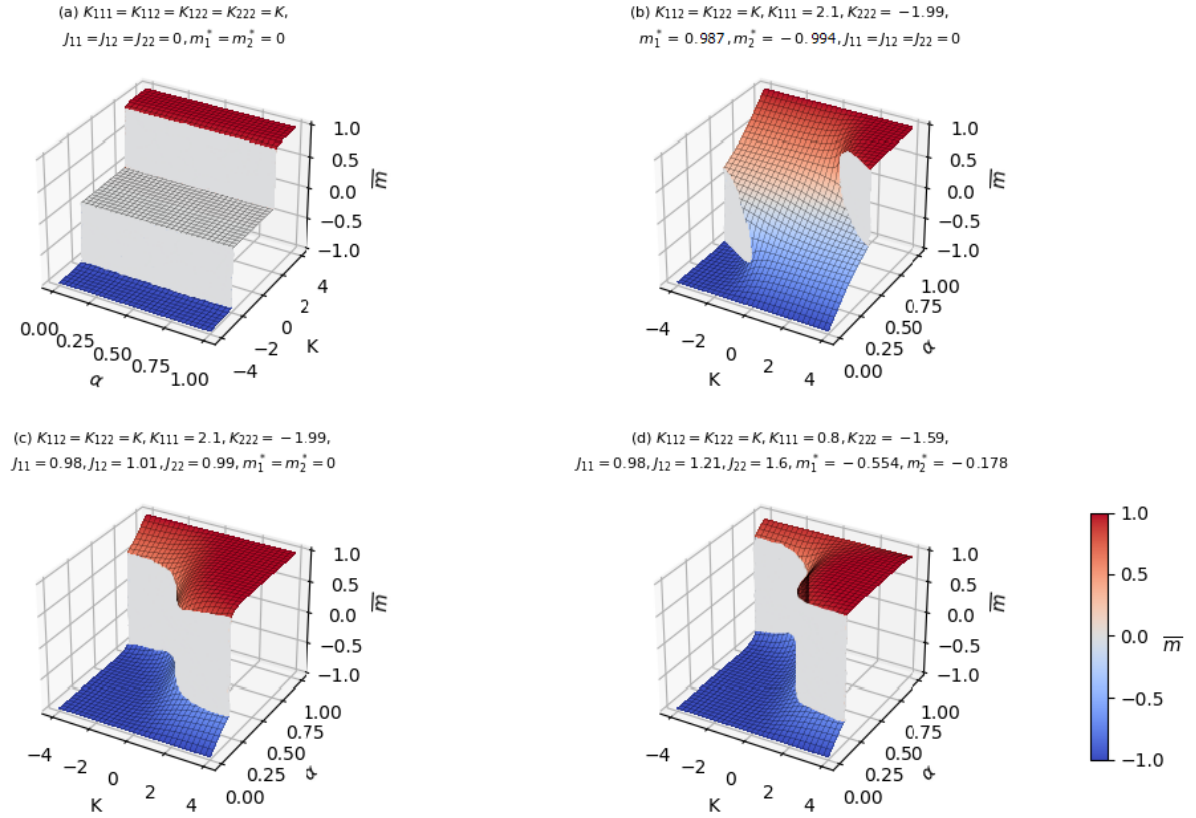
Figure 6.2: Total average opinion surfaces of the two component cubic mean-field model. In panel **(a)** we observe first order phase transitions at K_c. Here, α is constant in K. When the cubic interactions are fixed (i.e. $K_{111} = K_{112} = K_{122} = K_{222} = K$) the proportion of AI and Human agents present in the system has no effect on their average opinion as observed in panel **(a)**. Two distinct jumps in $\overline{m}$ are observed in panel **(b)** for certain values of K and α. For panel **(c)** and **(d)** α varies smoothly for the total average opinion and then observe sudden jump to another phase.
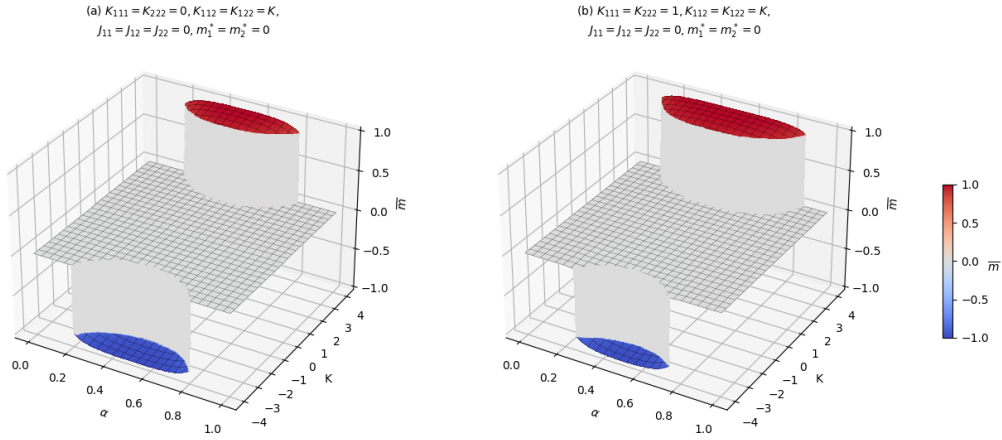
Figure 6.3: Average opinion for $K_{111} = K_{222} = 0$ and $K_{111} = K_{222} = 1$ with $K_{112} = K_{122} = K$ varying. In the left panel, panel **(a)**, the cubic in-group interaction for the AI agents and that of humans are set to zero (i.e., $K_{111} = K_{222} = 0$) and in **(b)** to one (i.e., $K_{111} = K_{222} = 1$) with varying inter-group interaction.

i.e., sudden jumps of the opinion resulting in abrupt changes of colour in the picture. This is illustrated in Figure 6.4. The α-value found in correspondence of the black line indicates the proportion of AI agents required for Human opinion to lose its prevalence over the entire population.

The simulation of the results obtained for suitable values of the model parameter in Figure 6.4**(a)** suggests that even in the case where there is very small fraction of AI agents we can still observe abrupt behaviours in opinion formation within the Human AI ecosystem. This observation is likewise similar to that of panel **(d)** of Figure 6.4, which illustrates that for a system where there is less interaction among Human agents (K_{222}), smaller fraction of the AI agents may lead to phase transition and hence prevalent opinion formation.

6.4.2 Discussion

A noteworthy feature of the cubic mean-field model stems from the fact that we can observe three distinct phases depending on the parameter values in the absence of interaction bias of the agent(s) in the ecosystem (see for instance Fig 6.2(a) and Fig 6.3). Unlike the quadratic mean-field model, where we observe a jump from negative to positive state, instead one can observe a jump from the negative
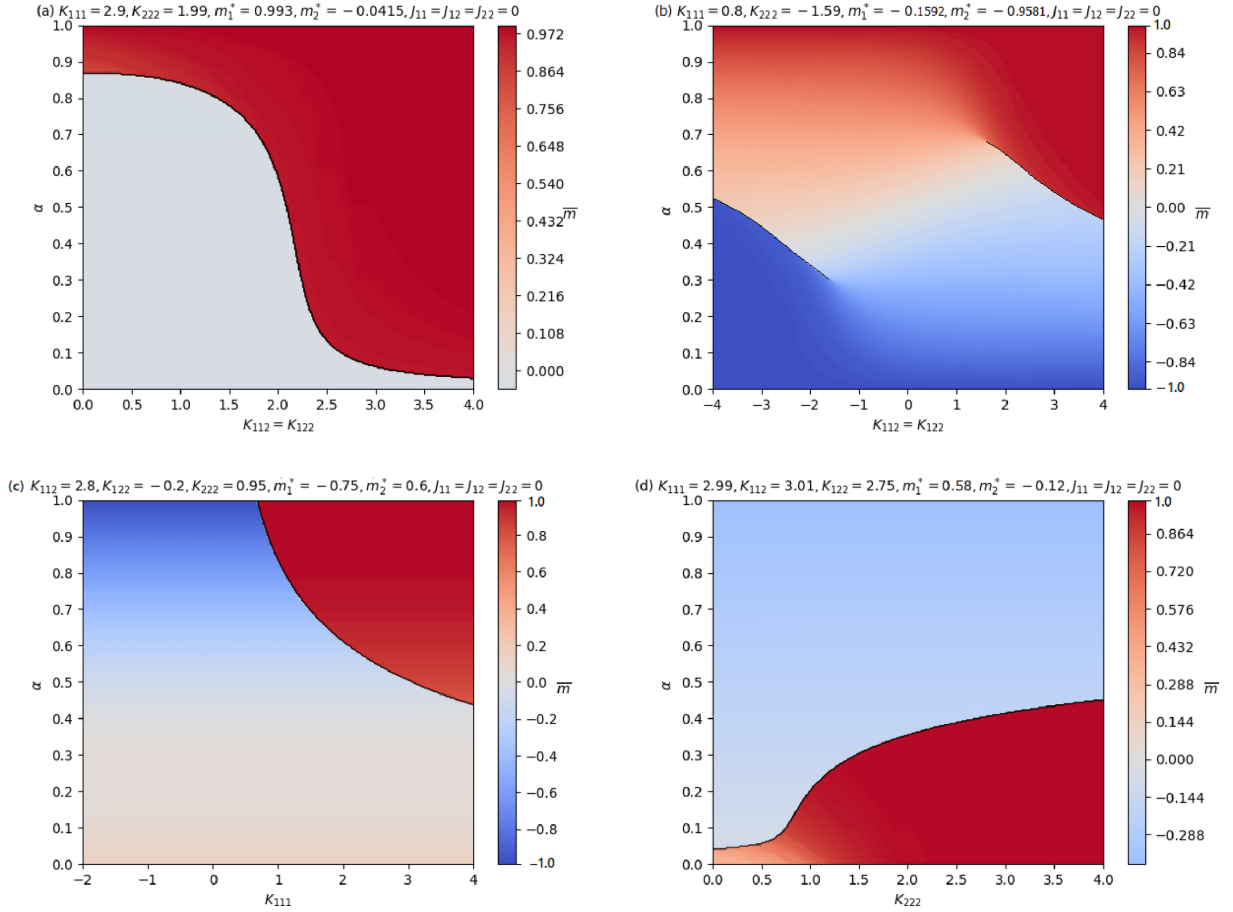
Figure 6.4: Phase diagram for fixed parameters of the cubic mean-field model. In panel **(a)**, when $K_{112} = K_{122}$ is small the system require a larger fraction (i.e., α) of the AI agents to observe a phase transition and as $K_{112} = K_{122}$ increases, the proportion of AI agents required for a phase transition decreases. In this scenario, the relative fraction of the AI agents corresponding to the black line is a decreasing function of $K_{112} = K_{122}$. While panel **(b)** illustrate two separate jumps in the average opinion depending on the values of $K_{112} = K_{122}$ and α. We observe from panel **(c)** that when interaction among AI agents (K_{111}) increases their proportion needed to observe a phase transition decreases. While in panel **(d)**, when interaction among Human agents (K_{222}) increases, the fraction of AI agents needed to effect a phase transition increases and vice versa.

average opinion to a zero average opinion and a jump to a positive average opinion when three-body interaction is considered. The zero average opinion, which is a stable paramagnetic state, is an indication of symmetry in opinion such that the agents have no preference for one over the other. As K increases or decreases, the symmetry in opinion is broken, and the total average opinion of the agents in the ecosystem shifts to either a positive or negative state.

The results illustrated in this work are some of the possible simulation for a wide class of values of the parameters. The model used and the whole statistical mechanics approach presented might also be used to infer the values of those parameters starting from real data as it was done in [60, 63, 64, 78].

Clearly, our approach has limitations. First, the dynamics leading to the stationary statistical distribution described by the pressure per particle is a special one, while in reality opinion dynamics may be quite different as reflected in the numerous models introduced to study it [79]. However, we believe that our simplified model is sufficient for calling the attention to a possible source of criticality, namely that the dependence of the outcome in a Human-AI ecosystem depends very non-linearly on the composition of the participants and this may have severe consequences.

A further aspect is that in realistic settings time should play an important role, which has been completely ignored here. With reference to the example above about the decision making process in a critical situation in health care, there is probably not enough time to achieve a complete equilibrium state of the participating opinion carriers. Another source of non-stationarity could be that the system is driven by a continuous flow of data. Therefore, more realistic models have to be dynamic in nature.

The above critical points give a guide to us in which direction one should continue the research on the Human-AI ecosystem. An important step should be to collect and use data of related systems as a starting point for the developments of adequate models.

Chapter 7

General Conclusions and Outlook

In this thesis, a complete characterisation of the phase properties of the mean-field Ising model with three-spin interaction is given. The three-spin interaction, which provides a spin-flip symmetry-breaking parameter, induces phase transitions with novel properties in the mean-field setting. The presence of a stable paramagnetic phase and the fact that, also in the antiferromagnetic regime, the model presents phase transitions and phase coexistence are interesting for applications in socio-technical environments [35] and possibly in other fields [45, 80]. Particularly noteworthy is the phase coexistence of magnetised and symmetric states without the need for more than two spin states, as observed in the Potts model [36].

An interesting advancement is made in the analysis of fluctuations in magnetisation, both in the single-block model and the multi-populated model. The validity of the Central Limit Theorem (CLT) provides a theoretical foundation for the parametric analysis in Chapter 5, as the magnetisation density tends to approximate a normal distribution for a sufficiently large sample size. This leads to intriguing possibilities, such as extending the results of the inverse problem in two directions: (1) to the critical point where some observables, such as χ and ψ, diverge, and (2) to the multi-populated case studied in Chapter 6, where the model finds applications in describing Human-AI ecosystems [35]. This would provide a more viable framework for applying the models to real-world data.

It is worth mentioning that the results in Chapter 5 can be refined using methods from Bayesian parametric analysis. In this way, the parameters of interest are sampled from the posterior of the likelihood, allowing for a more flexible exploration

131

of the behaviour of the likelihood function. This is in contrast to relying solely on moments, which may have limitations when dealing with the recovery of a nonidentifiable set of parameters or at the critical point of the system. Moreover, in the presence of a phase transition, refined methods such as the density clustering algorithm are employed, whereas the Bayesian method explores more freely. In [81], this issue is thoroughly investigated using methods from Bayesian analysis that capture the geometry of the likelihood function [82].

A possible research development will be to extend the results obtained in Chapters 3 and 4 to the multi-populated model introduced in Chapter 6. Furthermore, intriguing open problems lie in extending the results presented here to $O(N)$ vector mean-field models, a direction that will be explored in future investigations. Observe that in the case of two-spin interaction, Stein's method provides stronger results (Berry-Esseen type bounds) on the rate at which the convergence to the normal distribution takes place (see [83, 84]). The extension of the above method to the model introduced in Chapter 3 of this thesis has recently been discussed in [85]. Extending such results to more general, higher-order interactions is an interesting open problem.

Appendix A

Technical tools

A.1 Approximation lemmas

In this section, standard mathematical approximations which played a crucial role in Chapters 3, 4, and 6 are stated.

Lemma A.1.1. *(Riemann Approximation). Let $f : [a, b] \to \mathbb{R}$ be a differentiable function and let $\{x_0, x_1, \ldots, x_n\}$ be any partition of $[a, b]$, i.e., $a = x_0 < x_1 < \ldots < x_n = b$. Furthermore, if f' is the derivative of f and it is continuous on $[a, b]$ and $\epsilon = \max_{1 \leq i \leq n}(x_i - x_{i-1})$ denotes the mesh size of the partition, then:*

$$\left| \int_a^b f(x)\, dx - \sum_{i=1}^n f(c_i) \cdot (x_i - x_{i-1}) \right| \leq \frac{\epsilon(b-a)}{2} \max_{a \leq x \leq b} |f'(x)|.$$

where c_i is any point in the $i-$th subinterval $[x_{i-1}, x_i]$.

Lemma A.1.2. *(Laplace Approximation). Let $a < b$ be fixed real numbers, $g : [a, b] \longrightarrow \mathbb{R}$ be a differentiable function on (a, b), and $q_n : [a, b] \longrightarrow \mathbb{R}$ be a sequence in (a, b) that is bounded away from both a and b, satisfying $q_n'(x^*) = 0$ and $q_n''(x^*) < 0$ such that $q_n(x^*) > q_n(x)$ for all $x \in (a, b)$. Then for $\alpha \in (0, \frac{1}{6}]$ we have as $n \longrightarrow \infty$:*

$$\int_{x^* - n^{-\frac{1}{2}+\alpha}}^{x^* + n^{-\frac{1}{2}+\alpha}} g(x) e^{nq_n(x)} dx = \sqrt{\frac{2\pi}{n|q_n''(x^*)|}} g(x^*) e^{nq_n(x^*)} \left(1 + \mathcal{O}(n^{-\frac{1}{2}+3\alpha})\right) \quad \text{(A.1)}$$

Lemma A.1.3 (Multivariate Riemann Approximation)**.** *Let $Q = [a_1, b_1] \times [a_2, b_2] \times \ldots \times [a_r, b_r]$ be a rectangular domain in $\mathbb{R}^r$, and let $\{(x_{1,0}, x_{2,0}, \ldots, x_{r,0}), (x_{1,1}, x_{2,1}, \ldots, x_{r,1}), \ldots,$*

$(x_{1,m}, x_{2,m}, \ldots, x_{r,m})\}$ *be any partition of* Q, *where* $a_i = x_{i,0} < x_{i,1} < \ldots < x_{i,m} = b_i$ *for each* $i = 1, 2, \ldots, r$.

Assume that g is differentiable on Q and that its partial derivatives $\frac{\partial g}{\partial x_i}$ are continuous on Q for all $i = 1, 2, \ldots, r$. Let $\epsilon_i = \max_{1 \leq j \leq m}(x_{i,j} - x_{i,j-1})$ denote the mesh size of the partition along the i-th variable. Then, the Riemann approximation lemma for the multivariate case states:

$$\left| \int_Q g(\mathbf{x}) \, d\mathbf{x} - \sum_{j_1=1}^{m_1} \sum_{j_2=1}^{m_2} \ldots \sum_{j_r=1}^{m_r} g(\mathbf{c}_{j_1,j_2,\ldots,j_r}) \cdot \prod_{i=1}^{r}(x_{i,j_i} - x_{i,j_i-1}) \right| \leq \frac{\epsilon_1 \epsilon_2 \ldots \epsilon_r}{2} \cdot \max_{\mathbf{x} \in Q} |\nabla g(\mathbf{x})|,$$

where $\mathbf{c}_{j_1,j_2,\ldots,j_r}$ *is any point in the* j_1-*th subinterval along the first variable,* j_2-*th subinterval along the second variable, and so on, up to the* j_r-*th subinterval along the* r-*th variable.*

Lemma A.1.4 (Multivariate Laplace Approximation). *Let* $Q \subset \mathbb{R}^r$ *be an open set,* $\mathbf{x}_N^*$ *a vector in* Q, *and* $\mathbf{q}_N : Q \longrightarrow \mathbb{R}$ *a differentiable sequence in* Q *that is bounded away from the boundary of* Q, *satisfying* $\nabla \mathbf{q}_N(\mathbf{x}_N^*) = \mathbf{0}$ *and* $\nabla^2 \mathbf{q}_N(\mathbf{x}_N^*)$ *is negative definite, such that* $\mathbf{q}_N(\mathbf{x}_N^*) > \mathbf{q}_N(\mathbf{x})$ *for all* $\mathbf{x} \in Q$. *Given that* $\mathbf{N} = (N_i)_{i \leq r}$ *and* $\alpha \in (0, \frac{1}{6}]$, *as* $N_1 \to \infty, N_2 \to \infty, \ldots, N_r \to \infty$, *then multivariate Laplace approximation is:*

$$\int_{\mathbf{x}_N^* - \mathbf{N}^{-\frac{1}{2}+\alpha}}^{\mathbf{x}_N^* + \mathbf{N}^{-\frac{1}{2}+\alpha}} g(\mathbf{x}) e^{N\mathbf{q}_N(\mathbf{x})} d\mathbf{x} =$$

$$= \sqrt{\frac{(2\pi)^r}{\prod_{l=1}^{r} N_l \det(-\nabla^2 \mathbf{q}_N(\mathbf{x}_N^*))}} g(\mathbf{x}_N^*) e^{N\mathbf{q}_N(\mathbf{x}_N^*)} (1 + \mathcal{O}(\mathbf{N}^{-\frac{1}{2}+\alpha})). \quad \text{(A.2)}$$

Here, $\nabla \mathbf{q}_N$ is the gradient vector and $\nabla^2 \mathbf{q}_N$ is the Hessian matrix of $\mathbf{q}_N$.

Proof. Observe from the left hand side of equation (A.2) that:

$$\mathcal{L} = \int_{\mathbf{x}_N^* - \mathbf{N}^{-\frac{1}{2}+\alpha}}^{\mathbf{x}_N^* + \mathbf{N}^{-\frac{1}{2}+\alpha}} g(\mathbf{x}) e^{N\mathbf{q}_N(\mathbf{x})} d\mathbf{x} =$$

$$= \int_{x_N^*(1) - N_1^{-\frac{1}{2}+\alpha}}^{x_N^*(1) + N_1^{-\frac{1}{2}+\alpha}} \cdots \int_{x_N^*(r) - N_r^{-\frac{1}{2}+\alpha}}^{x_N^*(r) + N_r^{-\frac{1}{2}+\alpha}} g(x_1, \ldots, x_r) e^{N\mathbf{q}_N(x_1,\ldots,x_r)} dx_1 \cdots dx_r. \quad \text{(A.3)}$$

Notice from the above that $\mathcal{L}$ is only used here to denote the Laplace approximation. Now, let's consider the following change of variables $t_l = \sqrt{N_l}(x_l - x_N^*(l))$ for $l = 1, \ldots, r$. Then it follows that: $x_l = \frac{t_l}{\sqrt{N_l}} + x_N^*(l)$ and $dx_l = \frac{dt_l}{\sqrt{N_l}}$. We have that:

$$\mathcal{L} = \int_{-N_1^\alpha}^{N_1^\alpha} \cdots \int_{-N_r^\alpha}^{N_r^\alpha} g\left(\frac{t_1}{\sqrt{N_1}} + x_N^*(1), ..., \frac{t_r}{\sqrt{N_r}} + x_N^*(r) \right) e^{N\mathbf{q}_N \left(\frac{t_1}{\sqrt{N_1}} + x_N^*(1), ..., \frac{t_r}{\sqrt{N_r}} + x_N^*(r) \right)}$$

$$\cdot \left(\prod_{l=1}^{r} N_l \right)^{-1/2} dt_1 \cdots dt_r. \quad (A.4)$$

For any $t_l \in [-N_l^\alpha, N_l^\alpha]$, by application of Taylor expansion around the vector $\mathbf{x}_N^*$, we have that:

$$e^{N\mathbf{q}_N \left(\frac{t_1}{\sqrt{N_1}} + x_N^*(1), ..., \frac{t_r}{\sqrt{N_r}} + x_N^*(r) \right)} = e^{N\mathbf{q}_N(\mathbf{x}_N^*) + \frac{1}{2}\langle \mathcal{H}_{\mathbf{q}_N}(\mathbf{x}_N^*)\mathbf{t}, \mathbf{t} \rangle} \left(1 + \mathcal{O}\left(\left(\frac{\mathbf{t}}{\sqrt{\mathbf{N}}} \right)^3 \right) \right) \quad \text{and}$$

$$g\left(\frac{t_1}{\sqrt{N_1}} + x_N^*(1), ..., \frac{t_r}{\sqrt{N_r}} + x_N^*(r) \right) = g(\mathbf{x}_N^*) + g'(\mathbf{x}_N^*)\left(\frac{\mathbf{t}}{\sqrt{\mathbf{N}}} \right) =$$

$$= g(\mathbf{x}_N^*)\left(1 + \mathcal{O}\left(\frac{\mathbf{t}}{\sqrt{\mathbf{N}}} \right) \right) \quad (A.5)$$

where $\mathbf{t} = (t_1, ..., t_r)$ and $\mathcal{H}_{\mathbf{q}_N}(\mathbf{x}_N^*)$ is the Hessian of $\mathbf{q}_N$ evaluated at $\mathbf{x}_N^*$. Now, following from (A.5), the right side of (A.4) becomes:

$$\mathcal{L} = \left(\prod_{l=1}^{r} N_l \right)^{-1/2} \left(1 + \mathcal{O}\left(\mathbf{N}^{\alpha-1/2} \right) \right) g(\mathbf{x}_N^*) e^{N\mathbf{q}_N(\mathbf{x}_N^*)} \int_{-\mathbf{N}^\alpha}^{\mathbf{N}^\alpha} e^{\frac{1}{2}\langle \mathcal{H}_{\mathbf{q}_N}(\mathbf{x}_N^*)\mathbf{t}, \mathbf{t} \rangle} d\mathbf{t} =$$

$$= \left(1 + \mathcal{O}\left(\mathbf{N}^{\alpha-1/2} \right) \right) \sqrt{ \frac{(2\pi)^r}{\prod_{l=1}^{r} N_l \det\left(-\mathcal{H}_{\mathbf{q}_N}(\mathbf{x}_N^*) \right)} } g(\mathbf{x}_N^*) e^{N\mathbf{q}_N(\mathbf{x}_N^*)}. \quad (A.6)$$

Notice that we have bounded $\mathbf{t}$ by its limit $\mathbf{N}^\alpha$. This completes the proof of Lemma A.1.4. $\square$

A.2   Implicit function theorem

This section of the appendix presents some useful technical results applied in the work. We begin by stating the Berge's maximum theorem in the following Proposition without providing its proof.

Proposition A.2.1. *Let $f : [-1, 1] \times \mathbb{R}^n \to \mathbb{R}$ and $c : \mathbb{R}^m \to [-1, 1]$ be continuous functions.*

(a) The following function is continuous:

$$F : \mathbb{R}^n \times \mathbb{R}^m \to \mathbb{R}, \quad F(x, y) = \max_{v \in [-1, c(y)]} f(v, x).$$

(b) *Suppose that for all $x, y \in \mathbb{R}^n$ the function $v \mapsto f(v, x)$ achieves its maximum on $[-1, c(y)]$ in a unique point. Then also the following function is continuous:*

$$T : \mathbb{R}^n \times \mathbb{R}^m \to [-1, 1], \quad V(x, y) = \arg \max_{v \in [-1, c(y)]} f(v, x).$$

The following proposition partially states Dini's implicit function theorem. Then we provide two simple corollaries that are used in this thesis.

Proposition A.2.2. *Let $F : \mathbb{R}^n \times \mathbb{R} \to \mathbb{R}$ be a C^∞ function. Let $(x_0, y_0) \in \mathbb{R}^n \times \mathbb{R}$ such that $F(x_0, y_0) = 0$ and $\frac{\partial F}{\partial y}(x_0, y_0) \neq 0$. Then there exist $\delta > 0, \epsilon > 0$ and a C^∞ function $f : B(x_0, \delta) \to B(y_0, \epsilon)$ such that for all $(x, y) \in B(x_0, \delta) \times B(y_0, \epsilon)$*

$$F(x, y) = 0 \quad \Longleftrightarrow \quad y = f(x)$$

Corollary A.2.1. *Let $F : \mathbb{R}^n \times \mathbb{R} \to \mathbb{R}$ be a C^∞ function. Let $\varphi : \mathbb{R}^n \to \mathbb{R}$ be a continuous function such that for all $x \in \mathbb{R}^n$ such that $F(x, \varphi(x)) = 0$ and $\frac{\partial F}{\partial y}(x, \varphi(x)) \neq 0$, then $\varphi(x) \in C^\infty(\mathbb{R}^n)$.*

Corollary A.2.2. *Let $F : \mathbb{R}^n \times \mathbb{R} \to \mathbb{R}$ be a C^∞ function. Let $a, b : \mathbb{R}^n \to \mathbb{R}$ be a continuous function such that for all $a < b$. Suppose that for all $x \in \mathbb{R}^n$ there exists a unique $y = \varphi(x) \in (a(x), b(x))$ such that $F(x, \varphi(x)) = 0$. Moreover, suppose that for all $x \in \mathbb{R}^n$, $\frac{\partial F}{\partial y}(x, \varphi(x)) \neq 0$, then $\varphi(x) \in C^\infty(\mathbb{R}^n)$.*

Bibliography

[1] Curie, P. (1895). Propriété ferromagnetiqué des corps a diverse températures, Ann. de Chim. et de Phys., 7e série, V: 289.

[2] William, L. (1920). Beitrag zum Verständnis der magnetischen Eigenschaften in festen Körpern. Phys. Zeitschr, 21, 613–615.

[3] Stephen, G. B. (1967). History of the Lenz-Ising model. Rev. Mod. Phys, 39(4).

[4] Weiss, P. (1907). L'hypothèse du champ moléculaire et la propriété ferromagnétique. J. Phys. Theor. Appl. 6, no. 1, 661–690. doi:10.1051/jphystap:019070060066100

[5] Duminil-Copin, H. (2022). 100 Years of the (Critical) Ising Model on the Hypercubic Lattice. International Mathematical Union Preliminary version, to appear in Proc Int. Cong. Math, 2022. doi: 10.4171/ICM2022/204.

[6] Ising, E. (1925). Beitrag zur theorie der ferromagnetismus. Z. Phys. 31, 253–258.

[7] Onsager, L. (1944). Crystal Statistics. I. A Two-Dimensional Model with an Order-Disorder Transition, Phys. Rev. 65, 117–149, 0, American Physical Society, doi/10.1103/PhysRev.65.117.

[8] Heisenberg, W. (1928). Zur Theorie des Ferromagnetismus. Zeitsch. fùr Physik, 49, no. 9, 619–636.

[9] Kadanoff, L. P. and Wegner, F. J. (1971). Some Critical Properties of the Eight-Vertex Model, Phys. Rev. B, 4, 3989–3993, doi:10.1103/PhysRevB.4.3989.

[10] Baxter, R. J. and Wu, F. Y. (1973). Exact Solution of an Ising Model with Three-Spin Interactions on a Triangular Lattice, Phys. Rev. Lett. 31, 1294.

[11] Baxter, R.J. and Wu, F.Y. (1974). Ising Model on a Triangular Lattice with Three-spin Interactions. I The Eigenvalue Equation. Aust. J. Phys. 27, 357-367.

[12] Subramanian, B., Lebowitz, J. (1999). The study of a three-body interaction Hamiltonian on a lattice. J. Phys. A Math Gen. 32:6239.

[13] Ginibre, J. (1970). In Cargese lectures in physics. Gordon and Breach, New York.

[14] Froyen, S., Sudbo, A. A. S., Hemmer, P. C. (1976). Ising models with two- and three-spin interactions: Mean field equation of state, Physica A: Statistical Mechanics and its Applications, Volume 85, Issue 2, 399-408, ISSN 0378-4371, https://doi.org/10.1016/0378-4371(76)90058-3.

[15] Bidaux, R., Boccara, N., and Forgàcs, G. (1986). Three-Spin Interaction Ising Model with a Nondegenerate Ground State at Zero Applied Field, Journal of Statistical Physics, Vol. 45, Nos. 1/2.

[16] Alberici, D., Contucci, P., Mingione, E., Molari, M. (2017). Aggregation models on hypergraphs. Ann. Phys. (N. Y.). 376, 412–424. https://doi.org/10.1016/j.aop.2016.12.001

[17] Battiston, F., Cencetti, G., Iacopini, I., Latora, V., Lucas, M., Patania, A., Young, J.-G., Petri, G. (2020). Networks beyond pairwise interactions: Structure and dynamics. Phys. Rep. 874, 1–92. https://doi.org/10.1016/j.physrep.2020.05.004

[18] Bianconi, G. (2022). Higher-Order Networks: An introduction to simplicial complexes. Cambridge University Press, (Elements in Structure and Dynamics of Complex Networks) Cambridge, England.

[19] Benson, A. R., Abebe, R., Schaub, M. T., Jad-Babaie, A., Kleinberg, J. (2018). Simplicial closure and higher order link prediction, Proc. Proc. Proc. Natl Acad. Sci. USA. 115.

[20] Ellis, R. S. (2006). Entropy, large deviations, and statistical mechanics. Classics in Mathematics. Springer Verlag, Berlin, Reprint of the 1985 original.

[21] Ellis, R. S., Newman, C. M. (1978). The statistics of Curie-Weiss models. J. Stat. Phys. 19, 149–161. https://doi.org/10.1007/bf01012508

[22] Ellis, R.S., Newman, C. M., Rosen, J. S. (1980). Limit theorems for sums of dependent random variables occurring in statistical mechanics II. Conditioning,

multiple phases, and metastability. Z.Wahrscheinlichkeitstheorie verw. Geb. 51, 153–169.

[23] Mukherjee, S., Son, J. & Bhattacharya, B. B. (2021). Fluctuations of the Magnetization in the p-Spin Curie–Weiss Model. Commun. Math. Phys. 387, 681–728, https://doi.org/10.1007/s00220-021-04182-z.

[24] Friedli, S. and Velenik, Y. (2017). Statistical mechanics of lattice systems: A concrete mathematical introduction. Cambridge University Press, ISBN=9781107184824, Cambridge, England.

[25] Dembo, A. and Zeitouni, O. (2010). Large deviations techniques and applications, volume 38 of Stochastic Modelling and Applied Probability. Springer-Verlag, Berlin, Corrected reprint of the second (1998) edition.

[26] Opoku, A. A., & Osabutey, G. (2018). Multipopulation spin models: A view from large deviations theoretic window. Journal of Mathematics, 2018, 1–13. doi:10.1155/2018/9417547

[27] Barra, A. (2008). The mean field Ising model through interpolating techniques, J. Stat. Phys. 145: 234-261.

[28] Guerra, F., Toninelli, F. L. (2002). The Thermodynamic Limit in Mean Field Spin Glass Models, Communications in Mathematical Physics 230.

[29] Ruelle, D. (1999). Statistical mechanics: Rigorous results, World Scientific, Singapore.

[30] Talagrand, M. (2003). Spin glasses: a challenge for mathematicians: cavity and mean field models (Vol. 46). Springer Science & Business Media.

[31] Rudin, W. (1976). Principles of Mathematical Analysis, McGraw-Hill Book Co., New York, NY, USA, 3rd edition.

[32] Varadhan, S. R. S. (1966). Asymptotic probabilities and differential equations. Comm. Pure Appl. Math., 19:261286.

[33] Touchette, H. (2009). The large deviation approach to statistical mechanics. Phys. Rep., 478(1-3):169.

[34] Contucci, P., Mingione, E., & Osabutey, G. (2024). Limit theorems for the cubic mean-field Ising model. Annales Henri Poincaré, pp. 1–26. https://doi.org/10.1007/s00023-024-01420-7

[35] Contucci, P., Kertész, J. and Osabutey, G. (2022). Human-AI ecosystem with abrupt changes as a function of the composition. PLoS ONE 17(5): e0267310. https://doi.org/10.1371/journal. pone.0267310.

[36] Ellis, R. S., Wang, K. (1990). Limit theorems for the empirical vector of the Curie-Weiss-Potts model. Stochastic Processes and Their Applications, 35, 1, 59–79.

[37] Ok, E. A. (2007). Real Analysis with Economics Applications (Princeton University Press, Princeton, 2007), pp. 306–311.

[38] Alberici, D., Contucci, P. and Mingione, E.(2014). A mean-field monomer-dimer model with attractive interaction. The exact solution, Journal of Mathematical Physics 55, 063301:1-27.

[39] Osabutey, G. (2023). Phase properties of the mean-field Ising model with three-spin interaction. http://dx.doi.org/10.2139/ssrn.4469835

[40] Contucci, P., Osabutey, G., & Vernia, C. (2023). Inverse problem beyond two-body interaction: The cubic mean-field Ising model. Physical Review. E, 107(5–1), 054124. doi:10.1103/PhysRevE.107.054124

[41] Jaynes, E. T. (1957). Information theory and statistical mechanics, The Physical review, 106(4), pp. 620–630. doi: 10.1103/physrev.106.620.

[42] Mackay, D. J. C. (2003). Information Theory, Inference, and Learning Algorithms. Copyright Cambridge University Press.

[43] Battiston, F., Cencetti, G., Iacopini, I., Latora, V., Lucas, M., Patania, A., Young, J.-G. & Petri, G. (2020). Networks beyond pairwise interactions: Structure and dynamics. Physics Reports, 874, 1–92. doi:10.1016/j.physrep.2020.05.004

[44] Battiston, F., Amico, E., Barrat, A., Bianconi, G., Ferraz de Arruda, G., Franceschiello, B., Petri, G. et. al. (2021). The physics of higher-order interactions in complex systems. Nature Physics, 17(10), 1093–1098. doi:10.1038/s41567-021-01371-4

[45] Majhi, S., Perc, M., & Ghosh, D. (2022). Dynamics on higher-order networks: a review. Journal of the Royal Society, Interface, 19(188), 20220043. doi:10.1098/rsif.2022.0043

[46] Benson, A. R., Abebe, R., Schaub, M. T., Jadbabaie, A., & Kleinberg, J. (2018). Simplicial closure and higherorder link prediction, Proc. Proc. Natl Acad. Sci. USA, 115, E11221E-11230.

[47] Alvarez-Rodriguez, U., Battiston, F., de Arruda, G. F., Moreno, Y., Perc, M., & Latora, V. (2021). Evolutionary dynamics of higher-order interactions in social networks. Nature Human Behaviour, 5(5), 586–595. doi:10.1038/s41562-020-01024-1

[48] Nguyen, H. C., Zecchina, R. and Berg, J. (2017). Inverse statistical problems: from the inverse Ising problem to data science, Advances in physics, 66.

[49] Baldassi, C., Gerace, F., Saglietti, L., & Zecchina, R. (2018). From inverse problems to learning: a Statistical Mechanics approach. Journal of Physics. Conference Series, 955, 012001. doi:10.1088/1742-6596/955/1/012001

[50] Beentjes, S. V. and Khamseh, A. (2020). Higher-order interactions in statistical physics and machine learning: A model-independent solution to the inverse problem at equilibrium, Physical Review E, 102(5–1), p. 053314. doi: 10.1103/PhysRevE.102.053314.

[51] Mezard, M., Parisi, G. and Virasoro, M. A. (1987). Spin glass theory and beyond: An introduction to the replica method and its applications. World Scientific Publishing.

[52] Schneidman, E., Berry, M., Segev, R. and Bialek, W. (2006). Weak pairwise correlations imply strongly correlated network states in a neural population, Nature 440, 1007.

[53] Mzard, M. and Mora, T. (2009). Constraint satisfaction problems and neural networks: A statistical physics perspective, Journal of physiology, 103.

[54] Schug, A., Weigt, M., Onuchic, J. N., Hwa, T. and H. Szurmant, H. (2009). High-resolution protein complexes from integrating genomic information with molecular simulation, Proceedings of the National Academy of

Sciences of the United States of America, 106(52), pp. 22124–22129. doi: 10.1073/pnas.0912100106.

[55] Morcos, F., Pagnani, A., Lunt, B., Bertolino, A., Marks, D. S., Sander, C., Zecchina, R., Onuchic, J. N., Hwa, T. and Weigt, M. (2011). Direct-coupling analysis of residue coevolution captures native contacts across many protein families, PNAS 108, E1293.

[56] Geman, G., Graffigne, C. (1986). Markov random field image models and their applications to computer vision, in Proceedings of the International Congress of Mathematicians, p. 14961517.

[57] McFadden, D. (2001). Economic choices, American Economic Review 91, 351.

[58] Durlauf, S. N. (1999). How can statistical mechanics contribute to social science? Proceedings of the National Academy of Sciences of the United States of America, 96(19), 10582–10584. doi:10.1073/pnas.96.19.10582

[59] Brock, W. A. and Durlauf, S. N. (2001) Discrete choice with social interactions, The Review of Economic Studies, 68(2), pp. 235–260. doi: 10.1111/1467-937x.00168.

[60] Burioni R, Contucci, P., Fedele, M., Vernia, C., Vezzani, A. (2015). Enhancing participation to health screening campaigns by group interactions, Scientific reports, 5(1), p. 9904. doi: 10.1038/srep09904.

[61] Gallo, I., Barra, A., Contucci, P. (2009). Parameter evaluation of a simple mean-field model of social interaction. Mathematical Models & Methods in Applied Sciences: M3AS, 19(supp01), 1427–1439. doi:10.1142/s0218202509003863

[62] Osabutey, G., Opoku, A. A., & Gyamfi, S. (2020). A statistical mechanics approach to the study of energy use behaviour. Journal of Applied Mathematics, 2020, 1–14. doi:10.1155/2020/7384053

[63] Barra, A., Contucci, P., Sandell, R., Vernia, C. (2015). An analysis of a large dataset on immigrant integration in Spain. The Statistical Mechanics perspective on Social Action. Scientific Reports, 4(1). doi:10.1038/srep04174

[64] Opoku, A. A., Osabutey, G., & Kwofie, C. (2019). Parameter evaluation for a statistical mechanical model for binary choice with social interaction. Journal of Probability and Statistics, 2019, 1–10. doi:10.1155/2019/3435626

[65] Contucci, P., Vernia, C. (2020). On a statistical mechanics approach to some problems of the social sciences. Frontiers in Physics, 8. doi:10.3389/fphy.2020.585383

[66] Fedele, M., Vernia, C., & Contucci, P. (2013). Inverse problem robustness for multi-species mean-field spin models. Journal of Physics. A, Mathematical and Theoretical, 46(6), 065001. doi:10.1088/1751-8113/46/6/065001

[67] Fedele, M., & Vernia, C. (2017). Inverse problem for multispecies ferromagnetic like mean-field models in phase space with many states. Phys. Rev. E, 96.

[68] Contucci, P., Luzi, R., & Vernia, C. (2017). Inverse problem for the mean-field monomer-dimer model with attractive interaction J. Phys. A: Math. Theor, 50.

[69] Itoy, N. and Kohring, G. A. (1993). Cluster vrs single-spin algorithms–Which are more efficient? International Journal of Modern Physics C, World Scientific Publishing Company, DOI:10.1142/S0129183194000027, Corpus ID: 119441633.

[70] Decelle, A. & Ricci-Tersenghi, F. (2016). Solving the inverse Ising problem by mean-field methods in a clustered phase space with many states. Phys. Rev. E 94, 012112.

[71] Rodriguez, A., & Laio, A. (2014). Clustering by fast search and find of density peaks. Science (New York, N.Y.), 344(6191), 1492–1496. doi:10.1126/science.1242072

[72] Chau, H. N. and Berg, J. Mean-Field Theory for the Inverse Ising Problem at Low Temperatures. Physical Review Letter 109, 050602 (2012).

[73] Gallo, I., Barra, A., Contucci, P. (2009). Parameter evaluation of a simple mean-field model of social interaction. Math. Models Methods Appl. Sci. 19, 1427–1439. https://doi.org/10.1142/s0218202509003863

[74] Contucci, P., Gallo, I., Ghirlanda, S. (2008). Equilibria of culture contact derived from ingroup and outgroup attitudes, vol. 5.

[75] Kincaid, J. M. and Cohen, E. G. D. (1975). Phase diagrams of liquid helium mixtures and metamagnets: Experiment and mean-field theory, Physics Reports, vol. 22, no. 2, pp. 57–143.

[76] Galam, S., Yokoi, C. S. O. and Salinas, S. R. (1998). Metamagnets in uniform and random fields, Physical Review B, Vol. 57, 14.

[77] Contucci, P., Gallo, I., Menconi, G. (2008). Phase transitions in social sciences: two-population mean field theory, Int. Jou. Mod. Phys. B, Vol. 22, N. 14: 1-14.

[78] Contucci, P., Ghirlanda, S. (2007). Modeling society with statistical mechanics: an application to cultural contact and immigration. Qual Quant. 41:569–578. doi: 10.1007/s11135-007-9071-9.

[79] Xia, H., Xuan, Z. (2011). Opinion Dynamics: A Multidisciplinary Review and Perspective on Future Research. International Journal of Knowledge and Systems Science, 2:72–91.

[80] Liggett, T. M., Steif, J. E., & Tóth, B. (2007). Statistical mechanical systems on complete graphs, infinite exchangeability, finite extensions and a discrete finite moment problem. Annals of Probability, 35(3), 867–914. https://doi.org/10.1214/009117906000001033.

[81] Osabutey, G., Richardson, R., Page, G. L. (2024) Bayesian inverse Ising problem with three-body interactions, https://doi.org/10.48550/arXiv.2404.05671.

[82] Girolami, M. and Calderhead, B. (2011). Riemann manifold langevin and hamiltonian monte carlo methods: Riemann manifold langevin and hamiltonian monte carlo methods. Journal of the Royal Statistical Society. Series B, Statistical methodology, 73(2):123–214.

[83] Eichelsbacher, P., & Löwe, M. (2010). Stein's method for dependent random variables occuring in statistical mechanics. Electronic Journal of Probability, 15, 962–988. doi:10.1214/ejp.v15-777.

[84] Chatterjee, S., & Shao, Q. M. (2011). Nonnormal approximation by Stein's method of exchangeable pairs with application to the Curie–Weiss model, The Annals of Applied Probability, Vol. 21, No. 2, pp. 464-483, 20.

[85] Eichelsbacher, P. (2024). Stein's method and a cubic mean-field model. doi:10.48550/arxiv.2404.07587